ENHANCED ENZYMATIC HYDROLYSIS OF CELLULOSIC FIBERS BY CATIONIC POLYELECTROLYTES

A Dissertation
Presented to
The Academic Faculty

by

John Timothy Reye

In Partial Fulfillment
of the Requirements for the Degree
Doctor of Philosophy in the
School of Chemical and Biomolecular Engineering

Georgia Institute of Technology
May 2011

ENHANCED ENZYMATIC HYDROLYSIS OF CELLULYTIC FIBERS BY CATIONIC POLYELECTROLYTES

Approved by:

Dr.Sujit Banerjee, Advisor
School of Chemical and Biomolecular Engineering
Georgia Institute of Technology

Dr. Spyros Pavlostathis
School of Civil and Environmental Engineering
Georgia Institute of Technology

Dr. Jim Bradbury
NewPage Corporation
Wisconsin Rapids, WI

Dr. Athanassios Sambanis
School of Chemical and Biomolecular Engineering
Georgia Institute of Technology

Dr. Yulin Deng
School of Chemical and Biomolecular Engineering
Georgia Institute of Technology

Date Approved: November 23, 2010

To my wife Elizabeth and son Colin

ACKNOWLEDGEMENTS

Throughout my thesis work I have been fortunate to receive help from many people, which made the completion of this research possible. Of these people, I first thank my advisor Dr. Sujit Banerjee. Dr. Banerjee provided me a great opportunity to explore and develop my thesis topic, and through the research and discussions with him an important discovery was made providing a new method for enhancing the performance of hydrolytic enzymes. Next, I would like to thank my loving wife, Elizabeth, for her support during my thesis work. I know at times it was a challenge being around me, and I appreciate her unconditional love. I also thank my parents, Lawrence and Patricia, for their love and support throughout my entire studies which has led me to Georgia Tech. I would like to thank my thesis committee Sujit Banerjee, Jim Bradbury, Yulin Deng, Spyros Pavlostathis, and Athanassios Sambanis for their constructive evaluations, which has made my thesis that much better. I also thank Ken Matthews and Danny Hanes at Eka Chemicals for their support during my thesis work. If the risk pays off, Eka Chemicals will be launching new polymer sales in the biofuels market. Finally, I would like to thank my former and current lab mates, Kendra Maxwell, Jian Lu, Sandeep Mora, Adam Brancato, Swati Rao, and Tuan Le, and the Georgia Tech faculty and staff for their instruction and advice along the way; among the Georgia Tech staff I would like to specially thank Mike Buchanan for his collaboration with the Banerjee Group.

TABLE OF CONTENTS

LIST OF TABLES

LIST OF FIGURES

LIST OF EQUATIONS

SUMMARY

A new method for enhancing rates of enzymatic hydrolysis for cellulosic fiber is presented. By adding a cationic polyelectrolyte to a cellulase/cellulose hydrolytic system, the polyelectrolyte binds to the cellulase and fiber forming flocs. The cellulase is bound by a patching mechanism. By using this technique, the rate of enzymatic hydrolysis can be enhanced. This thesis covered observations made about the cellulase/cationic polyelectrolyte/fiber interactions. A mechanism was proposed based on the experimental results.

Dynamic light scattering results generally showed non-specificity for cellulase-polyelectrolyte interactions with regard to varying cationicity; however, increasing molecular weight was less favorable for binding. Adsorption of cellulase increased with the addition of polyelectrolytes. The differences between polyelectrolytes appeared non-specific and were not significant; however, the increase in cellulase binding with and without polyelectrolyte was significant at approximately a 40% increase. Binding/rate of reaction phenomena compete as a function of temperature. Shorter fibers and fines have higher surface area than longer fibers. An adsorption coefficient for fines was found to be three times greater than for long fibers. Long fibers having a lower surface area proportional to the bound enzymes results in a greater amount of free enzymes not bound. The cellulase binding is a function of temperature, but given the negative charge of the cellulase and cellulose fibers, there is also a resistance to adsorption because of a repulsive electrical double layer. Measurements of polyelectrolyte layer thicknesses (40-

70 nm) were found to be significantly lower than the repulsive double layer thickness (250-1000 nm). The polyelectrolyte adsorption may reduce the negative surface charge of the fiber, thus reducing the repulsive layer thickness. Additionally, the binding of cellulase to the polyelectrolyte layer through a flocculation mechanism brings the cellulase and cellulose closer for binding and allows for the reaction to occur. Without agitation, the surface area of the fiber flocs is reduced offsetting the benefit of the polyelectrolyte flocculation. The increase in binding cellulase to fiber in the presence of a cationic polyelectrolyte is believed to be the main reason for the increase in enzymatic hydrolysis rate and extent. If the polyelectrolyte is added to long fibers, initially no enhancement will be observed. Polyelectrolyte addition appears to benefit when short fibers and fines are present. Polyelectrolyte addition at a point where short fibers and fines are appreciable facilitates the polyelectrolyte rate and extent enhancement. This process works for a variety of different cationic polyelectrolytes, thus demonstrating the generalized process. The process has been found to work with virgin fiber, paper mill sludge, and corn starch. Thus, the effect of the cationic polyelectrolyte is non-specific in that it can boost the performance of completely different systems.

CHAPTER 1

INTRODUCTION

Over the past 60 years, there has been an increasing interest in utilizing renewable biomass resources as feedstock for the chemical industry and for biofuels. Thermochemical technology is being developed to produce bio-oils, which could be integrated into the oil economy. Other research is developing bioethanol from first generation corn ethanol and second generation ethanol from cellulose. Improving the saccharification of plant biomass has been one of the areas of research. Through chemical and enzymatic technologies various strategies have been developed. Many chemical techniques produce undesirable byproducts that are inhibitory to downstream processes (Weil et al., 2002; Soderstrom et al., 2003; Gray et al., 2006).

With the invention of the kraft process in 1879 and its first use in 1890 (Biermann, 1993), the pulp and paper industry has been a leader in the processing of lignocellulose biomass for over a century. Pulping technology has provided strategies that researchers continue to study for better biomass processing. The paper industry also uses various chemical additives for strength and retention. Flocculants, commonly cationic polyelectrolytes, are utilized to retain cellulose fines and filler materials.

This thesis aims to introduce a new method for the saccharification of cellulosic fiber. Cationic polyelectrolyte flocculants have been found to act as accelerants for the enzymatic hydrolysis of biomass. From the results of this project, a mechanism to explain how the cationic polyelectrolyte enhances enzymatic hydrolysis will be proposed. Chapter 2 reviews the literature on aspects of biomass, hydrolytic enzymes, flocculants, polymer conformation and its measurement, and current methods for hydrolyzing

biomass. Chapter 3 outlines the objectives of this research project. Chapter 4 outlines the experimental techniques and procedures used to complete this research. Following this, the results of this project are discussed. Chapter 5 reports the findings on enzyme-polyelectrolyte interactions and complexing. This leads into sections reporting findings on enzyme and polyelectrolyte adsorption onto cellulose. A section reporting kinetic results demonstrating the use of the cationic polyelectrolyte accelerant is then given. A mechanism is proposed from the results. Chapter 6 provides a few suggestions on future work and discusses briefly industrial application of the thesis work.

CHAPTER 2

BACKGROUND AND LITERATURE REVIEW

2.1 Introduction

The literature review begins by discussing lignocellulose biomass and the enzymes needed to break down the material. A brief discussion regarding pulping and bleaching technology is reviewed, explaining established methods for freeing cellulosic fibers from biomass. The review continues to discuss advances in biofuels production such as biomass pretreatment, saccharification, and fermentation processes. The literature review finishes by discussing flocculants and their traditional uses.

2.2 Lignocellulose Biomass

Agriculture and forestry derived lignocellulose biomass is a plentiful and diverse natural renewable resource and is the major constituent of most plant life. Abundant usable lignocellulose biomass includes both herbaceous and woody crops. Examples of herbaceous (non-woody) crops include switchgrass, wheat straw, and corn stover. Examples of woody crops include both coniferous (softwood) trees and deciduous (hardwood) trees. Common examples of softwoods include redwood, pine, and Douglas fir, while common examples of hardwoods include maple, oak, elm, and aspen.

Lignocellulose biomass is composed of a complex structuring of cellulose, hemicellulose, lignin, extractives, proteins, inorganics, and silicon dioxide. The term holocellulose is

used to describe the total carbohydrate (cellulose + hemicellulose) content of fibers. The main components of the woody and non-woody feedstocks consist mainly of cellulose, hemicellulose, and lignin. Table 2.1 shows a summary of woody and non-woody chemical compositions (Stenius and Pakarine, 1999).

Table 2.1. Typical chemical compositions of woody and non-woody feedstocks.

Component	Woody Feedstock	Non-Woody Feedstock
Holocellulose	65%-80%	50%-80%
Cellulose	40%-45%	30%-45%
Hemicellulose	25%-35%	20%-35%
Lignin	20%-30%	10%-25%
Extractives	2%-5%	5%-15%
Proteins	<0.5%	5%-10%
Inorganics	0.1%-1%	0.5%-10%
Silicon Dioxide	<0.1%	0.5%-7%
Note: % of the feedstock dry solids basis		

Woody feedstocks are by far the most abundant sources of cellulose fibers and the greatest source utilized in North America. Since the 1950s, improvement has been made to increase the yield development in southern pine (softwood) plantations in the United States (Wann and Rakestraw, 1998). Using intensive culturing, Union Camp Corporation reported crop yield of about 12 wet tons per acre per year produced in their forest plantations with half of the mass coming from water. In comparison De La Torre et al. (2000) reported that hybrid popular (hardwood) grown in the Southeast produce approximately 4.5 dry tons/acre/year.

The composition of lignin in softwoods is normally greater than it is in hardwoods, whereas hardwood contains more hemicellulose than do softwoods. The greater amount of lignin found in softwood makes it more of a challenge to pulp than hardwood. The average compositions of softwoods and hardwoods are reported in Figure 2.1.

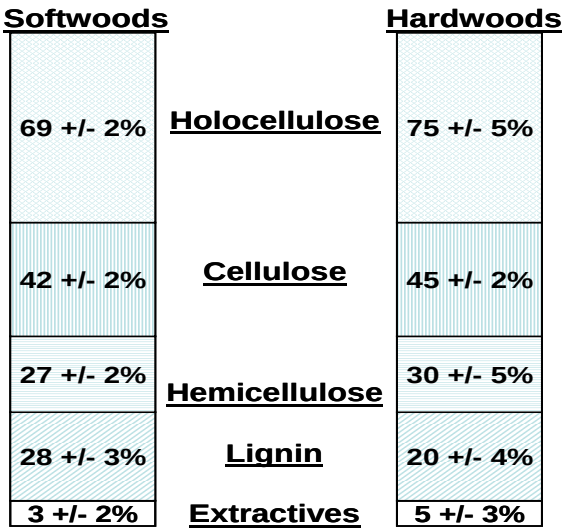

Figure 2.1. Comparison between the principal components of softwood and hardwood (Smook, 1982).

Through pulping processes, pulped fibers can be extracted from almost any vascular plant found in nature (Smook, 1982). Because of differences in the lignin composition, softwoods and hardwoods are pulped separately. Depending on the desired structural properties, these fibers can then be processed for the manufacturing of a multitude of pulp-derived products.

2.2.1 Cellulose

Cellulose is the major polysaccharide constituent found in lignocellulose biomass. The chemical formula for cellulose is $(C_6H_{10}O_5)_n$, where n is the number of repeating sugar units or the degree of polymerization (DP). The recurring structural unit of cellulose is composed of two consecutive glucose anhydride units, known as a cellobiose unit. Native cellulose (in situ) has a degree of polymerization of 3500 to 10,000 whereas commercial wood pulp DPs range from 600 to 1,500 (Smook, 1982; Lee, 1981). The linkage consists completely of D-glucopyranose monomers linked via β-1,4 glycosidic bonds, creating long-chain polymers referred to as elemental fibrils (Gray et al., 2006; Kontturi, 2005). Bundles of elemental fibrils form larger microfibrils. Microfibrils are made up of glucose chains consisting of DPs of approximately 250. As a consequence of how cellulose is synthesized into extended chains, cellulose molecules fit snugly together over long segments, giving rise to powerful associative forces, e.g. van der Waals forces and hydrogen bonds that are responsible for the great strength of cellulosic materials (Vries and Visser, 2001). Bundles of microfibrils make up cellulose fibers found in two main ordered states of orientation, (1) amorphous and (2) crystalline, where the majority of the cellulose present is in a highly crystalline form (Wyman, 1996). In general, 70% of native cellulose is comprised of the crystalline form, where a unit crystal is comprised of four tightly connected glucose residues (Lee, 1981). Thus, crystalline cellulose is resistant to degradation as enzymes and other biological compounds are too large to access the linkages needed for breakage (Gray et al., 2006). By contrast, the relatively more amorphous form is readily penetrated by solvents and reagents and is more susceptible to hydrolysis reactions (Garcia-Conesa et al., 1999). Long-chain cellulose is

known as alpha-cellulose. A shorter cellulose chain where the DP is between 15 and 90 is called beta-cellulose. When the DP is less than 15 the cellulose chain is referred to as gamma-cellulose (Smook, 1982).

Woody cellulose pulped fibers have different fiber characteristics depending on whether they are hardwood or softwood. Table 2.2 summarizes average fiber length, diameters, and wood density for various common hardwoods and softwoods found in North America. Softwoods normally have longer average fibers lengths and longer fiber diameters.

Table 2.2. Properties of North American pulp-woods (Smook, 1982).

Wood Species	Fiber length (mm)	Fiber Diameter (μm)	Wood Density (lbs.cu. ft)
Softwood			
Black Spruce	3.5	25-30	30
Douglas fir	3.9	35-45	34
Redwood	6.1	50-65	25
Southern Pine	4.6	35-45	36
Hardwood			
Aspen	1.04	10-27	27
Oaks	1.4	14-22	46
Birch	1.85	20-36	38

2.2.2 Hemicellulose

Hemicellulose provides bonding between cellulose fibers through hydrogen bonding and direct linkages. In contrast to cellulose, which is constructed exclusively from glucose, hemicelluloses are complex, amorphous, carbohydrate-based polymers made up of various six carbon sugars (hexoses) and five carbon sugars (pentoses); the DPs range from 100 to 200.

During chemical or enzymatic treatment of lignocellulose biomass, the hemicellulose structure changes dramatically. Owing to its loose amorphous structure, it is more easily degraded and dissolved as compared to cellulose, which is both crystalline and amorphous. There are generally two different forms of hemicellulose, heteropolysaccharides based on either xylans or galactoglucomannans (Palonen, 2004; Perez et al., 2002).

The principal form of a hemicellulose polymer found in softwoods is galacto-glucomannan, which consists of a backbone made of β-D-manno-pyranose and β-D-glucopyranose linked together by a β-1,4 linkage with β-D-galactopyranose side branches. There are two forms of galactoglucomannan that have been identified and subdivided, water-soluble (acetyl containing) and water-insoluble (acetyl lacking). Other biomasses have even more diverse forms (Vries and Visser, 2001; Wyman, 1996).

The principal forms of hemicellulose polymers found in hardwoods are various xylan-based polymers. Xylan structures can vary greatly in the cell well of plants, depending on their origin with a universal backbone of β-1,4-linked D-xylose monomers. The

greatest difference in the forms of xylan comes from the distribution of the types of side branches. Both softwoods and hardwoods contain building block units such as D-xylose, D-mannose, D-galactose, D-glucose, L-arabinose, 4-O-methyl-glucuronic acid, acetyl and feruloyl groups, D-galacturonic acid, and D-glucuronic acid. Different types of plants each contain their own diversity and types of hemicellulose (Vries and Visser, 2001; Wyman, 1996).

2.2.3 Lignin

Lignin is a complex, amorphous, highly polymerized and cross-linked phenolic macromolecule. It is present in the middle lamella. The lignin cements the fibers together providing thermoplasticity and a hydrophobic barrier. The structure of lignin consists primarily of phenyl propane monomer units, referred to as monolignols, linked together in three dimensions. There are three main phenyl propane monomers: p-hydroxyphenyl monomer units (H) derived from the precursor trans-p-coumaryl alcohol, guaiacyl monomer units (G) derived from the precursor trans-coniferyl alcohol (also referred to as guaiacyl propanol), and syringyl monomer units (S) derived from trans-sinapyl alcohol (Perez et al., 2002).

Softwoods contain guaiacyl lignin, which is made up primarily of coniferyl alcohol. Hardwoods contain guaiacyl-syringyl lignin, which is primarily both coniferyl alcohol and sinapyl alcohol. Different plants have varying monolignol ratios and, therefore, varying structures. For example, lignin from softwoods such as pine have a monolignol ratio G:S:H of 86:2:13 (Palonen, 2004).

2.2.4 Extractives

In addition to holocellulose and lignin, a number of diverse substances may be present in native fibers depending on their plant source, e.g. resin acids, fatty acids, terpenoid compounds, and alcohols. Extractives make up a group of chemicals that provide fungal and insect resistance and affect the permeability and physical properties of lignocellulose biomass. Most of these substances are soluble in water or neutral organic solvents and are collectively called extractives (Smook, 1982). The Southern pines have a high extractive content, which provides substantial amount of raw tall oil, e.g. rosins, fatty acids, abietic acid, and turpentine as byproducts from alkaline pulping operations.

2.3 Pulping and Bleaching Processes to Create Bleached Kraft Pulp

The kraft process involves cooking wood chips in a solution of sodium hydroxide and sodium thiol. Typical cooking times are from 2 to 4 hours, a liquid pH of ~13, and a cooking temperature in the range of 170 to 180^{o}C (Smook, 1982). Following cooking, pulping chemicals are washed off the pulped fibers and they are sent to be bleached.

Bleaching is performed to further remove lignin from the pulp and brighten the pulp. The bleaching process is carried out in order to further remove lignin in a step-wise sequential order that utilizes such chemicals as chlorine dioxide and sodium hydroxide. The result is a bleached kraft pulp very low in lignin content and rich in cellulose fiber.

2.4. Cellulose Degrading Enzymes

Cellulases are a group of enzymes that synergistically hydrolyze cellulose into its constituents, monosaccharide (glucose) and disaccharide (cellobiose), as was observed in a study where cellulosic fabric was degraded by cellulases (Mandels and Reese, 1964). Early studies identified the individual enzyme components of the cellulase system and observed the individual action of these purified components on cellulose (Wood, 1968). These components have since been named endoglucanases, exoglucanases, and ß-glucosidases. These enzymes, along with hemicellulases and lignin degrading enzymes, work synergistically to break down lignocellulose biomass (Vries and Visser, 2001; Kirk and Jeffries, 1996). They are normally found in fungi and bacteria; hemicellulase and lignin degrading enzymes will not be further expanded on. Two of the most commonly used fungal systems used to produce lignocellulose degrading enzymes are *Phanerochaete chrysosporium* and *Trichoderma species* (Palonen, 2004; Kersten and Cullen, 2004; Keating et al., 2006). In addition, among all the cellulase-producing microorganisms, the soft rot fungus *T. reesei* and its mutants are acknowledged to be the leading strain for the industrial production of cellulases. This is due to its complete composition of cellulase complex, high productivity and stability during the saccharification process (Kadam and McMillan, 2003).

Cellulases are categorized into three major groups: endoglucanases, exoglucanases, and ß-glucosidases. Endoglucanase, EG (EC 3.2.1.4), hydrolyzes internal bonds of 1,4-ß-D-glucosidic linkages in cellulose chains to disrupt the crystalline structure of cellulose, and to expose individual cellulose chains by creating new cellulose chain ends. Next, the

exoglucanases, known as 1,4-ß-D-glucan cellobiohydrolases, CBH (EC 3.2.1.91), cleave 2-4 units from the ends of the exposed chain ends resulting in tetrasaccharides or disaccharides such as cellobiose (Barr et al., 1996). There are two main types of cellobiohydrolases, one type proceeding from the reducing end, and the other type proceeding from the non-reducing end of cellulose. The enzyme at the reducing end is known as cellobiohydrolase I (CBH I) and the non-reducing end is cellobiohydrolase II (CBH II) (Palonen, 2004; Barr et al., 1996).

The reducing end of a cellulose chain contains a free hemiacetal, or aldehyde group at the C-1 atom, while the non-reducing end contains a free hydroxyl group at the C-4 atom. The defining part of an acetal is the central carbon atom which becomes the carbon atom in the carbonyl C=O. This carbon atom is the anomeric carbon or the anomeric center. The end where there is a C-1 carbon atom that is not involved in a glycosidic bond is called the reducing end, while the other end, where the C-1 carbon atom which is involved in a glycosidic bond, is called the non-reducing end. An illustration of this is provided in Figure 2.2.

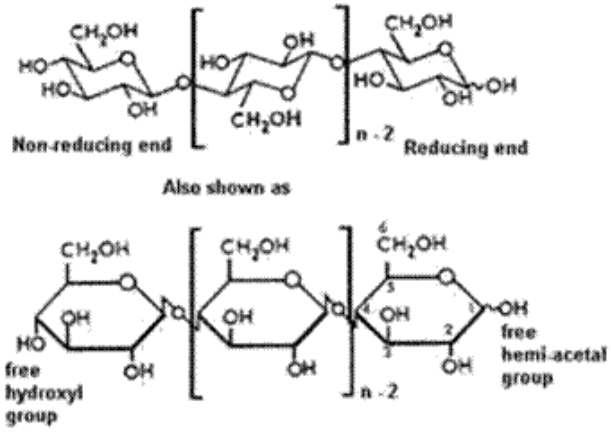

Figure 2.2. Illustration of a cellulose strand.

The last type of cellulase is known as ß-glucosidase, also referred to as cellobiase, βG (EC 3.2.1.21) which creates glucose by cleaving the cellobiose disaccharide. The overall synergistic relationship between the different cellulosic enzymes is illustrated in Figure 2.3. Table 2.3 also summarizes bioinformatic information on each cellulase.

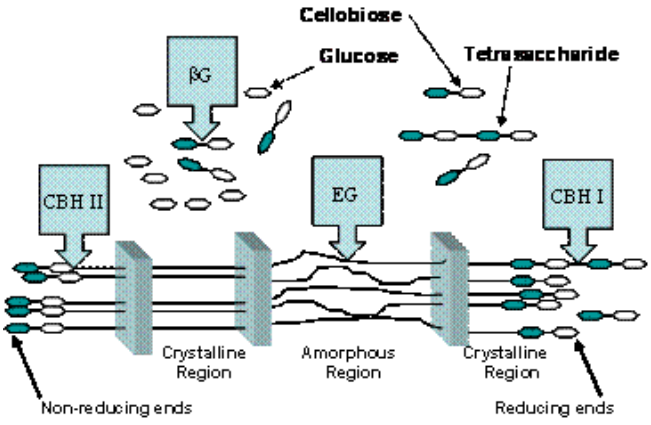

Figure 2.3. Illustration of the major hydrolytic enzymes for cellulose degradation. Cellulase designations: Endoglucanase (EG), Exoglucanase (CBH I and CBH II), and β-Glucosidase (βG).

Table 2.3. Bioinformatic properties of *T. Reesei* cellulases (NCBI, 2010).

E.C. No.	Name	MW (kDa)	Genes	No. of Residues
3.2.1.4	Endo-1,4-β-glucanase	48, 50-55, 25, 23, 55	Cel5A, Cel7B, Cel12A, Cel45A, Cel61A	397, 437, 218, 225, 344
3.2.1.91	1,4-β-cellobiohydrolase (CBH I)	59-68	Cel7A	497
3.2.1.91	1,4-β-cellobiohydrolase (CBH II)	50-58	Cel6A	447
3.2.1.21	β-Beta-1,4-D-glucosidase	114, 75	Cel1A, Cel3A	700, 713

2.4.1 Hydrolysis Kinetics

Kinetic models of cellulose hydrolysis have been developed and are based on oligosaccharide and sugar analysis through methods using dinitrosalicylic acid (DNS), total organic carbon (TOC), differential refractive index, and high performance liquid chromatography (HPLC) (Lee, M. et al., 2007). Additionally, kinetic models have been generated evaluating surface properties of softwood and hardwood chemical pulp fibers (Hilden et al., 2005). Jeoh et al. (2010) investigated how pretreatment of cellulosic biomass limits cellulase digestibility because of cellulose accessibility. Those pretreatment schemes that rendered the cellulosic biomass more digestible reduced the crystallinity of the cellulose and increased the accessible surface area of the fiber in biomass cell walls. Romani et al. (2007) reported on the saccharification of cellulosic biosludge from a water treatment plant of a kraft pulp mill. The results demonstrated how mill sludge solid residue, which shows high enzymatic digestibility, does not require pretreatment for saccharification. Fan et al. (2004) attempted converting bleached kraft paper mill sludge to ethanol in a semicontinuous solids-fed reactor. The results attempt

to partially address issues associated with near-term commercial applications of technology for producing cellulosic ethanol from sludge.

Cellulase adsorption to cellulosic fiber is also important to the reaction kinetics (Medve et al., 1994; Banka and Mishra, 2002). Wu and Ju (1998) reported on how nonionic surfactants affect the enzymatic hydrolysis of waste newsprint. Partial irreversible adsorption of cellulase on cellulose has been proposed as a reason for enzyme deactivation. Surfactant addition has been shown to minimize irreversible binding, which is proposed to explain increases in enzymatic hydrolysis. Methods adaptable for measuring adsorption onto cellulose include X-ray photoelectron spectroscopy (XPS), ellipsometry, quartz crystal microbalance (QCM), and polyelectrolyte charge titration.

In addition to adsorption phenomena, studies have also been reported on the immobilization of hydrolytic enzymes. The benefits of immobilizing may potentially include improved thermal stability, storage stability, operational stability, or improve recovery. For example, Ho et al. (2008) constructed core-shell nanoenzyme particles consisting of polymethylmethacrylate (PMMA) cores and cellulase shells where the particle size was about 100 nm. The immobilized cellulase showed a broader working pH range and better thermal stability. In an associated study, Arica et al. (2000) immobilized hydrolytic enzymes onto a spacer-arm attached to magnetic PMMA/ microspheres. Operational, thermal, and storage stabilities were found to be increased with immobilization. Tethering the hydrolytic enzymes to the surface of PMMA microspheres (the inert substrate) resulted in better overall temperature stability.

2.4.2 Cellulase Inhibition

The accumulation of cellobiose during cellulose hydrolysis is known to inhibit the enzyme activities of both endo and exo-glucanases by reversibly binding to the enzymes to form inhibited enzyme complexes (Berghen et al., 1975; Holtzapple et al., 1984). By inhibiting the endo and exo-glucanase, the hydrolysis rate and sugar yields are reduced (Maguire, 1977; Sternberg et al., 1977). It has also been discovered that β-glucosidase is inhibited by glucose (Gong et al., 1977). Therefore, glucose indirectly inhibits endo- and exo-glucanases by its inhibition of cellobiose reduction. This situation is illustrated by the following figure (Sun, 2002).

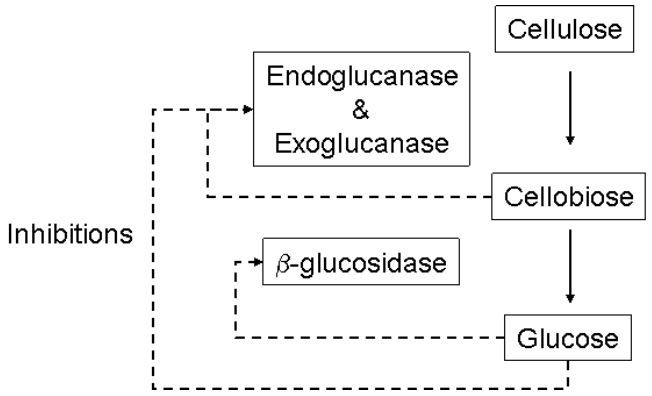

Figure 2.4. Product inhibition of cellulose through cellulase. The solid lines represent reactions and the dashed lines represent product inhibitions.

Although many commercial cellulase preparations are synthesized from *Trichoderma reesei*, it has been reported that *T. reesei* produces an insufficient amount of β-glucosidase (Woodward, 1982; Ryu and Mandels, 1980; Tangnu et al., 1981). However, it has been found that *Aspergillus* produces large quantities of β-glucosidase, and the addition of *Aspergillus* β-glucosidase to the *Trichoderma* cellulases greatly improved the

glucose yield (Duff et al., 1985; Duff et al., 1987; Spindler et al., 1989; Stockton et al., 1991). The supplementation of β-glucosidase, within certain ranges, will result in enhanced glucose yield, but will also add to the cost of the enzymes.

2.5 Hemicellulose Degrading Enzymes

The backbone of softwoods is made of mostly galactoglucomannans. Owing to the large number of sugars and linkages in the fibers, many enzymes are needed for the breakdown of the biomass. Galactoglucomannan is degraded by a number of enzymes that are categorized into three main groups: endo-acting enzymes, exo-acting enzymes, and accessory enzymes (Wyman, 1996). For endo-acting enzymes, endomannase (EC 3.2.1.78) hydrolyzes random 1,4-β-D-mannosidic linkages in glucomannans, galactomannans, and mannans.

2.6 Lignin Degrading Enzymes

Delignification by oxidative enzymes carries out a significant function in the degradation of lignocellulosic biomass. Currently, there are two main families of extracellular oxidative enzymes, derived from white-rot basidiomycetes that break down lignin: laccases (EC 1.10.3.2) and peroxidases (Bonnarme and Jeffries, 1990). Two types of peroxidase exist, lignin peroxidases, LiP (EC 1.11.1.14) and manganese-dependent peroxidases, MnP (EC 1.11.1.13).

Laccase, an enzyme isolated from white rot fungi, can oxidize phenolic compounds, but is relatively ineffective against lignin. Both the laccase enzyme and lignin are large

molecules and the two moieties do not line up well for the oxidation to proceed. Lignin oxidation can occur in the presence of a substrate mediator. Laccase oxidizes lignin, and in the process reduces O_2 to H_2O. The process begins with oxygen being consumed by laccase to form an oxidized "activated" form of laccase as shown in the following figure.

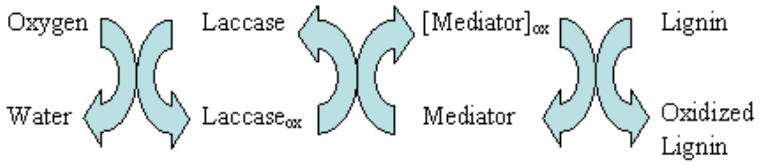

Figure 2.5. Illustration of the mediated oxidation of lignin by Laccase.

This oxidized laccase form oxidizes the mediator and reverts back to its resting state. Through the mediator, the laccase oxidizes lignin. The most effective laccase mediators usually consist of N-OH functional groups. Examples of such mediator include 1-hydroxybenzotrizole (HBT), N-hydroxy-N-phenylacetamide (NHA), violuric acid (VIO), 2-nitroso-1-naphtol-4-sulfonic acid (HNNS) and 2,2'-azino-bis(3-ethylbenzothiazoline-6-sulfonic acid (ABTS). Laccases generate phenoxy radicals from the phenol units of lignin.

2.7 Biofuel Technology

Biofuels are a wide range of fuels derived from biomass. This has led to different efforts for developing different types of biofuels. The released sugars are either fermented or run through simultaneous saccharification and fermentation (SSF). The above technologies and processes have mainly been applied to first and second generation biofuels.

First generation biofuels are made from sugar, starch, vegetable oil, or animal fats using conventional technology. The basic feedstocks for producing these biofuels are often grains and seeds, which are pressed to yield vegetable oil that can be used in biodiesel; animal fats can be also used to make biodiesel. Starches can be mechanically ground and saccharified, and the resulting sugars fermented into ethanol. Second generation biofuels focus on using non-food crops (Gomez et al., 2008). These include biomass waste, corn stover, wheat stalks, and woody biomass. The most popular example of a second generation biofuel is cellulose derived ethanol; however, processes are being developed to produce biohydrogen, biomethanol, 2,5-dimethylfuran and bio-dimethyl ether, biohydrogen diesel, mixed alcohols, and wood diesel.

2.7.1 Biomass Pretreatments

First generation biofuels have had some commercial success. Second generation biofuels have yet to go commercial and have technological hurdles to overcome. The bottleneck for lignocellulose-based biofuels is the pretreatment of the biomass required to improve the polysaccharide accessibility. Pretreatments may include using some combination of mechanical, chemical, or enzymatic pretreatment. Initial treatment of biomass by dry grinding, wet milling, or mechanical refining can be a necessary first step to reduce material and increase accessible surface area for further chemical and enzymatic treatment (Brethauer and Wyman, 2010; Smook, 1982). Chemical treatment is a vital part in the bioconversion of lignocellulosic biomass. Several methods have been tested; their standard conditions are summarized in Table 2.4 (Mosier et al., 2005; Wyman et al., 2005).

Table 2.4. Technologies and reaction conditions for biomass pretreatment.

Pretreatment Technology	Chemicals used	Temp. (°C)	Pressure (atm)	Reaction time (min)	Solids (wt.%)	Increase accessible surface area	Removes hemi-cellulose	Removes lignin / alter structure
Dilute sulfuric acid	0.5%-3.0% sulfuric acid	130-200	3-15	2-30	10-40	M	M	m / M
Ammonia fiber explosion (AFEX)	100% (1:1) anhydrous ammonia	70-90	15-20	<5	60-90	M	m	m / M
Ammonia Recycle Percolatin (ARP)	10-15 wt. % ammonia	150-170	9-17	10-20	15-30	M	m	m / M
Lime	0.05-0.15 g Ca(OH)2 / g biomass	70-130	1-6	1-6 h	5-20	M	m	M / M
Lime + air	0.05-0.15 g Ca(OH)2 / g biomass	25-60	1	1 week – 2 months	10-20	M	m	M / M
Major effect: M, Minor effect: m, Not determined: ND								

Dilute sulfuric acid treatments have been found to effectively remove and recover the majority of hemicellulose as dissolved sugars, up to 90% yields, while disrupting the lignin enough to increase the cellulose susceptibility to enzyme attack. Glucose yields approach 100% for complete hemicellulose hydrolysis. However, dilute acid pretreatments have a downside of costly materials, neutralization and conditioning of the hydrolysate prior to the biological steps, and competitive binding of cellulose hydrolyzing enzymes to lignin (Wyman, 1996). Dilute sulfuric acid pretreatment also increases accessible surface area for enzymes by removing hemicelluloses and modifying the lignin structure. All methods had major effects for altering lignin structure.

All of the above methods are based on either acid or alkaline technologies. Both acid and alkaline biomass treatments have harmful side effects on the biomass. Acidic processes have the greatest effect on both cellulose and hemicellulose fibers, as demonstrated by a

two-step dilute acid pretreatment (Soderstrom et al., 2003). Acidic pretreatments can break down pentoses, which can lead to dehydrogenation, where they lose three water molecules to become furfural. This is an inhibitory compound, a hindrance to the effectiveness of product recovery of carbohydrates. Alkaline methods, on the other hand, have the greatest effect on lignin degradation. They produce ferulate and acetate in the hydrolysate and leave both hemicellulose and cellulose relatively unbroken (Gray et al., 2006).

2.7.2 Saccharification and Fermentation

Ethanol produced from biomass sources such as agricultural and forestry residues, grasses, and wood is widely considered as a sustainable feedstock source for liquid transportation fuels. Brethauer and Wyman (2010) discussed in a recent review the state of hydrolysis and fermentation for ethanol production. Traditionally, biomass is broken-down into sugar, and in a separate step the sugars are fermented to ethanol. This has since been streamlined into a one-step process referred to as simultaneous saccharification and fermentation (SSF). Ethanol yields have been lower than desired because as glucan was consumed, lower than desired xylose consumption was observed in the one-step process. Mingjie et al. (2010) developed a two-step simultaneous saccharification and co-fermentation (SSCF) system, in which xylan was hydrolyzed and fermented first followed by the hydrolysis and fermentation of glucan. Two-step SSCF shows higher xylose consumption and higher overall ethanol yields. Other investigators have also been investigating the two-step SSF (Li et al., 2010). As an alternative approach, work has been reported where investigators are genetically engineering strains

of *saccharomyces cerevisiae* to effectively ferment mixed glucose-xylose substrates (Krahulec et al., 2010). Improvements continue to be made in pretreatment, hydrolysis, and fermentation of various biomass sources.

2.8 Flocculation

Figure 2.6 shows visually what effect a flocculant can have on a fiber suspension.

Figure 2.6. Effect of flocculant on fiber suspension. (left) fiber suspension and (right) fiber flocs formed and settling after flocculant addition.

In a related flocculation study, Hartley and Banerjee (2008) showed that the degree of flocculation increases with fiber length, with the best flocs being formed with mixtures of short and long fibers. Short fibers did not flocculate by themselves but were captured by flocs formed with longer fibers. The short fibers strengthen the floc and give it shear resistance.

2.9 Co-Polymers of Acrylamide Based Flocculants

A review of flocculants is provided because the focus of the thesis work is to explain a new application for flocculants. While acrylamide based flocculants are known for

acting as flocculants and retention aids, they may also serve as a binding aid that increases the rate at which hydrolytic enzymes can hydrolyze its corresponding substrate (Reye et al., 2009).

The largest use of acrylamide-based co-polymers is to flocculate or coagulate solids in a liquid. These processes are applied to wastewater treatment, and to processes in papermaking. Polyacrylamide (PAM) is synthesized with varying degree of substitution (DS); 0% being pure polyacrylamide and 50% being half substituted monomer positions. When the co-polymers produced contain electrolytic properties the co-polymers are polyelectrolytes. An example of a co-monomer used to synthesize acrylamide co-polymers is (acryloyloxy)ethyltrimethylammonium chloride. The addition of this monomer provides cationic moieties to the polymer chain creating a cationic polyelectrolyte. Example cationic polyelectrolytes are illustrated in the following figure (Griebel and Kulicke, 1992).

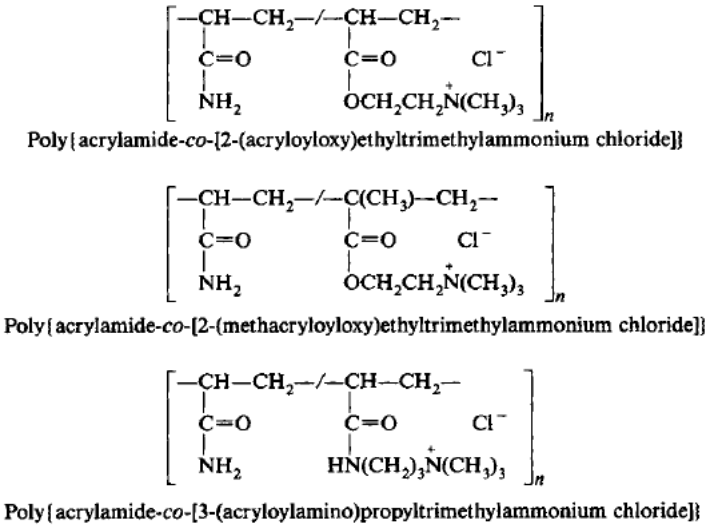

Figure 2.7. Sample structures of acrylamide based co-polymers.

The cationic moieties were investigated for stability. At pH ≥7.0 the cationic branch is hydrolyzed off a PAM chain. At pH between 8 and 10, the half-life for the hydrolysis of the cationic polyelectrolytes is in the range of 2-15 minutes (Kamiti et al., 1995). At pH 4.5, it was found that the cationic polyelectrolytes were stable and no change was observed within a day (Kamiti and van de Ven, 1995). These functionalized charge groups bond readily to negatively charged surfaces such as papermaking fibers. Hence, cationic polyacrylamides have been developed into a commonly used retention aid in the papermaking industry and as a flocculant in sludge dewatering (Nasser and James, 2006).

Two of the main flocculation mechanisms are patching and bridging mechanisms. Shorter polymers are more suited for patching while longer polymers are more suited for bridging. Figure 2.8(B) illustrates the bridging mechanism. The low-molecular-mass polymer (A) does not cause bridging flocculation, since it adsorbed conformation does not extend beyond the range of strong electrostatic forces of repulsion between the surfaces. The high-mass polymer (B) remains in an extended conformation long enough to allow attachment to two surfaces, even in the presence of net repulsive electrostatic forces between the surfaces.

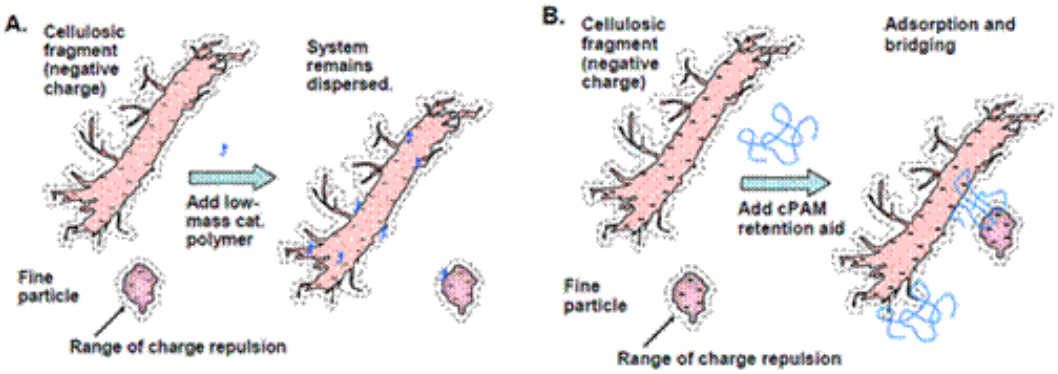

Figure 2.8. Polymer bridging of cellulose (Hubbe et al., 2009).

Typically, the charge patch mechanism occurs with using highly charged cationic polyelectrolytes having molecular masses ranging from approximately $1x10^5$ to $2x10^6$ g/mole. Lower relative molecular mass polymers may not allow bridging flocculation since the adsorbed conformation may not extend beyond the range of strong electrostatic forces of repulsion between the surfaces (Figure 2.8(A)); however, if electrostatic repulsive forces are low enough, patching may also occur. Bridging polyelectrolytes typically are high molecular weight, greater than $1x10^6$ g/mole and up to approximately $20x10^6$ g/mole (Eklund and Lindstrom, 1991; Neimo, 1999). The patching and bridging processes require the polyelectrolyte to have sufficient surface area and extend beyond the electrical double layer of the fiber or particle in order to allow particles to floc.

Charge at the surface of a particle affects the distribution of ions surrounding the interfacial region, resulting in an increased concentration of counter ions close to the surface. Thus, an electrical double layer exists around each particle. Figure 2.9 illustrates the double layer (Diffuse + Stern layers) for a particle with a negatively charged surface surrounded by an electrical double layer.

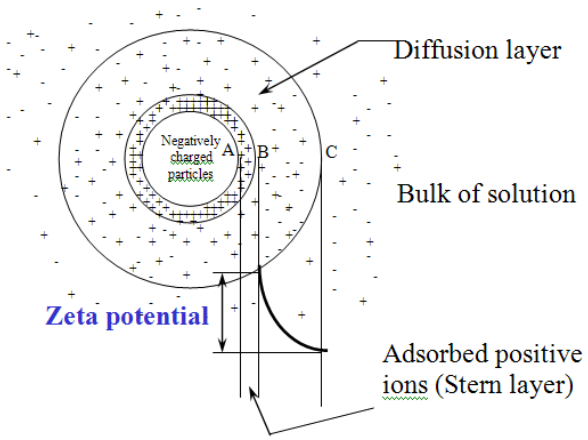

Figure 2.9. Schematic of the repulsive electric double layer comprised of the sum of the Diffusion and Stern layers (Chen, 2009).

The liquid layer surrounding the particle exists as two parts; an inner region (Stern layer) and an outer region (diffuse layer). In the Stern layer, ions are strongly bound with a net cationic or counter ion layer. Within the diffuse layer is a boundary within which the particle acts as a single entity. The electrostatic potential at the particle surface decreases through the Stern layer and along the diffuse layer and reaches zero charge at the outer boundary of the diffuse layer where the bulk of the solution is encountered. The diffuse layer, or at least part of it, can shift under changes in potential, which introduces a slipping plane that separates the mobile bulk fluid from the fluid that remains attached to the surface. The zeta potential is the electrical potential at this plane. The presence of the double layer can be overcome by patching and bridging processes, which require the polyelectrolyte to extend beyond the electrical double layer allowing flocculation to occur.

The adsorption of cationic polyelectrolytes has been visualized using transmission electron microscopy (TEM). Studies have reported that flocculants attached to cellulosic

surfaces can become extended because of flow past the surface (Nanko and Pan, 2003; McNeal et al., 2005; Nanko et al., 2006). TEM micrographs reported in Figure 2.10 show negatively charged gold nanoparticles used to visualize the positions of the polyelectrolyte strands of positively charged flocculants.

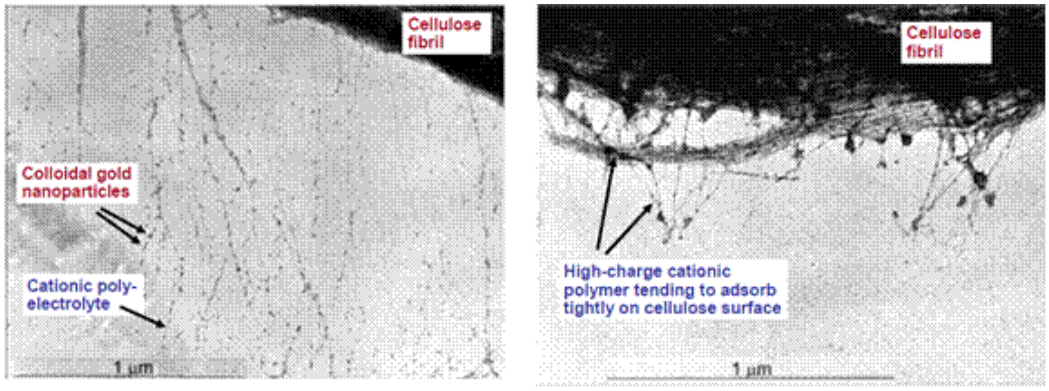

Figure 2.10. TEM images of cationic acrylamide co-polymers attached to cellulosic fibrils. (Left): High molecular-mass, low-charge density polyelectrolyte; (Right): High charge density cationic polyelectrolyte of similar molecular mass.

In the case of a high-charge density cationic polyelectrolyte, Figure 2.10(right) shows a more collapsed polyelectrolyte conformation. The more condensed conformation is consistent with a stronger interaction between the opposite charges of the dissolved polymer and the substrate. The stretched nature of Figure 2.10(left) shows extended linear shape of the polymer chains.

Nanko and Pan (2003) and McNeal et al. (2005) have imaged bridging (as summarized in the following figure). The left image shows clay particles bound by long polymer bridges; the right image illustrates clay particles held close to cellulosic fibril by polymer bridges.

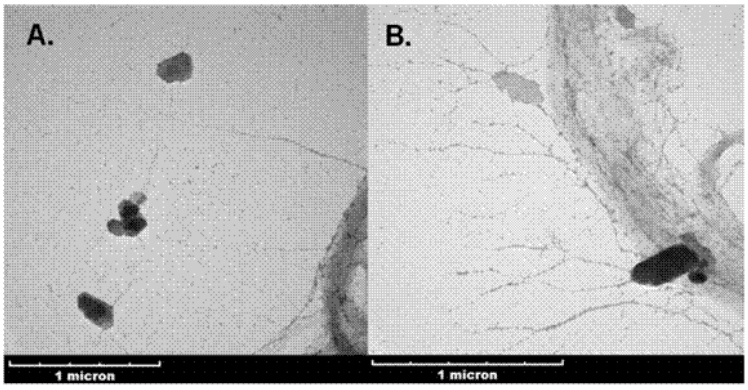

Figure 2.11. TEM micrograph showing cationic polyacrylamide bridges between cellulose fibrils and Kaolinite particles.

The authors suggest that the short bridge in micrograph B is a result from chaotic flow events, which matted the clay particle down onto a fiber. True patches would be more likely with shorter polyelectrolyte chains.

Polyelectrolyte adsorption on cellulose fiber using bridging and patching processes continues to be an area of study for the paper making industry (Wagberg and Odberg 1989; Odberg et al. 1993; Wagberg 2001; Hubbe et al. 2009). Theoretical treatment of flocculation describes polyelectrolyte adsorption by Flory-Huggins solution theory (Bohmer et al. 1990, Fleer et al. 1993, Flory 1941 and 1942, and Huggins 1941).

Commonly used papermaking retention aid systems include: (i) addition of a high-charge cationic polymer followed by the addition of a very-high molecular mass cationic polymer (e.g. c-PAM or PEI copolymers), (ii) a high-charge cationic polymer followed by the addition of a very-high-mass anionic polymer (usually a-PAM), or (iii) a very high-mass cationic polymer followed by the addition of an anionic microparticle (Hubbe, 2010). It has been reported in the literature for various applications that negatively

charged dissolved colloids form complexes with cationic polymers (Pelton et al. 1980; Wagberg et al. 1995; Swerin and Odberg, 1997; Nassman et al. 1998; Allen et al. 1996 Dunham 2000, 2002; Nurmi et al. 2003). A new application utilizing the complexing of negatively charged enzymes with a negatively charged active substrate will be introduced in the following thesis work. An enhanced binding of the enzymes with the active substrate will be shown to lead to improved biomass hydrolysis.

CHAPTER 3

THESIS OBJECTIVES

The goal of this research is to provide a new method for enhancing the rates of enzymatic hydrolysis and to propose the likely mechanism through which the process occurs. Experimental methods were used to directly determine cationic polyelectrolytes and cellulase interactions, how both adsorb to cellulose, and how the polyelectrolyte affects the enzymatic hydrolysis of cellulose. First, substrates, enzymes, and polyelectrolytes were characterized. Next, dynamic light scattering determined how varying conditions and polyelectrolyte properties influenced interactions with cellulase. Thirdly, an adsorption study investigated how cationic polyelectrolytes affect the adsorption of cellulase to cellulosic fiber. Lastly, with the help of kinetic experimental results a mechanism for the process was developed.

The specific objectives of this thesis were to:

1. Develop a new method for enhancing rates of enzymatic hydrolysis.
2. Determine how variations in polyelectrolyte properties affect interactions with cellulase.
3. Determine how adsorption of enzyme is affected by polyelectrolytes.
4. Determine how a polyelectrolyte affects enzyme hydrolysis.
5. Use the results to propose a mechanism for the rate enhancement.

CHAPTER 4

EXPERIMENTAL METHODS AND MATERIALS

4.1 Introduction

Chapter 4 describes experimental techniques and procedures used throughout the thesis work. This will include explanations of methods for characterization of enzymes, polyelectrolytes, substrates, and using techniques such as dynamic light scattering and atomic force microscopy to probe how these constituents interact together.

4.1.1 Method Development for Glucose Determination

The need to measure glucose has been important throughout many avenues of science. Such glucose determination methods include hydrometry, DNS, HPLC, refractometry, TOC, and enzyme assays. Hydrometry is a method of measuring the density of a solution. A hydrometer is placed into a measuring cylinder full of a sugar (e.g. glucose and fructose) solution and a density reading is taken from the hydrometer scale at the surface of the liquid (Baldy, 1997). A hydrometer can be used to measure the disappearance of sugar during a fermentation process. This method is still practiced in the alcoholic beverage industry. Hydrometry is a simple method with the drawback that it cannot discriminate between other components that will affect density; however, for sugar solutions produced by the saccharification of biomass, a hydrometer is an inexpensive and reliable method for monitoring sugar solutions. The dinitrosalicylic acid (DNS) method utilizes a reagent whose main component consists of 3,5 dinitrosalicylic acid (Miller, 1959). The DNS reagent has a high pH of approximately 13.0. This reagent

immediately stops the cellulase reaction. Upon boiling samples containing DNS reagent and reducing sugars, e.g. glucose, a colored reaction mixture is produced, where the degree of color-development correlates linearly to the amount of reducing sugars present. This method requires an incubation water bath, a boiling water bath, and an ice bath. Samples are analyzed with a UV-VIS spectrophotometer at 562 nm. Refractometry has been used throughout the fruit growing industries as a method for measuring the sugar content in fruit juices and is also suited as a method for measuring sugar concentration from the saccharification of biomass during biofuel production. As with hydrometry, refractometry is a measure of the density of a given sugar solution with units expressed in "degrees Brix"; 10 degrees Brix has 10 gram of sugar per 100 grams of solution.

D-glucose can be conveniently measured using commercially available assay kits based on colorimetric enzyme assay procedures. Two well-known assays are hexokinase/glucose-6-phosphate dehydrogenase (HK/G6P-DH) format and glucose oxidase/peroxidase (GOPOD) format assays (Kunst et al., 1988; Trinder, 1969; Blakeney and Matheson, 1984; McCleary and Codd, 1991). Megazyme International Ireland Ltd. supplied assay kits for such D-glucose analysis. In the first assay the hexokinase (HK) enzyme phosphorylates D-glucose with adenosine-5'-triphosphate (ATP) to form the products glucose-6-phosphate (G-6-P) and adenosine-5'-diiphosphate (ADP). In a second reaction, in the presence of G6P-DH, G-6-P is oxidized by nicotinamide-adenine dinucleotide phosphate (NADP+) to gluconate-6-phosphate and the reduced form of nicotinamide-adenine dinucleotide phosphate (NADPH). The amount of NADPH produced in this reaction system is stoichiometric with the amount of D-glucose reacted.

NADPH was measured by the increase in absorbance at 340 nm. An illustration of this reaction pathway is given in Figure 4.1.

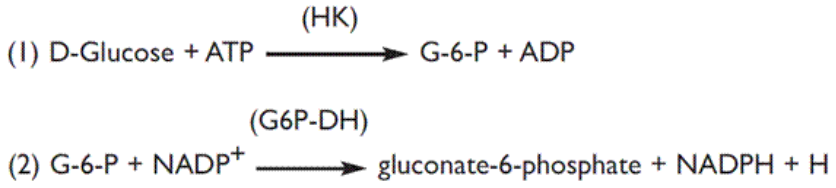

Figure 4.1. Reactions associated with (HK/G6P-DH) format assay.

In the second assay, the glucose oxidase (GO) enzyme oxidizes D-glucose in the presence of oxygen and water to produce D-gluconate and hydrogen peroxide. In a second reaction, in the presence of peroxidase (POD), two hydrogen peroxide molecules react with p-hydroxybenzoic acid and 4-aminoantipyrine to produce quinoneimine dye and water. The reaction is illustrated in Figure 4.2. The amount of quinoneimine dye produced in this reaction system was stoichiometric with the amount of D-glucose reacted. The quinoneimine dye was measured by the increase in absorbance at 510 nm.

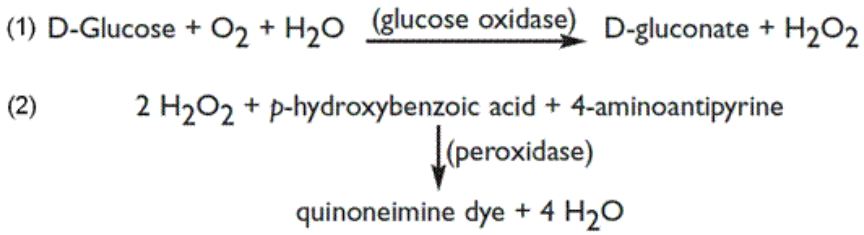

Figure 4.2. Reactions associated with (GOPOD) format assay.

It appears that use of either D-glucose (HK/G6P-DH) or D-glucose (GOPOD) formats would have been acceptable; however, most commercially available D-glucose kits are

based on GOPOD. Secondly, the price per assay was not similar between the two. The HK/G6P-DH format assay kit cost $315 per 220 assays per kit for a cost of $1.44 per assay. The assay takes approximately 5 minutes to complete and runs at room temperature. The GOPOD format assay kit cost $240 per 660 assays per kit for a cost of $0.37 per assay. The assay takes approximately 20 minutes to complete and is run at 50^{o}C. Therefore, based on the above information it was decided that the GOPOD format was more cost-effective.

4.1.2 D-Glucose Measurement Procedure

When running the Megazyme GOPOD format assay the following recommended assay parameters and conditions were used:

Table 4.1. Summary of D-glucose assay conditions.

Wavelength:	510 nm
Temperature:	40^{o}C - 50^{o}C
Light path:	1 cm
Read against:	Reagent Blank

Calibration standards were prepared by dilution over the range 0 – 1000 μg/mL using a standard certified 1.0 mg/mL glucose solution supplied by Megazyme. In performing the assay manually, 3.0 mL of GOPOD reagent was combined with 0.1 mL of sample solution containing D-glucose in an 8 mL screw cap tube, and incubated for 20 minutes at 50^{o}C. A linear calibration curve was constructed from the calibration standards. Unknown samples were diluted into the range of the calibration curve and glucose concentrations were estimated.

A calibration curve was prepared from the same standard certified 1.0 mg/mL glucose solution supplied by Megazyme. The measurement was automated with a DA 3500 discrete analyzer from OI Analytical. The DA 3500 prompts the user to input the concentration of a standard solution and to set a range of dilutions of that standard solution. The DA 3500 used 10x less GOPOD reagent and less sample than that required for the manual procedure. The incubation time and temperature were 20 minutes at 37^{o}C; it was verified during the application development that 37^{o}C was acceptable.

4.1.3 Testing Glucose Analysis for Interference

D-glucose solutions were prepared from dextrose corn sugar (Sigma G-8270) purchased from Sigma-Aldrich Co. St. Louis MO. The Megazyme GOPOD format D-glucose assay was tested for interference through use of spiked samples. Standard solutions of 1.0 mg/mL glucose were prepared in conjunction with spiked glucose solutions of 2.0, 5.0, and 10.0 mg/mL. Solutions of 100 mg/L and 1000 mg/L of a cationic polyelectrolyte (XP10035, 35% cationicity), supplied by Eka Chemicals, were prepared with ultrapurified water. It was important to give the polyelectrolyte enough time for dissolution, i.e. 2 hours. A magnetic stir bar / magnetic stir plate setup was used to mix the solution.

4.1.3.1 Test for Interference on the GOPOD-Format Assay

Glucose measurements were performed using the GOPOD format D-glucose assay kit. Earlier work was performed with this assay manually. A linear regression represented the calibration well, with the correlation coefficient for the linear regression being

0.9968. Later, the GOPOD format D-glucose assay was adapted to the DA 3500 analyzer.

To verify that the GOPOD format assay was free from polyelectrolyte interferences, tests were performed with various concentrations of an 80% cationicity (high cationicity) polyelectrolyte and 1.0 mg/ml D-glucose. The error between the known value and the measurement was less than 4% as summarized in Table 4.2. The percent error increased with increasing cationic polyelectrolyte. No significant deviation was detectable.

Table 4.2. Cationic polyelectrolyte interface test for D-glucose assay.

Polyelectrolyte (mg/L)	D-Glucose (mg/mL)	± D-Glucose (mg/mL)	% $Error_{true}$
0	0.993	0.002	0.7
100	0.984	0.018	1.6
1000	0.961	0.086	3.9

When the glucose assay was adapted to the DA 3500 analyzer a more formal interference analysis was performed with a 40% cationicity polyelectrolyte of high molecular weight with varying glucose, enzyme, and polyelectrolyte content. A 20% up/down interference test was done for D-glucose measurements; that is measuring at 20% and 80% of the full range not to be too close to zero or 100% of the full range. First, D-glucose solutions of 200, 800, and 1000 ppm were analyzed for their glucose content. Next, these solutions were spiked with some combination of enzyme and polymer. The results, reported in Table 4.3 show a maximum error of 6.4%.

Table 4.3. Summary for interference with GOPOD format assay.

Sample No.	Sample	Average Glucose Concentration (mg/L)	Standard Deviation of Glucose Concentration (mg/L)	% $E_{rel.}$	% E_{true}
1	Standard 1000 ppm	943	29	3.0	5.7
2	200 ppm glucose	207	3	1.2	3.6
3	800 ppm glucose	762	13	1.7	4.7
4	200 ppm glucose + 1 mg/mL cellulase (BLX)	192	3	1.3	4.0
5	800 ppm glucose + 1 mg/mL cellulase (BLX)	758	1	0.1	5.3
6	200 ppm glucose + 1000 ppm 40% cationicity	213	4	1.7	6.4
7	800 ppm glucose + 1000 ppm 40% cationicity	761	15	2.0	4.9
8	200 ppm glucose + 1 mg/mL cellulase (BLX) + 1000 ppm 40% cationicity	210	10	4.7	5.0
9	800 ppm glucose + 1 mg/mL cellulase (BLX) + 1000 ppm 40% cationicity	788	51	6.4	1.5

4.1.4 Method Development for Protein Analysis

The concentration of proteins in solution could be quantified using any of a number of total protein assays. Commonly used assays include the Bradford, Lowry, and BCA Protein Assay Methods (Bradford 1976; Lowry et al. 1951; Smith et al. 1985). Pierce Protein Research Products supplied assay kits used in this thesis work. Each used colorimetric detection for quantification of the amount of protein in solution. The Bradford protein assay was faster and easier to use than the BCA protein assay while the BCA protein assay was faster and easier than the Lowry protein assay. From comparing the three methods, the BCA method was compatible with many ionic and nonionic

detergents and reported less variation between different proteins, making the BCA method an overall good choice.

The BCA Protein Assay formulation is based on bicinchoninic acid (BCA) for the colorimetric detection and quantification of total protein in solution. This method combines the well-known reduction of Cu^{2+} to Cu^{+} by protein in an alkaline medium (the biuret reaction) with the highly sensitive and selective colorimetric detection of the cuprous cation (Cu^{+}) in the BCA containing working reagent. The assay is a two-part reaction where in the first reaction a cupric ion (Cu^{2+}), in the presence of peptide bonds, reacts with multiple amino acid residues to reduce the cupric ion to produce a cuprous ion (Cu^{+}). In the macromolecular structure of protein, the number of peptide bonds interacting with the cupric ion is reportedly responsible for color development with the BCA reagent (Wiechelman et al. 1988). Wiechelman et al. also reported that with di-, tri- and tetrapeptides it was more than the simple sum of individual color-producing functional groups that caused the extent of color development. In the second reaction chelation of two molecules of bicinchoninic acid with one cuprous ion forms a water-soluble, color-developing complex that exhibits a strong absorbance at 562 nm that is nearly linear with increasing protein concentrations over a broad working range (20-2000 mg/mL). The BCA assay was not a true end-point method in that the final color continued to develop. However, following incubation, the rate of continued color development was slow enough to allow a number of samples to be assayed together. Pierce Protein Research Products supplied the BCA™ Protein Assay Kits. Protein

concentrations were determined and reported with reference to standards of a common protein, bovine serum albumin (BSA), which was provided in the assay kit.

4.1.5 BCA Total Protein Assay Procedure

When running the BCA protein assay the following parameters and conditions were used:

Table 4.4. Summary of BCA assay conditions.

Wavelength:	562 nm
Temperature: Room temperature 37°C 60°C	Incubation time: 2 hours 30 minutes 30 minutes
Light path:	1 cm
Reference:	Reagent Blank

Calibration standards were prepared by dilution over the range 0 – 2000 μg/mL using a standard certified 2.0 mg/mL bovine serum albumin (BSA) solution supplied in the Pierce assay kit. The assay kit also comes with manufacturer prepared chemical reagents. In performing the assay 3.0 mL of working reagent (Reagent A: Reagent B; preparation ratio 50:1) was combined with 0.1 mL of sample solution containing protein in a 4.5 mL optical grade polystyrene cuvette. The cuvette was covered with Parafilm® and incubated for two hours at room temperature. A linear calibration curve was constructed from the calibration standards. Samples were diluted into the range of the calibration curve and total protein concentrations were estimated. Absorbance measurements were made directly with the assay cuvettes after incubation.

To automate the BCA method a calibration curve was prepared from the same standard certified 2.0 mg/mL BSA solution supplied by Pierce. The DA 3500 prompts the user to input the concentration of a standard solution and to then set a range of dilutions of the standard. The incubation time and temperature were 30 minutes at 37^{o}C, which is one of the incubation conditions suggested by the manufacturer.

4.2 NREL Cellulase Activity Assay

The National Renewable Energy Laboratory (NREL) released a method describing a procedure for measuring cellulase activity using International Union of Pure and Applied Chemistry (IUPAC) guidelines (Adney and Baker, 1996). The procedure is to measure cellulase activity in terms of "filter-paper units" (FPU) per milliliter of original (undiluted) enzyme solution. For quantitative results the enzyme preparations must be compared on the basis of significant and equal conversion. The method uses a value of 2.0 mg of reducing sugar as D-glucose from 50 mg of filter paper (4% conversion) in 60 minutes, which has been designated as the criterion for estimating filter paper cellulase activity units (FPU) by IUPAC.

The reducing sugar yield may not be a linear function of the amount of enzyme in the assay mixture (Ghose, 1987). It is not necessarily true that twice the amount of enzyme yields twice the reducing sugar in an equal amount of time. Therefore, the assay procedure focused on finding a dilution of the original enzyme stock such that a 0.5 mL aliquot enzymatically hydrolyzed 4% of the 50 mg filter paper in 60 minutes. This was accomplished by finding two dilutions that bracket the 4% conversion point so closely

that the required dilution could be obtained by interpolation. The dilution was then used to calculate the cellulase activity (in FPU/mL) of the original stock from the dilution required. FPU activity units were calculated by using the following equation 4.1:

$$\text{Filter Paper Activity} = \frac{0.37}{[enzyme]\ \text{releasing 2.0 mg glucose}}\ units/mL \qquad (4.1)$$

where [*enzyme*] is simply the proportion of original enzyme solution present in the directly tested enzyme dilution (the enzyme dilution of which 0.5 mL was added to the assay mixture).

4.2.1 Modified Cellulase Activity Assay Procedure

It became evident that a modification to the NREL procedure was necessary to make it compatible with the DA 3500 analyzer. The NREL procedure for filter paper activity from Adney and Baker (1996) detects the β-1-4 glycosidic bond cleavage of cellulose for three categories of experimental tubes: assay mixtures, blanks and controls, and glucose standards. The substrate was a 50 mg strip of Whatman No. 1 filter paper, approximately 1.0 x 6.0 cm in dimensions and 50 ± 0.4 mg in order to achieve less than 1% error. The piece of 50 mg filter paper was rolled and placed into a test tube. A 1.0 mL aliquot of buffer was added to the tube saturating the filter paper strip. Samples were then equilibrated in a 50^{o}C water bath. The assay began when 0.5 mL of enzyme dilution was added to a tube. The samples were incubated at 50^{o}C for exactly 60 min. When the incubation period was completed, the samples were removed from the water bath, placed into an ice bath, and the enzyme reactions stopped by immediate addition of 3.0 mL of 10% (w/v) trichloroacetic acid (TCA). Samples were left to settle or were filtered with a

0.2 μm GHP syringe filter and an aliquot of each analyzed with the GOPOD-format assay kit. The effect of TCA on the GOPOD assay was tested by running two calibrations, one with and the other without TCA. The calibration slopes differed by 2.5% relative error confirming that there was no significant difference in the calibration with or without addition of 3.0 mL 10 (w/v)% TCA solution as a stopping reagent. The recommended enzyme dilution range suggested in the NREL procedure was between 0.01 and 0.001 depending on the specific enzyme preparation being evaluated and the current age and condition of that preparation. The NREL procedure recommended determination of FPU activity from a graph of cellulase dilution vs. glucose concentration. Cellulase activity was reported in terms of "filter-paper units" (FPU) per milliliter of original undiluted enzyme solution and was calculated using equation 4.1. The FPU activity units of μmol $min^{-1}mL^{-1}$ appear similar to International Units per mL (IU per mL). Because the D-glucose release in the activity assay was non-linear with respect to time, the use of IU units is inappropriate; IU units are based on initial reaction velocities where the initial linear rate of reaction produces the same rate of product formation during each minute of the reaction (Ghose, 1987). Hence, FPU units were used to measure cellulase activity.

A number of different sources of cellulase were used, all of which were preparations from *Trichoderma reesei*, which is a mesophilic and filamentous fungus. A summary of these cellulases is shown in Table 4.5. Genencor and Novozymes were the major suppliers of hydrolytic enzymes. Early supplies were acquired as gifts from Georgia Pacific and Buckman Laboratories.

Table 4.5. Summary of activities for commercial cellulase preparations.

Commercial Cellulase Preparation	Filter Paper Activity (FPU/mL)	Total Charge Density (C/g)	Total Protein Concentration (mg/mL)
Pergalase 7547	54 ± 1	-7 ± 1	130 ± 1
Buckman Laboratories BLX – 13271	46 ± 2	-7 ± 1	117± 1
Optimase CX 40L	50 ± 2	-12 ± 1	119 ± 1
Novozym 22CG	165 ± 5	-7 ± 1	153 ± 1
Cellic Ctec	95 ± 4	-7 ± 1	155 ± 1
Cellic Ctec 2	119 ± 1	-	204 ± 3

4.2.2 Amylase Activity Assay Procedure

An amylase activity assay was adapted from the cellulase activity assay described previously in Section 4.2.1. Only two changes were made: (1) the 50 mg of filter paper were replaced with 50 mg raw cornstarch and (2) the cellulase enzyme stock was replaced with the amylase enzyme stock. As with cellulase activity assays, quantitative activity for commercial amylase preparations was compared based on equal conversion. The production of 2.0 mg of reducing sugar as D-glucose from 50 mg of cornstarch (4% conversion) in 60 minutes has been designated as the criterion for estimating cornstarch amylase activity units. This can be applied to both alpha-amylase and glucoamylase. The enzyme activity can then be reported as μmoles glucose equivalents released per minute averaged over 60 minutes per milliliter of original (undiluted) enzyme solution.

Buckman's Buzyme 2506 is a bacterial alpha-amylase produced by submerged fermentation of a select strain of *Bacillus amyloliquefaciens*. The systematic enzyme name is 1,4-alpha-D-glucan glucano-hydrolase. An amylase activity assay was created from the cellulase activity. The only difference between the cellulase activity assay and

the amylase modified assay is that 50 mg of Whatman #1 filter paper is replaced by 50 mg of raw cornstarch and instead of using dilutions of cellulase we used appropriate dilutions of amylase. The activity was reported as the number of μmoles glucose equivalents released in 60 min per mL enzyme solution, which follows the filter paper protocol. The alpha-amylase activity was measured to be 11.4 ± 1 μmoles glucose equivalents released in 60 min per mL enzyme solution (stock solution 20 ± 1 mg total protein per mL). The total charge density for the Buzyme 2506 was -35 C/g ± 10 C/g. The cellulase charge density averages less than half the charge density of the amylase.

4.3 Method for Charge Determination for Colloids and Polyelectrolytes

The surface charge density of particles and the amount of soluble charged species in colloidal and polyelectrolyte systems are significant in determining the state of particle aggregation and how various additives function to change properties of the solution or to simply stabilize the system. Generally speaking, particles with like charges stabilize a suspension because of the repulsion forces among them. The stable condition may be further enhanced by the addition of dispersants. Conversely, flocculant dosages will destabilize the suspension.

The surface charge is the electric charge present at an interface. In the case of colloids, polyelectrolytes, and similar heterogeneous fluid based systems, it is not possible to directly measure the surface charge due to the small sizes of the objects. Instead, the zeta potential measurements yield information for assessing surface charge. There are two general methods for determining the charge for colloidal and polymer systems (1)

electrokinetic titration and (2) charge titration. Electrokinetic titration is a method for measuring zeta potential, which is an intensive property of a bulk colloidal system. Charge titration, also referred to as colloidal titration, requires the need for appropriate surface-active chemical titrants. Charge titration can be used to evaluate polyelectrolyte adsorption and complexation. These are examples of extensive property measurements where the adsorption and complexation do not depend on system size. Traditional applications utilizing charge titration found in the paper industry include identifying the charge of solids, e.g. fibers and fillers, in the process waters as well as the widespread anionic and cationic trash levels found in the water supply.

When titrating for the cationic or anionic demand, either can be determined by direct or back titration. Examples of commonly used titrants, illustrated in Figure 4.3, include polydimethyl diallyl-ammonium chloride (PDADMAC), a cationic polyelectrolyte, and potassium poly (vinyl sulfate) (PVSK), a negative polyelectrolyte. Literature from the manufacturer states the average molecular weights of PDADMAC and PVSK to be 107,000 and 170,000 grams/mole respectively. BTG Americas, Inc., Norcross GA supplied 0.001 N titrant standard solutions in 1-liter bottles.

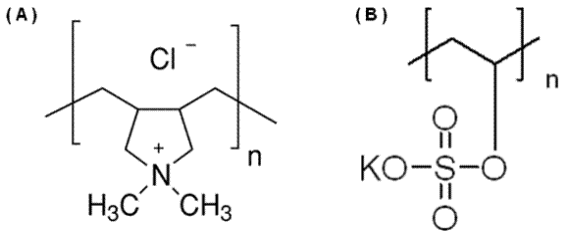

Figure 4.3. Polyelectrolytes used as titrants during charge titration. (A) Poly (diallyldimethylammonium chloride) (pDADMAC), positively charged polyelectrolyte and (B) potassium poly (vinyl sulfate) (PVSK), negatively charged polyelectrolyte.

The streaming current method is a common means for detecting the endpoint of a charge demand titration, which is measured using a Mutek Particle Charge Detector (PCD) 03. The main components of the particle charge detector consist of a cylindrical test cell with a fitted displacement piston. A schematic for a PCD detector standard test cell, holding approximately 10-30 mL capacity, is shown in the following figure.

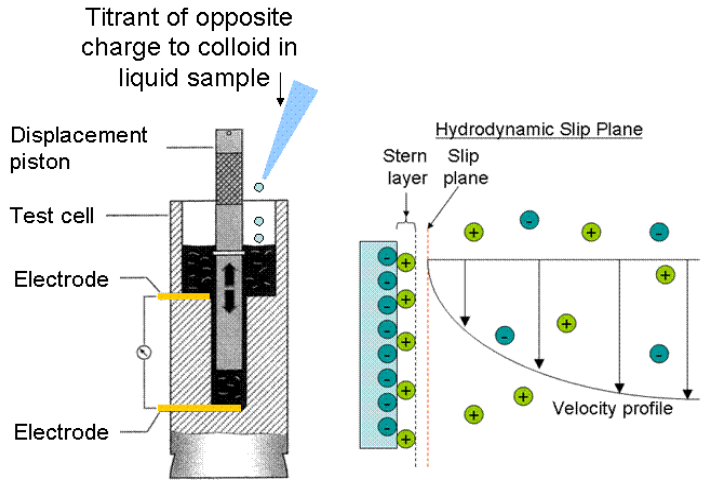

Figure 4.4. Schematics of a Mutek Particle Charge Detector Cell (left) and the hydrodynamic slip plane (right).

Under the action of van der Waal forces, the charged macromolecules are adsorbed at the surface of the test cell and the adjacent displacement piston. The oscillating piston (~ 4 sec^{-1}) forces the sample liquid to flow along the plastic wall of the test cell. Gold electrodes are positioned vertically at either end of the test cell. The flowing liquid, between the oscillating piston and the test cell wall, carries along any counter-ions opposite in charge to the adsorbed colloidal sample that lie outside the hydrodynamic slip plane at the plastic surface where the streaming current is induced. During an evaluation of colloidal charge of an aqueous sample, an oppositely charged titrant is added until the

potential goes past the zero point; the detector interpolates the zero point. In theory, the zero point condition occurs when neutral complexes between the titrant and components of the sample become less stable, begin to precipitate, and cover the probe surfaces.

By measuring the streaming current, the PCD provides for quantitative determination of the charges of polyelectrolytes and particles. The original charge amount is calculated from the consumption of the titrant of known concentration. Streaming potential is measured in mV and the specific charge amount is calculated and reported in units of (meq/g) or (C/g); the unit conversion is 1 meq/g = 96.5 C/g. The detection limit of an active substance in the PCD is approximately 1 ppm depending on sample specifications.

The particle charge detector (PCD) 03 is a Mutek brand system. Either the titrant can be added manually with a hand pipette or automatically; an automated Mutek PCD-Titrator is accompanied by the PCD. The total charge amount calculation is as follows:

$$Q = \frac{V \cdot c}{m} \cdot F \tag{4.2}$$

where, Q is the total charge amount (C/g; 96.5C/g = 1 meq/g), V is the consumption of titrant (L), c is the titrant concentration (mole/L, 0.001N), m is the amount of active substance in the sample (grams), and F is Faraday's constant (96,485 C/mole).
The total coulombic charge of an active material of either a positive or a negative charge can easily be measured.

4.3.1 Procedures for Charge Titration

Charge titration was performed on enzymes, polymers, and substrates using the Mutek Particle Charge Detector. If the active material being titrated was positively charged then the negatively charged PVSK titrant was used. Conversely, if the active substance being treated was negatively charged then the positively charged PDADMAC titrant was used. Commercial preparations of enzyme stock solutions were diluted to appropriate measureable levels (e.g. approximately $0.1\% \leq$ dilution $\leq 10\%$ (v/v)). The Mutek PCD cell was filled with 10 mL of ultra purified water. Various amounts of enzyme dilution were added to the cell. The piston was turned on and allowed to oscillate until a stable steaming potential was observed from the output display. Once stable, the sample was auto titrated and the particle charge detector interpolated the amount of titrant necessary to achieve zero millivolts. The data were then used to calculate the amount of charge associated with a given amount of active substance.

The same direct titration approach was applied to measuring other colloidal and polymer changes. The Mutek PCD cell was filled with 10 mL of ultra purified water. Various amounts of 100 mg/L polyelectrolyte solution were added to the cell, the piston was turned on, and once a stable streaming potential was reached the sample was autotitrated until a zero millivolt endpoint was reached.

In concept, suspensions of either starch or cellulosic fiber may be directly charge titrated; however, for concentrations able to run on the Mutek (max. 1000 mg/L) the starting streaming potential signal was not stable around zero, indicating that the active substance

was under the detection limit. Therefore, back titration was attempted with a low concentration and low cationicity polyelectrolyte (20 mg/L, XP10023L, 10% cationicity). Handsheets of varying weight or 5% to 10% (w/w) cornstarch were added to a 20 mL screw cap glass vial with 10 mL of the PDADMAC or XP10025L polyelectrolyte solution; samples were shaken and left to settle at room temperature for one hour. A sample was slowly pipetted out from the top of the supernatant so as not to disturb the settled solids. The supernatant contained cationic polyelectrolyte that did not adsorb to the fiber or starch, and was charge titrated with PVSK. The amount of titrant (PVSK) corresponded to the amount of PDADMAC or the XP10023L polyelectrolyte that did not adsorb to the active substrate, whereas 10 mL minus the amount of titrant corresponded to the amount of polyelectrolyte that did bind to the active substrate. The back titration gave an estimate of the total coulombic charge for bleached softwood kraft pulp and cornstarch.

4.4 Cellulosic Fiber and Starch Characterization

The morphology of cellulose fiber and starch granules was determined using light scattering techniques. The structural properties and changes in the structural properties of these plant materials play an important role in their enzymatic hydrolysis and degradation. The following two sections outline different techniques for characterizing cellulosic fibers and starch granules.

4.4.1 Cellulosic Fiber and Procedure

The TAPPI 271 standard, "Fiber Length of Pulp and Paper by Automated Optical Analyzer Using Polarized Light" is an automated testing method by which the numerical and weighted average fiber lengths and fiber length distributions of cellulosic fiber samples can be measured utilizing light polarizing optics in the range of 0.1 mm to 7.2 mm. First, the fibers are diluted in water and the fiber suspension is routed through a fiber orienting channel (F.O.C.) where the projected lengths of individual fibers are measured. The F.O.C. is placed between a light source and a photosensor matrix. The elements of the matrix indicate the length of the fiber from the projected image of the fiber. When the fiber reaches a certain point, it covers some of the diodes, and based on the number covered, the length of the fiber can be determined. On either side of the F.O.C. crossed polarizers are positioned to eliminate the effect of objects other than fibers, e.g., non-optically active fillers and air bubbles, which are not able to change the direction of polarization. Available to students at IPST is a fiber quality analyzer (FQA) sold by OpTest Equipment Inc. Ontario, Canada. The system is designed to meet the specifications of the TAPPI 271 Standard Method, and was the unit used for this research.

Three general types of cellulosic fiber were used throughout this study: bleached kraft softwood pulp, bleached kraft hardwood pulp, and Whatman grade 1 filter paper. Bleached softwood kraft pulp was procured from Weyerhauser's Grande Prairie mill in Alberta, Canada. The softwood pulp was produced at the Grande Prairie Mill in Alberta, Canada and is a mix of white spruce, lodgepole pine, and a minimal amount of balsam

fir. The Southern mixed hardwood elemental chlorine-free (ECF) kraft pulp was procured from Alabama River Pulp Company, Inc. in Perdue Hill, Alabama USA. The hardwood pulp was produced at the Claiborne Mill Complex in Claiborne, Alabama and is a mix of Southern hardwood wood species. Finally, Whatman filter paper grade 1 is a specific grade filter paper made from high-quality α-cellulose cotton linter. This filter paper is produced to have medium porosity and flow rate, 0.06% ash content, medium crystallinity, and retains particles of an 11 micron size; the part number is 1001-917.

4.4.2 Starch Characterization and Procedure

The size characterization of cornstarch can be accomplished by a light scattering technique. The Malvern Series 2600 Droplet and Particle Size Analyzer performs particle size analysis based on the principles of laser diffraction in the range of 1 to 1,800 microns of particulate in suspensions and emulsions by wet measurements. The detector is an array of 31 solid-state detector elements. The setup also contains a particle suspension unit, which provides a uniform liquid suspension and pumps the solution through the fluid path.

Large particles scatter light at low angles while smaller particles scatter light at higher angles, as illustrated in Figure 4.5. The number of particles needed in the beam to obtain an adequate measurement of the scattering is approximately 100 to 100,000, dependent on the particle size. One instantaneous measurement of the scattering will result in a size distribution based on the small cross section of material. As the sample flowing through the fluid sample holder passes through the laser beam the measured light scattering continuously changes producing an instantaneous integral of the material illuminated by

the analyzer beam. Suspensions of cornstarch in water were flowed through the system at ambient conditions and particle size distributions were collected. Because of the measuring limitations of the system, particle sizes for submicron particles were unobtainable.

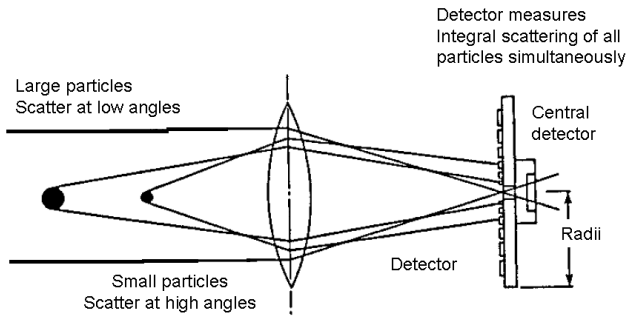

Figure 4.5. Properties of particles in scattered light.

Raw commercial cornstarch (Cream Cornstarch 100% pure), and cornstarch from Sigma Aldrich, were both analyzed using the particle size analyzer. At ambient conditions, aqueous solutions of both starches were prepared with distilled water. The suspension unit was run to maintain a homogenous solution, which prevented the starch from settling and creating gradients in the sampling. Starch solutions were pumped through the flow cell. Particle size distributions were immediately generated. The flow cell and suspension unit were flushed and cleaned out between starch samples.

4.5 Dynamic Light Scattering (DLS)

Photon correlation spectroscopy (PCS), sometimes referred to as dynamic light scattering (DLS) or quasi-elastic light scattering (QELS), is a technique that can be used to

determine the size distribution of particles in a suspension or polymers in solution (Bohren and Huffman, 1998; Chu, 1974). DLS uses a 15 mW solid state laser, 635 nm. When the light source is a monochromatic laser, the light scattering generates a time-dependent fluctuation in the light scattering intensity. The fluctuations are due to small particles undergoing Brownian motion and so the distance between the particles in solution is constantly changing with time. From the changes in intensity, the translational diffusion coefficient (D) can be found by the autocorrelation function equation 4.3.

$$g^{(2)}(\tau) = \frac{\langle I(\tau)I(0)\rangle}{\langle I(0)\rangle^2} = B + A\left(e^{(-Dq^2\tau)}\right)^2 \qquad (4.3)$$

In the above equation, I is the signal intensity, τ is the time delay between measurements, A is an optical constant, B is the background constant, and q is the magnitude of the scattering wave vector.

The translational diffusion coefficient is the principal quantity measured by DLS and is useful for probing interactions between macromolecules. Using the Stokes-Einstein equation, the diameter for a spherical particle moving through a liquid with a low Reynolds's number is related to the translational diffusion coefficient as shown in equation 4.4:

$$D = \frac{k_B T}{3\pi\eta d}, \left[cm^2 / \sec\right] \tag{4.4}$$

where k_B is Boltzmann's constant, T is the temperature of the medium in K, η is the viscosity of the liquid medium (in centipoise) in which the particle is moving, and d is the particle diameter. Appendix A provides more detail regarding DLS theory. Cellulase is a more rigid colloid while the cationic polyelectrolytes are collapsed into random coiled structures. DLS was used to investigate how cellulase and polyelectrolytes interact together under various conditions.

4.5.1 Materials and Methods Used in DLS Study

Cationic polyelectrolyte and cationic polyelectrolyte-cellulase solutions were analyzed with dynamic light scattering (DLS) using a Brookhaven 90 Plus Nanoparticle Size Analyzer. Solutions were prepared in citrate buffer, pH 4.8, at various ionic strengths. The purpose was to gain insight into what variables influence the interaction between the two components. Cationic polyelectrolytes were supplied by Eka Chemicals for this study. Commercially available cellulase produced from *Trichoderma reesei* was supplied by Buckman Laboratories (Atlanta, GA). As received, this enzyme preparation was too crude for DLS because of microbial debris present in the concentrated enzyme solution; DLS showed large debris. Samples were centrifuged for 10 minutes at 10^{o}C at 175,000 rcf in a Beckman Ultra Centrifuge L80 using a Beckman Type 80Ti rotor. Thin walled polyallomer tubes (16x76 mm) with nominal fill capacity of 10.4 mL were purchased from Beckman Instruments. Charge titration and the BCA protein assay confirmed that

ultracentrifugation created debris free solutions. There was no loss of protein and the charge was also maintained. Protein melting experiments were also performed where polyelectrolyte-cellulase solutions were heated by ramping the DLS cell from room temperature to 70^{o}C at a 1^{o}C/point interval and the particle size was monitored.

DLS was also used to examine polyelectrolyte layer thickness on a model substrate. A NIST Traceable Particle Size Standard (3090A) was used as an adsorbent. First, a feasibility study to estimate the layer thickness on the NIST particle was attempted using the 0.001 N analytical grade solution of PDADMAC (used in charge titration). Then XP series polyelectrolytes were used to estimate polyelectrolyte layer thickness for the higher molecular weight samples. Zeta potential was measured using either a Zetasizer 3000 from Malvern Instruments or a ZetaPlus system from Brookhaven Instruments Corporation. The difference in applied power in the two systems required that the polyelectrolyte-cellulase solutions be run in the Zetasizer; the ZetaPlus system denatured enzymes. Samples were flushed out of the Zetasizer cell between runs with excess water. Overall cleaning involved flushing excess amounts of ultrapure water and ethanol through the system to remove water soluble and organic molecules.

4.5.2 Zeta Potential Analysis of Cellulase – Polyelectrolyte Complexes

The isoelectric point for two proteins, cellulase and bovine serum albumin (BSA), were measured in order to confirm that the zeta potential can measure verifiable changes in the proteins. A -50±5 mV zeta potential standard was run to verify that the Malvern

Zetasizer 3000 was working properly. Samples, approximately 2 mL to 3 mL, were injected each time.

Optimase CX 40L was used to investigate the effect of adding polyelectrolyte to the cellulase. Solutions of 50 mg/L XP10023L, XP100025L, and 25 mg/L XP10033L were prepared and added at different ratios to cellulase solutions so as to total 10 mL. The mass ratio of polyelectrolyte to protein ranged from 0 to 0.06 g/g. These solutions were compared by measuring zeta potential and DLS.

4.6 Materials and Methods Used in Adsorption Study

Charge titration was performed using a Mutek PCD-03 system and was used as the primary method for monitoring adsorption of polyelectrolytes and cellulase to cellulosic fiber. Normally, an initial 10 mL of deionized water is added to the sample cell and then 1-10 mL of a given sample is added. These ranges are used so as not to overflow the cell by either sample or titrant. This procedure did not always lead to a stable starting point due to a low amount of active substance. Accordingly, 30 mL of the sample was added initially followed by the appropriate amount of titrant. Each sample was prepared by tearing fiber samples to the desired weight and then suspending in water. XP series L grade polyelectrolytes with cationicities of 10%, 40%, and 80% were used. Optimase CX 40L was used for testing enzyme binding. Standard polyelectrolyte solutions (0.001N) polydimethyl diallyl ammonium chloride (poly-DADMAC) and potassium poly (vinyl sulfate) (PVSK) were used to charge titrate colloidal solutions.

4.6.1 Adsorption of XP Series Polyelectrolytes on Dispersed Cellulosic Fiber

A test was performed to determine how much polyelectrolyte adsorbs to the cellulose fiber. Solutions of 800, 200, and 100 mg/L for 10%, 40%, and 80% cationicity respectively were prepared in ultra purified water; the dissolution was allowed to go for two hours. Samples were prepared by taking 50 mL of polyelectrolyte solution and adding it to 950 mL of fiber suspension. Samples were shaken and then allowed to stand for ten minutes. The sample was filtered using a 250 mL filter funnel with a stainless steel 304 150x150 mesh wire screen and the filtrate was charge titrated.

4.6.2 Adsorption of Cellulase on XP Series Polyelectrolyte Treated Dispersed Cellulosic Fiber

Samples were prepared with 10 grams of fiber and 900 grams of ultra purified water. For the three different cationicity polyelectrolytes (10%, 40%, and 80%) 50 mL of solution was prepared at (10%, 645 ppm; 40%, 143 ppm; 80%, 83 ppm). These dosages were estimates for approximately saturating the cellulose fiber. Additionally, 50 mL of cellulase solution was added to obtain approximately 1000 grams of total solution; final cellulase dosages were made at 0.25% and 0.50% (v/v). Activity assays, to be discussed later, show that cellulase activity at 4^{o}C is approximately 3% of the activity at the optimal 50^{o}C. Because cellulase does not appreciably hydrolyze cellulosic fiber at 4^{o}C all solutions, prior to addition and mixing, were cooled in a refrigerator to temperatures of about 4^{o}C. The amount of cellulase present in the liquid phase was estimated using charge titration (titrant PDADMAC). Samples were prepared with 1.0% consistency

dispersed bleached kraft softwood fiber and varying polyelectrolyte concentration ranging from 20 mg/L to 160 mg/L with a total volume of 10 mL for three XP series samples (10%, 40%, and 80% cationicity). Samples were shaken and allowed to rest for one hour after which they were sampled through a 150x150 mesh screen.

4.6.3 Adsorption of Cellulase on XP Series Polyelectrolyte Treated Cellulosic Fiber Handsheets

The binding of cellulase to fiber was measured with and without cationic polyelectrolyte treatments. Because cationic polyelectrolytes bind differently to fiber fines as compared to long fiber (Hartley and Banerjee, 2008), the fines were removed from a sample of bleached softwood kraft pulp with a 28-mesh screen. Measurements for the adsorption of cellulase were also conducted with softwood fiber made into handsheets. Fines and shorter fibers were removed with a Bauer-McNett type classifier, which corresponds to the TAPPI 233 standard method. Bleached softwood kraft pulp was used for making uniform handsheets.

The pulp fiber was formed into handsheets according to official TAPPI 205 testing method. Handsheets were prepared with basis weights of 53 ± 3 gsm and dried overnight. They were then placed on brass screens (35 mesh), dipped into 100 mL of 200 ppm polyelectrolyte for five minutes, and then allowed to air-dry overnight. An equivalent reference handsheet was dipped in the same volume of water for the same period. The handsheets were air-dried at room temperature and placed in 50 mL aliquots of 0.1%, 0.2%, 0.3%, 0.4%, and 0.5% (v/v) aqueous solutions of Pergalase 7547 at 4^{o}C

for 20 minutes. The enzyme remaining in the supernatant was measured with the BCA protein assay, and the amount of enzyme bound to the sheet determined by difference. Both linear and quadratic regressions of the BCA assay calibration resulted in a correlation coefficient greater than 0.99.

For adsorption measurements, approximately 1.0 gram OD softwood bleached kraft fiber was suspended in 50 mL water. Next, 50 mL of 2000 ppm XP series polyelectrolyte was added to the fiber suspension. The suspension was mixed by shaking/inverting and then left to rest for five minutes. Samples were vacuum filtered leaving a 5 to 10 gram wet filter cake. The sample was then suspended in ultrapure water to a total solution weight of 25 grams and put into a refrigerator at 4^{o}C. Next, 0.25% (v/v) cellulase (Optimase CX 40L) solution was prepared and stored at 4^{o}C. Finally, the 25 gram solution of cellulase solution was added to 25 g of fiber solution. Samples were shaken and incubated at 4^{o}C for one hour. Samples were collected and filtered with a 0.2 micron GHP (low protein binding syringe filter). The protein remaining in solution was measured and the amount of adsorbed cellulase was determined.

4.7 Atomic Force Microscopy (AFM) Study of Polyelectrolyte Treated Cellulosic Fiber

Scanning Probe Microscopy (SPM) encompasses several related technologies, most common being scanning tunneling microscopy (STM) and atomic force microscopy (AFM). SPM technologies share the concept of scanning an extremely sharp tip (3-50

nm radius of curvature) across an object surface. The tip is mounted on a flexible cantilever, allowing the tip to follow the surface profile. More theory and background on AFM can be found in Appendix C.

4.7.1 Materials and Methods Used in AFM Study

Softwood handsheets were prepared at approximately a 50 gsm basis weight and allowed to air-dry overnight. They were laid on brass screens and dipped into polyelectrolyte solutions for five minutes, removed, excess solution shaken off, and dried overnight. They were then stored in a desiccator until used. When ready, samples were cut to size, ranging from 0.5 cm^2 to 2 cm^2, and placed on a piece of double sided sticky tape, which was adhered to a round glass wafer. The wafer was placed into an environmental chamber, where environmental humidity could be controlled.

The AFM study was performed using an Asylum Research MFP-3D™ atomic force microscope with a MFP-3D Closed Fluid Cell and BioHeater. Ultrapure nitrogen gas was plumbed to the fluid cell through two parallel AALBORG mass flow meters flowing at 10 mL/min and a 20 kPa gauge pressure; one line was bubbled through and air-stone submerged in ultra pure water. Humidity in the closed fluid cell was controlled by changing the ratio between the dry and wet gas lines. The MFP-3D system is housed in an acoustic enclosure to minimize noise and vibrations.

The AFM probe, AC240TS, is manufactured by Olympus. This general application probe is made from silicon and has a reflective backside coating made from aluminum

(approximately 100 nm thick). The cantilever nominal spring constant is 2 N/m with a resonant frequency ranging from 50 kHz to 90 kHz. The cantilever has a rectangular shape with the width, length, and thickness of 30 ± 2, 240 ± 10, and 2.7 ± 1 micron respectably. The tip has a 3-sided triangular spike shape with the tip height of 14 ± 4 μm and an apex radius 9 ± 2 nm. The AC240TS probe is meant to be used in air and is commonly used in tapping mode and in force traces. Si tips have a native SiO_2 layer, which makes the tip surface hydrophilic. Results and discussion for the AFM work can be found in Appendix C.

4.8 Enzymatic Hydrolysis Kinetics

Hydrolases are hydrolytic enzymes that catalyze the hydrolysis of a chemical bond in a reaction with water. Commonly used hydrolytic enzymes such as cellulase, hemicellulase, and amylase each have high specificity and hydrolyze their respective glycosidic bonds (Wyman, 1996). Cellulose is hydrolyzed to glucose by a mixture of enzymes from *Trichoderma Reesei* and other organisms (Sun and Cheng, 2002; Hahn-Hägerdal et al., 2006). Endoglucanases randomly attack glucan linkages in fiber through a series of adsorption-desorption cycles (Linder and Terri, 1996). Exoglucanases work processively on the ends of cellulose chains releasing cellobiose, which is then converted to glucose by ß-glucosidase (Kipper et al., 2005). Commercial cellulase preparations perform optimally at about 50^{o}C as measured against substrates such as filter paper or crystalline cellulose (Adney and Baker, 1996).

4.8.1 Procedures Used in Temperature Dependence Kinetic Study

A commercial cellulase preparation (Cellic CTec) was provided by Novozymes; its activity was 66 FPU/mL. Three procedures were used to hydrolyze cellulose fibers. First, fibers were formed into handsheets (Lark et al., 1997), which were exposed at 33 g/l to a 0.19% enzyme solution. Glucose was determined after 1 hour. In effect, this is similar to the standard filter paper enzyme assay except that a handsheet was substituted for the filter paper that is conventionally used. The stopping reagent used in the assay was replaced with 10% (w/v) trichloroacetic acid solution in order to be compatible with the automated glucose analysis used in this study. In the second procedure, the fibers were dispersed in water instead of being formed into handsheets and the glucose determined after 1 hour. The suspension was not stirred. Both procedures were run at 30, 40 and 50^{o}C. The third procedure was similar to the second except the samples were shaken in an orbital water bath and glucose generation was monitored over several hours. Glucose was determined with the GOPOD method, which was automated with a DA3500 Discrete Analyzer from OI Corporation, College Station, TX.

Fiber length was measured with an Optest Fiber Quality Analyzer, Hawkesbury, Ontario, Canada. The values reported are length-weighted averages, the sum of the individual fiber lengths squared divided by the sum of the individual fiber lengths. This measure is preferred over the arithmetic average because the latter overemphasizes the effect of short fibers (Ring and Bacon, 1997; Robertson et al., 1999). The results were averaged from 5 measurements (each measurement counts 5,000 individual fibers). The softwood fiber was fractionated into 28 mesh and fines fractions through a series of screens; the

hardwood fiber was fractionated into a 48 mesh fraction. The 28 and 48 mesh sizes correspond to sieve openings of 0.6 and 0.3 mm, respectively. The fines are defined as fibers that are < 0.1 mm. Their presence in the 28 and 48 mesh fractions was very small as they were mostly removed during fractionation. Each fraction was suspended at 1% solids in pH 4.8 citrate buffer and the enzyme added to a concentration of 0.1% (v/v). The mixtures were shaken at 130 rpm at 30, 40 and 50^{o}C.

Cellulase binding to fiber was measured (in duplicate) by suspending 50 mg of fiber in 2.5 mL of 50 mM citrate buffer at pH 4.8. The samples were refrigerated at 4^{o}C for 24 hours and 2.5 mL of 0.2% (v/v) enzyme was added to each sample and the mixture shaken for 1 hour at 4^{o}. The suspension was filtered through a GHP 0.2 µm low protein binding syringe filter and the filtrates analyzed spectrophotometrically at 230 nm against a 50 mM citrate blank. Cellulase activity measured at 4^{o}C showed that the activity was 3% of that at 50^{o}C; hence very little hydrolysis occurred at 4^{o}C. The enzyme concentration was determined from a standard curve.

The crystallinity of softwood fiber was measured by FT-IR spectroscopy. The fibers were mixed with spectroscopic grade KBr and pelletized. FTIR spectra were recorded with a Nicolet 550P spectrometer at a resolution of 4 cm^{-1}. The crystallinity index is proportional to the ratio of absorbance at 1,430 and 894 cm^{-1}, *i.e.* A_{1430}/A_{894} (Sluiter et al., 2008; Akerholm et al., 2004).

4.8.2 Procedures Used in Screening Effect of Cationic Polyelectrolytes

Screening measurements to identify the best polymers were made with 22 commercial cationic polyelectrolytes varying in charge, molecular weight, and the degree of branching, which were supplied by Ashland Water Technologies, Wilmington, DE. No attempt was made to optimize the dosages or the conditions; our intent for the screening was merely to rank the relative effects of the polymer. The set of commercial polymers were screened for their effect on the performance of alpha amylase on cornstarch and cellulase on bleached softwood pulp fiber. The substrate (cornstarch or cellulose) was added at 10 g substrate/l; enzyme (cellulase or amylase) was also added at 10 g enzyme stock/l. The mixture was shaken at 50^{o}C for 6 h. The polymers were applied at 500 and 100 mg of polymer/l of solution for the cellulase and amylase applications, respectively.

4.8.3 Kinetic Study of the Effect of Cationic Polyelectrolyte on the Hydrolysis of Hardwood and Softwood Fibers

To achieve better mixing a bioreactor (2.5 L), BioFlo 3000 from New Brunswick Scientific, was used for its ability to control temperature and agitation. Time course experiments were conducted for hardwood and softwood fiber stocks. Hydrolysis reactions were stirred at 200 rpm with a ribbon mixer attachment. The fiber slurry (2-3% consistency) was heated to 50^{o}C, the polyelectrolyte dose was 250-380 mg/L and the pH was adjusted to 5.0 with 6N HCl. Samples were taken with a sampling tube with a screen at the end. The tube would be inserted into the reactor and a pipette was used to extract a sample. Samples were filtered through a 0.2 μm GHP syringe filter and analyzed for glucose or dissolved organic carbon, e.g. oligosaccharides.

4.8.4 Effect of Cationic Polyelectrolyte on Hydrolysis of Cellobiose

The effect of cationic polyelectrolyte on cellobiose hydrolysis was tested. Reaction solutions were prepared using varying XP10035 concentrations, 1 g Pergalase 7547/L, 1% (w/v) cellobiose (EMD Bioscience, ≥98% purity), and an total initial volume of 50 mL; a control was prepared with no enzyme or polyelectrolyte. Samples were taken at 2, 4, and 6 hour sampling times and analyzed for glucose content.

CHAPTER 5

RESULTS AND ANALYSIS

5.1 Examination of the Interactions of Cationic Polyelectrolytes and Cellulase through Dynamic Light Scattering (DLS)

Dynamic light scattering (DLS) was used to examine the interactions between cellulase and cationic polyelectrolytes to identify the properties that most affect the component interactions. First, interactions within solutions of polyelectrolytes, with and without cellulase present, were examined by varying polyelectrolyte properties and solution conditions. The diffusion coefficients of the cellulase-polyelectrolyte complexes were measured in order to determine the mobility of the cellulase-polyelectrolyte complex under different conditions. The cellulase-polyelectrolyte interactions may improve the thermal stability of the cellulase; protein melting experiments were performed to support such a claim. Polyelectrolyte layer thickness was also estimated using a rigid NIST particle to serve as a substrate in order to estimate the possible polyelectrolyte layer thickness. Lastly, analysis of zeta potential data was done to characterize the cellulase-polyelectrolyte interactions.

5.1.1 Characterization of Cationic Polyelectrolytes

The XP polyelectrolyte series from Eka Chemicals is based on co-polymers of acrylamide and [2-(acryloyloxy)ethyl] trimethylammonium chloride as illustrated in the following Figure 5.1.

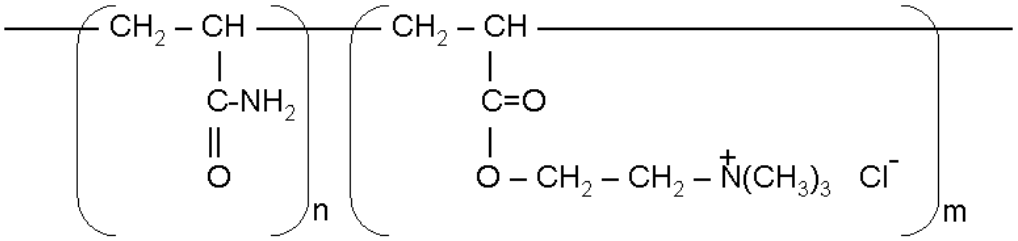

Figure 5.1. Illustration of XP series group structures.

The cationic polymers were titrated with polyvinylsulfate potassium salt (PVSK), an anionic polyelectrolyte. A summary of molecular weight ranges of these polymers is shown in Figure 5.2. All molecular weights are number averages. Various molecular weight grades exist for different polyelectrolytes. Samples with varying cationicity and molecular weight grades were used in the thesis work. Sample names are labeled along the top of the figure.

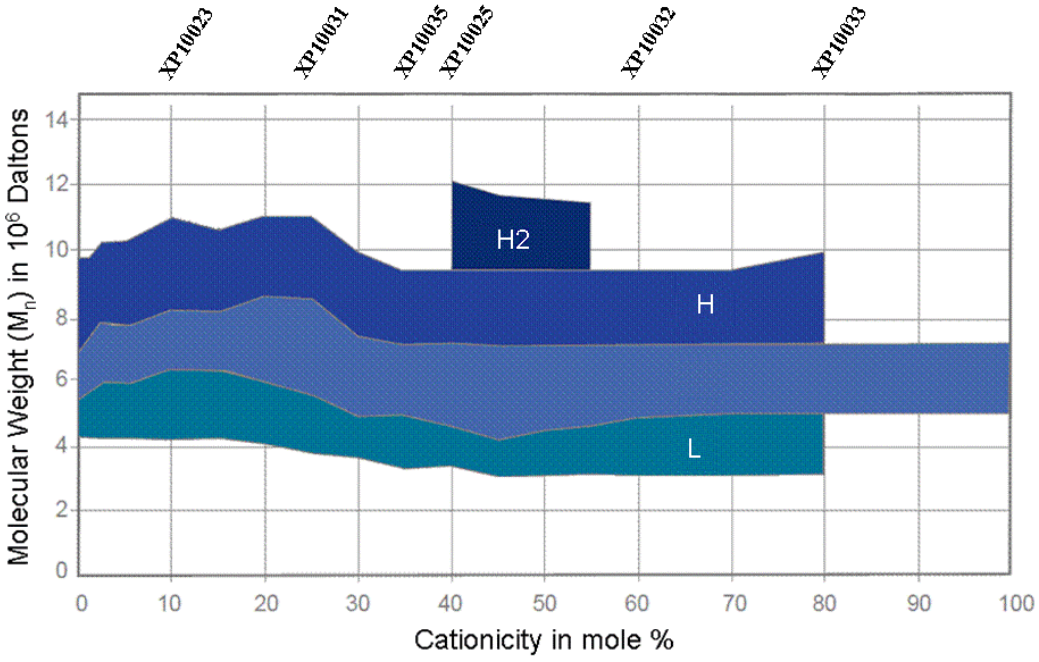

Figure 5.2. XP product summary of average M_n ranges for various cationicity polyelectrolytes.

Each sample was charge titrated at least three times. The charge was related to cationicity through equation 5.1.

$$[\text{Total charge (C/g)}] = 5.7 * [\text{Cationicity in mole\%}] + 88,\ r^2 = 0.88 \quad (5.1)$$

The low and high cationic charge samples, XP10023 and XP10033, were titrated for two different molecular weights. The results in Figure 5.3 show that polyelectrolytes of the same cationicity but different molecular weight have the same charge density. The H end suffix corresponds to a higher molecular weight sample.

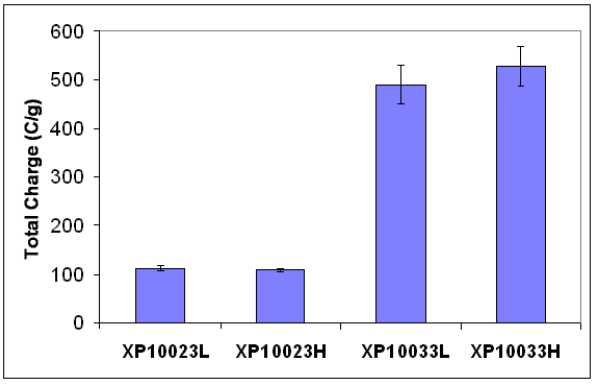

Figure 5.3. Charge density for low and high cationicity polyelectrolytes at two different molecular weights.

5.1.2 DLS of Cellulase

Optimase CX 40L cellulase (50 ± 2 FPU/mL) was used in the DLS work. The total protein concentration and charge density are 119 ± 1 mg/mL and -12 ± 1 C/g respectively. It was found that the commercial enzymes contained debris that interferes with measurement of the size of the proteins. Ultracentrifugation was performed to clean

the enzyme of larger debris. Before centrifugation, the effective diameter of the particles was typically >500 nm and ranged in the hundreds to thousands of nanometers. Given that the samples received were commercially prepared solutions, the debris most likely derives from residual fungus material that was not completely removed from the concentrated enzyme preparation. After centrifugation, the effective particle size ranged closer to 10 nm. In addition to using DLS for the verification of the cleanliness of the debris free cellulase, BCA analysis and charge titration were used to test the enzyme after centrifugation. There was no protein or charge loss. The average particle size distribution for the Optimase CX 40L mixture was measured for a series of dilutions, which are reported in Table 5.1. The dilutions were made with 50 mM citrate buffer pH 4.8. The average particle size was about 10 nm.

Table 5.1. Average particle size distribution of Optimase CX 40L.

(v/v)%	D(nm)	Std Error (nm)
25.0	11.6	0.4
12.5	10.1	0.2
6.25	9.0	0.2
2.50	9.1	0.2
0.50	10.1	0.2

Published data on the molecular structure of cellobiohydrolase I from *Trichoderma reesei* show that the enzyme consists of a long tail, the length and diameter of which are 18 nm and 4.4 nm, respectively, deduced from small-angle X-ray scattering (Schmuck et al., 1986). To show the diverseness of the cellulase mixture, Table 5.2 summarizes the amino acid count and molecular weight of the major components in the cellulase mixture.

These data were taken from The Universal Protein Resource (UniProt) database, which is a comprehensive resource for protein sequences.

Table 5.2. Summary of polypeptide length and molecular weight of cellulase mixture from *Trichoderma Reesei.*

EC #	Enzyme Name	# Amino Acids	kDa
3.2.1.4	Endoglucanase I, II	459, 418	48, 44
3.2.1.91	Cellobiohydrolase I, II	513, 471	54, 50
3.2.1.21	beta-glucosidase I, II	744, 466	78, 52

Results from the particle size analyzer are based on the assumption that the particles are spherical. With the mixture of enzymes this is not necessarily the case but will suffice for the scope of the thesis work.

The Optimase CX 40L stock was diluted to 1.0% (v/v) with 50 mM citrate buffer pH 4.8. Particle size distributions were averaged from triplicate measurements. DLS results summarized in Figure 5.4 are debris free enzyme solutions, which show a multimodal particle size distribution for the cellulase solution; the x-axis is the hydrodynamic diameter and the y-axis is a frequency of the particle size from light intensity measurements.

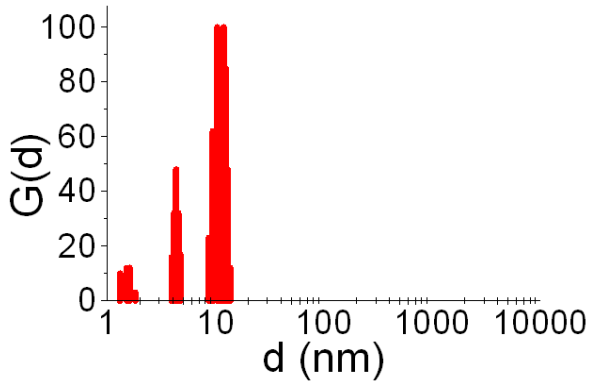

Figure 5.4. Particle size distribution of Optimase CX 40L. Dilutions prepared in 50 mM citrate buffer pH 4.8. The distribution is an average of 16 measurements. Average particle size is approximately 10 ± 1 nm.

The average size distribution was generally consistent with the CBH I dimensions reported by Schmuck et al. (1986).

5.1.3 DLS of Cationic Polyelectrolytes

DLS analysis was performed for multiple series of cationic polyelectrolytes. Each polymer was dissolved in 50 mM citrate buffer pH 4.8. Each sample was measured five times. Series of varying cationicity (10% - 80%) and molecular weight (3 – 12 MDa) were prepared at 10, 100, and 1000 ppm. All the polyelectrolytes used in the DLS study were supplied by Eka Chemicals; their properties are summarized in Table 5.3. The polymer grades are simply designations for the molecular weight ranges.

Table 5.3. Summary of polyelectrolyte properties.

Eka Polyelectrolyte	Percent Cationicity	Polymer Grade	Molecular Weight Range (MDa)
XP10023	10%	L	4.5 - 6.5
XP10031	25%	L	4 - 5.5
XP10025	40%	L	3.5 - 4.5
XP10032	60%	L	3 - 4.5
XP10033	80%	L	3 – 5
XP10025	40%		4.5 – 7
XP10025	40%	H	7 - 9.5
XP1025	40%	H2	9 – 12
XP10036 (branched)	38%		High

Sample polydispersities were approximately 0.35. A polydispersity close to zero (0.00 to 0.02) indicates a monodispersed sample while greater values indicate broader polydispersion. Figure 5.5 summarizes the effect of varying cationicity and polyelectrolyte concentrations on the particle size distribution of L grade XP polyelectrolytes. Each of the distributions is bimodal with a few minor exceptions. The bimodal character seems inherent for each polyelectrolyte sample. Two possible explanations for the bimodal character have been reported in the literature. For example, Ozeroglu et al. (1996) observed bimodal character when synthesizing polyacrylamide. HPLC results distinguished between free single polymer chains and a larger polymer-metal complex consisting of multiple chains. In another case, Fundin et al. (1996, 1999) report bimodal character in relaxation time distributions from light scattering data for cationic acrylate and acrylamide based co-polymers. Fast relaxation modes were attributed to a single polyelectrolyte chain and slow modes attributed to multichain clusters (interpolyion association).

The peaks shift to the right (polymer extension) with decreasing polyelectrolyte concentration. The major changes in the size distributions come from changes in polyelectrolyte concentration; they are insensitive to cationicity. For colloidal stability, the repulsive forces must be dominant. At lower concentrations, the polymer chains extend out to relieve the repulsion between positive moieties in the polyelectrolyte.

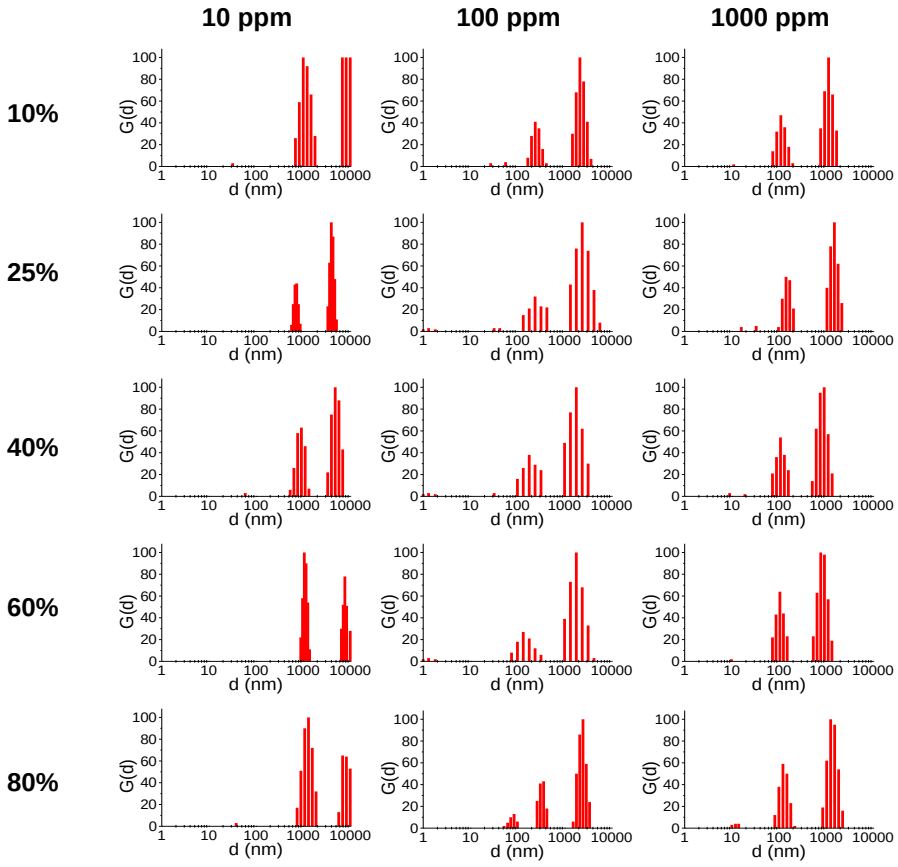

Figure 5.5. Cationic polyelectrolyte size distributions for varying cationicity and solution concentration.

Figure 5.6 summarizes the effect of varying molecular weight at different polyelectrolyte concentrations. As with cationicity, there was a bimodal distribution and there was no major difference in size distributions at a given polyelectrolyte concentration. Again, the

distributions shift right with decreasing polyelectrolyte concentration; the repulsions of cationic groups cause the polyelectrolyte to expand.

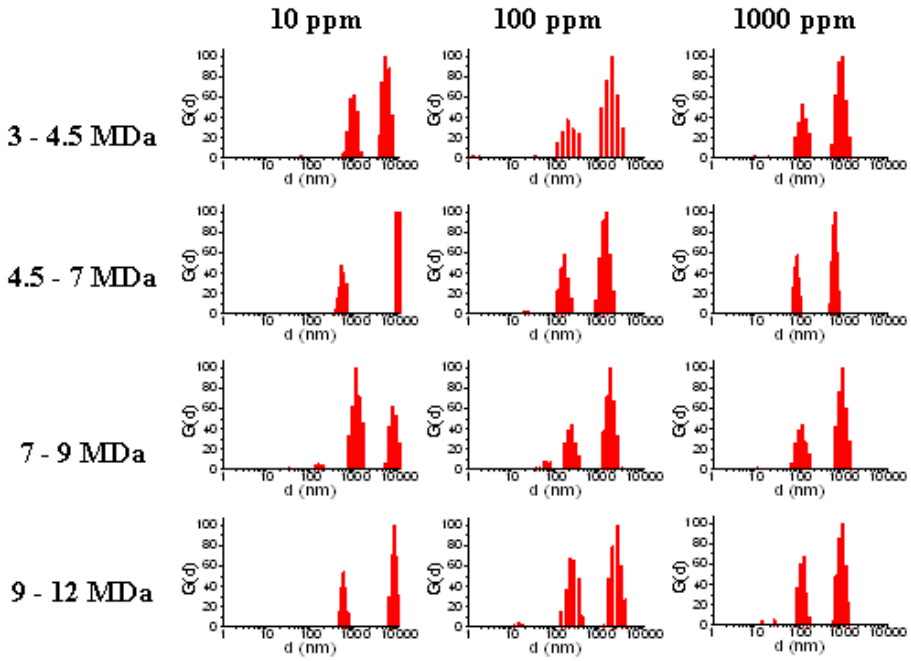

Figure 5.6. Cationic polyelectrolyte size distributions for varying molecular weight and solution concentration.

Next, the effect of ionic strength on the polyelectrolyte in solution was examined. At low ionic strength, polyelectrolytes tend to be stiff and expanded. As the electrolyte concentration increases, polyelectrolytes become dimensionally smaller because of an increased screening of the individual cationic charges on the polyelectrolyte, which reduces repulsive interactions (Richards and Dover, 1980). In a related study, Larrson et al. (1999) report static light scattering (SLS) data for a 10% cationicity polyacrylamide co-polymer, which is summarized in Table 5.4.

Table 5.4. Radius of gyration of 10% cationicity polyelectrolyte at varying salt concentrations (Larrson et al., 1999).

NaCl (mM)	R_G (nm)	μ_d (μm cm V^{-1} s^{-1})
1	250	1.3
5	195	0.7
10	170	0.6
25	140	0.4
50	113	0.3

The radius of gyration (R_G) and dynamic mobility (μ_d) both decrease with increasing ionic strength as reported in Table 5.4. DLS analysis was performed on a similar polyelectrolyte (XP10025L, 1000 ppm). Solutions were prepared over a range of ionic strengths: 5, 10, 50, 100, 500, 1000 mM citrate buffer pH 4.8. Figure 5.7 summarizes the effect of ionic strength in solutions with and without cellulase dosed at 1.0% (v/v). The cellulase peak (at 10 nm) is small because most of the cellulase is bound to the polymer. Both columns show a bimodal distribution. Effective diameters represent an average size of the particles in the sample and are an output of the DLS system. The enzyme reduces the effective diameter at low ionic strengths probably because it neutralizes the charge and promotes coiling of the polymer. This reduction disappears at high ionic strength because other effects predominate, as discussed below.

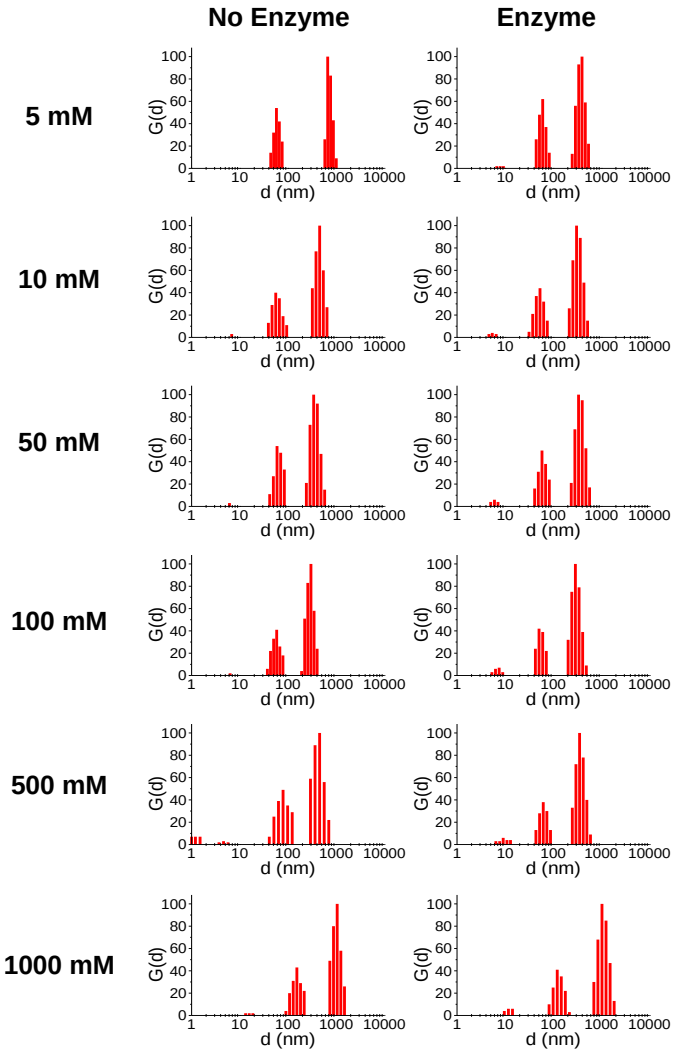

Figure 5.7. Cationic polyelectrolyte size distributions for varying ionic strength with and without cellulase.

Table 5.5. Mean diameter of polyelectrolyte complex with and without cellulase.

	Mean Effect Diameters (nm)	
Citrate buffer (mM)	Cellulase Free	Containing Cellulase
5	552 ± 16	261 ± 10
10	322 ± 11	240 ± 9
50	268 ± 10	265 ± 10
100	217 ± 8	222 ± 9
500	292 ± 12	276 ± 10
1000	737 ± 17	809 ± 18

The effective diameter first falls with increasing ionic strength, but then rises at citrate concentrations equal to greater than 500 mM as summarized in Table 5.5. This trend was also observed in the right column where each sample was dosed with 1% cellulase. This same phenomena was reported by Volk et al. (2004) where for a high molecular polyelectrolyte sample (PA2, $3.3x10^6$ g/mol) both the hydrodynamic radius and radius of gyration show the shrinking particle and an eventual increase in particle dimension at higher salt concentrations. As the electrolyte concentration is increased, electrostatic interactions are increasingly screened and the highly expanded polyelectrolyte coils begin to shrink. Eventually a minimum dimension was reached. At high enough electrolyte concentrations, there was a "salting out" of the polyelectrolyte (Eisenberg and Mohan, 1959; Eisenberg and Casassa, 1960; Ikegami and Imai, 1962). In such cases, phase separation occurs if the salt level is high enough. The salt concentration required to cause precipitation of the polyelectrolyte is high and independent of the polyelectrolyte concentration (Ikegami and Imai, 1962). With other varying polyelectrolyte concentrations (10 ppm and 100 ppm) there were minima observed at either 100 mM or 500 mM (data not shown). At higher electrolyte concentrations, there was an increase in the size of the previously collapsed polyelectrolyte coil. Cellulase containing polyelectrolyte solutions (10 ppm and 100 ppm) also showed the same trend supporting that salting out occurs at both low and high polyelectrolyte concentrations and may be independent of polyelectrolyte concentration. This salting out effect was likely the reason for observing an increase in the effective diameter of the solution complex.

5.1.4 DLS of Cationic Polyelectrolytes - Cellulase Interactions

DLS measurements were made with solutions of the same polyelectrolytes discussed above, but with cellulase present in the medium. Each sample had the same dose of cellulase. Since the polyelectrolyte structure in solution is significantly larger than that of the cellulase, the size of the complex should range more toward the size of the polyelectrolyte. The results in Figure 5.8 show a portion of unbound enzyme material in each distribution profile. For each sample there was a fraction of enzyme material that was not incorporated into the polymer peaks; at each polyelectrolyte concentration, this unbound fraction appears constant for each vertical set. For the 1000 ppm samples with varying cationicity, there was very little difference between samples. The enzyme peak G(d) was around 5 to 10%. The size distribution of the samples is relatively insensitive to the cationicity of the polyelectrolyte.

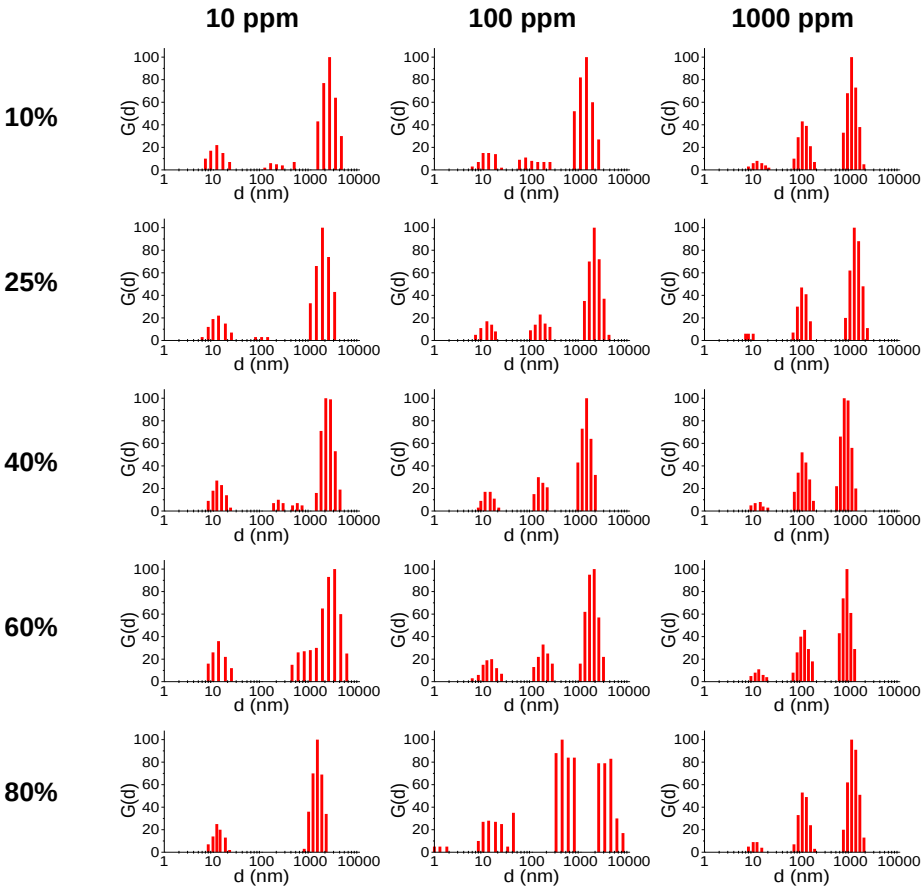

Figure 5.8. Effect of varying cationicity and polyelectrolyte concentrations on the DLS of polyelectrolyte-cellulase particle size distributions.

Figure 5.9 summarizes the effect of varying molecular weight for varying polyelectrolyte – cellulase ratios; the polyelectrolytes all of 40% cationicity. The results in Figure 5.9 show a portion of unbound enzyme material in each distribution profile. For each of the samples there was a fraction of enzyme material that was not incorporated into the polymer peaks. At 1000 ppm the vertical sample set, with varying molecular weight, showed little difference between samples. However, as polyelectrolyte concentration was decreased (100 and 10 ppm) it was observed that the unbound peak area increased with molecular weight in the vertical sets; this was most noticeable at 10 ppm.

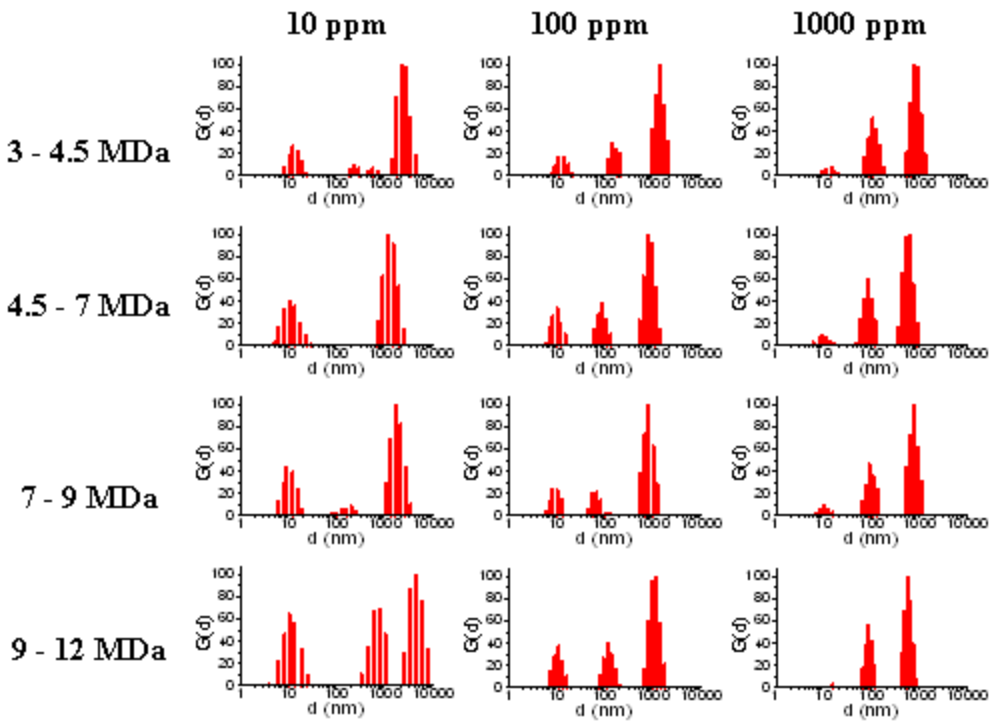

Figure 5.9. Effect of molecular weight on DLS of polyelectrolyte-enzyme solutions at various concentrations.

An overall summary of mean complex size for varying cellulase-polyelectrolyte samples was reported in Table 5.6; all cellulase-containing samples have 1% cellulase. The addition of the cellulase decreases the overall polyelectrolyte complex size. All samples appear to follow the same trends.

Table 5.6. Summary of effective diameter of polyelectrolyte complexes.

		Without enzyme		With Enzyme		
Ppm	Cationicity / Polymer Grade	Eff. Dia. (nm)	Std. Error (nm)	Eff. Dia. (nm)	Std. Error (nm)	Δd (nm)
1000	80% / L	449	16	374	15	75
100	80% D	869	61	656	45	213
10	80% D	1783	49	1141	50	642
1000	60% D	307	6	281	5	26
100	60% D	840	58	609	55	231
10	60% D	2079	306	1263	110	816
1000	40% D	323	7	293	3	30
100	40% D	669	29	501	20	168
10	40% D	1967	244	1088	51	879
1000	25% D	495	13	448	16	47
100	25% D	1001	36	810	58	191
10	25% D	1893	116	1185	62	708
1000	10% D	398	10	360	10	38
100	10% D	862	35	597	12	265
10	10% D	2241	347	1510	183	731
1000	40% HV	287	17	217	4	70
100	40% HV	614	89	301	15	313
10	40% HV	2363	999	805	24	1558
1000	40% HU	327	23	258	6	69
100	40% HU	574	64	308	44	266
10	40% HU	1524	166	679	39	845
1000	40% H	232	6	197	4	35
100	40% H	455	11	258	7	197
10	40% H	1419	127	644	24	775
1000	Eka XP 1067	280	8	248	5	32
100	Eka XP 1067	585	32	310	14	275
10	Eka XP 1067	1705	192	705	28	1000

The change in the size of the polyelectrolyte complex was estimated by taking the difference between the polyelectrolyte with and without the addition of cellulase (Δd). These size differences were plotted against polyelectrolyte concentration and are reported in Figure 5.10. The plot overlays results from nine polyelectrolyte samples. Although the samples vary in cationicity, molecular weight, and branching they all overlay closely and approach a minimum at high polymer concentration.

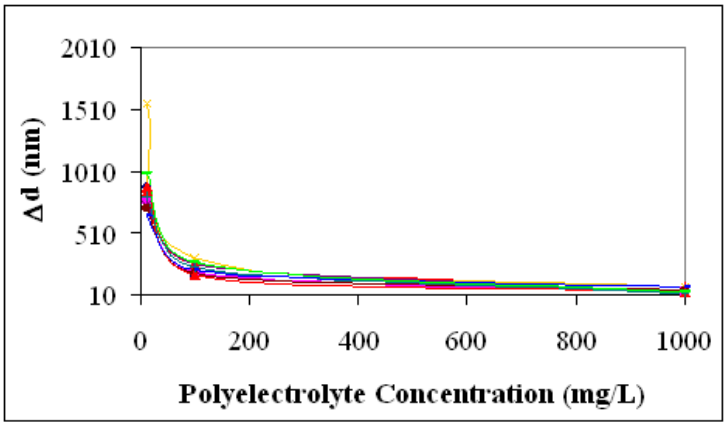

Figure 5.10. Plot of Δd vs. polyelectrolyte concentration from Table 5.6.

For the bimolecular equilibrium,

$$\text{Enzyme} + \text{Polyelectrolyte} \leftrightarrow \text{Enzyme}^{*}\,\text{Polyelectrolyte} \tag{5.2}$$

the equilibrium dissociation constant (K_d) can be expressed as:

$$K_d = \frac{[Enzyme]\ [Polyelectrolyte]}{[Enzyme * Polyelectrolyte]} \tag{5.3}$$

where the units are concentration. Since each of the polyelectrolytes overlay so closely a typical medium cationicity polymer was used (XP10025L, 40% cationicity) to generate a plot like Figure 5.10 with more resolution around the lower polymer concentrations; the enzyme was a debris- free sample of Optimase, whose activity was 50±2 FPU/mL. Figure I illustrates the change in complex size at various polyelectrolyte concentrations

(15, 20, 25, 50, 100, 200, and 400 mg/L) at an enzyme concentration of 1% (v/v). Each data point derived from at least 12 data points from which Δd values were calculated.

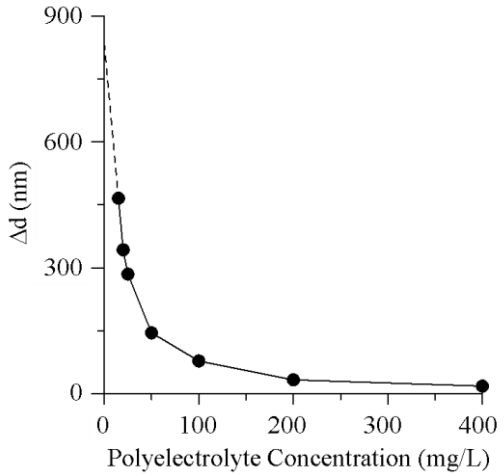

Figure 5.11. Plot of Δd vs. polyelectrolyte concentration. Relative error is ≤12% for each data point.

A fraction of enzyme bound (θ_{enzyme}) is estimated using the following equation:

$$\theta_{enzyme} = \frac{[Polyelectrolyte]}{K_d + [Polyelectrolyte]} \tag{5.4}$$

Equation 5.4 is analogous to a relationship known for a bimolecular equilibrium reaction (Blanch and Clark, 1997; Sauer et al. 2010). From this expression if [Polyelectrolyte] = K_d, then θ_{enzyme} = ½. Thus, half-maximal bound enzyme occurs when the free polyelectrolyte concentration is equal to K_d. It is assumed that the enzyme may proportionally bind to the polyelectrolyte. From Figure 5.11, Δd increases with decreasing polyelectrolyte concentration. It is assumed that the change in the size of the equilibrium complex is proportional to the fractional amount of enzyme bound to the polyelectrolyte so that:

$$\theta_{enzyme} \approx 1 - \frac{\Delta d_i}{\Delta d_0} \tag{5.5}$$

where Δd_i is the equilibrium size difference at any polyelectrolyte concentration and Δd_0 is the extrapolated equilibrium size difference of a single polyelectrolyte. If a power law relationship is assumed and fit for the data in Figure 5.11 then an (r^2=0.9982) results. This would not be usable in that a power law estimate for the Δd_0 would go to infinity for a single polyelectrolyte. The zero polyelectrolyte Δd (of 835 nm) was extrapolated linearly from the 15 and 20 mg/L data and represents a fully extended polyelectrolyte in the presence of excess enzyme. The fractions of bound enzyme (theta) were estimated from the data in Figure 5.11 and are summarized in Table 5.7.

Table 5.7. Summary of data for XP10025L (40% cationicity).

[P], mg/L	Δd (nm)	$\Delta d_i/\Delta d_0$	Theta	Theta / [P] (L/mg)
15	466±27	0.558	0.442	0.029±0.0017
20	343±45	0.411	0.589	0.029±0.0039
25	285±20	0.341	0.659	0.026±0.0019
50	145±14	0.174	0.826	0.017±0.0016
100	78±9	0.093	0.907	0.009±0.0011
200	33±4	0.040	0.960	0.005±0.0005
400	18±2	0.022	0.978	0.002±0.0003

Theta/[P] was plotted verses Theta and is reported in Figure 5.12.

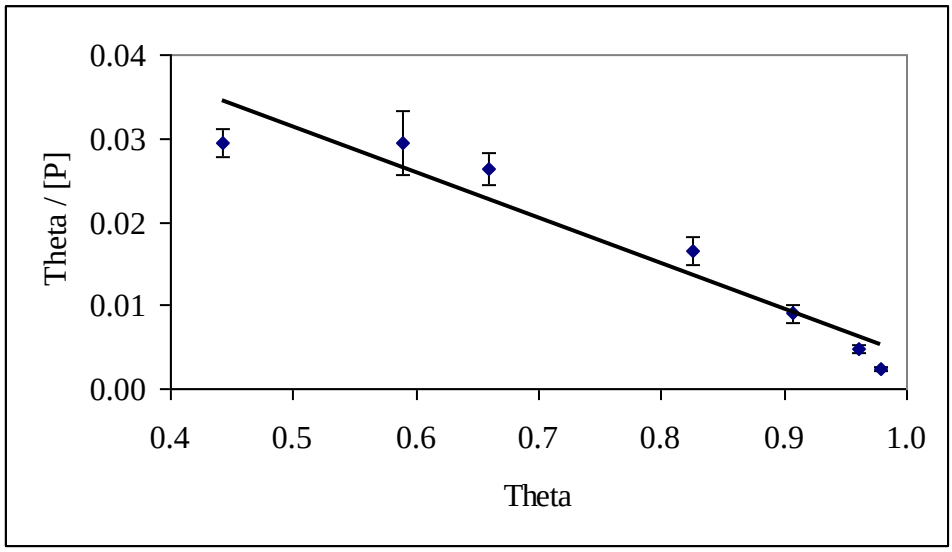

Figure 5.12. Plot of Theta / [P] vs. Theta for the data in Table 5.7.

The plot has a small curvature. If a linear relationship is assumed then a slope of -0.06 (r^2=0.92) results, which corresponds to a K_d of 17±6 mg/L (5±2 nM) results. The curvature likely derives from the interpolated value of 835 nm used for Δd_o. A linear interpolation was the only practical option available but the relationship in Figure 5.12 is curved at low polyelectrolyte concentrations and Δd_o is probably greater than 835 nm. If, for example, the Δd_o value is doubled to 1670 nm, then the regression coefficient (r^2) rises to 0.992 and K_d becomes 1.4±0.4 nM. However, the K_d value of 5 nM is reported here because the method of linear interpolation is more defensible.

This type of estimate for a dissociation coefficient has not been reported to date. The method will be further validated later in a results section where the K_d for the cellulase adsorbed to polyelectrolyte (XP10025L, 40% cationicity) treated fiber ranges between 3 to 7 nM. Goldstein et al. (1993), in a cellulase binding study, report that the measured cellulase carbohydrate binding domain (CBD) dissociation constant was in the 1 μM

range. The lower value of 5 nM obtained here suggest that cellulase binds much more tightly to polyelectrolyte-treated cellulose.

5.1.5 Discussion of DLS Results

Overall, the XP series polyelectrolytes behaved as expected. Varying ionic strength with the citrate buffer had a significant effect on the polyelectrolyte-cellulase interactions. At high ionic strength, there was a decrease in the interactions between the enzyme and polyelectrolyte and at some point the polyelectrolyte "salted out"; this coincides with a destabilization of the complex (Kam and Gregory 1999). Wittemann and Ballauff (2006) showed polyelectrolytes adsorbed proteins from solution only at low ionic strength and that at high ionic strength there is a marked resistance against protein adsorption. Additionally, Solberg and Wagberg (2003) showed that higher ionic strength decreased the amount of cationic polyacrylamide that would be adsorbed onto cellulosic fiber with 10 mM NaCl being more optimal than 100 mM NaCl for promoting adsorption. Most buffered work in this thesis was performed using 50 mM citrate buffer, which is standard for cellulase activity measurements. This would not be considered a high concentration. Even non-buffered systems contain some salt content coming from the enzyme preparations.

DLS did not show any noticeable contrast between different cationicity samples. At varying polyelectrolyte concentrations, the different cationicity samples followed the same general trends. The branched sample followed the same interaction trends with cellulase as the varying cationicity samples. However, there was some differentiation

between samples with constant cationicity (40%) and varying molecular weights. At low polyelectrolyte concentration (10 ppm) and increasing molecular weight, the free cellulase peak increased, suggesting that the higher the molecular weight the lower the adsorption interaction with the polyelectrolyte. At 10 ppm, lower molecular weight polyelectrolytes had smaller enzyme peaks than higher molecular weight polyelectrolytes, suggesting that lower molecular weight polymers bind better to the enzyme than higher molecular weight. This trend was also seen to a lesser extent at 100 ppm, but not at 1000 ppm. The DLS summary of Figure 5.10 shows that the polyelectrolyte-cellulase complexes regardless of cationicity, molecular weight, or branching shrank in the same manner as compared to the polyelectrolyte complex alone. An estimate for a dissociation constant between cellulase and polyelectrolyte suggests that there is strong binding between the two.

5.1.6 Diffusion Coefficient Analysis of Cellulase-Polyelectrolyte

The previous light scattering data suggests that the cellulase complexes with polyelectrolytes resulting in a tightly bound adsorption. Fundamental to light scattering is the generation of diffusion coefficients of the colloids in suspension. Diffusion coefficients of solutes in gas (~10^{-1} cm^2/s), liquids (~10^{-5} cm^2/s), solids (10^{-10} cm^2/s), and polymers (~10^{-8} cm^2/s) have been well studied (Lide, 1995). The diffusion coefficients for low-molecular-weight solutes in water are normally on the order of 10^{-5} cm^2/s, whereas the diffusion coefficients for high-molecular-weight polymeric gelants such as polyacrylamide or xanthan are typically about 10^{-8} cm^2/s (Southwick, 1982). Diffusion coefficient data were separately outputted from the DLS experimental results. An

analysis of diffusion coefficients was performed to confirm that the light scatting data were accurate, because regardless of the size distributions, if the diffusion coefficients do not correspond to appropriate values the data may not be reliable.

The effect of varying cationicity was tested and is reported in Figure 5.13. Here, the concentration affects the diffusion coefficient for the various cationicities. In Figure 5.13, at 1000 ppm the diffusion coefficients are of the same order of magnitude as polymers of same molecular weight. The diffusion coefficient decreases noticeably from 1000 ppm to 10 ppm, which correlates with the increase in effective diameter or elongation. Concentrations of 1000, 100, and 10 ppm correspond to the ranges of approximately 1.0 - 1.6x10^{-8}, 5.0 - 7.8x10^{-9}, and 2.0 - 3.0x10^{-9} cm^2/s across the range of cationicities, respectively. The diffusion coefficient was higher for the polyelectrolyte structures at higher concentrations. With increasing polyelectrolyte concentration, there is more variability in the polymer diffusion.

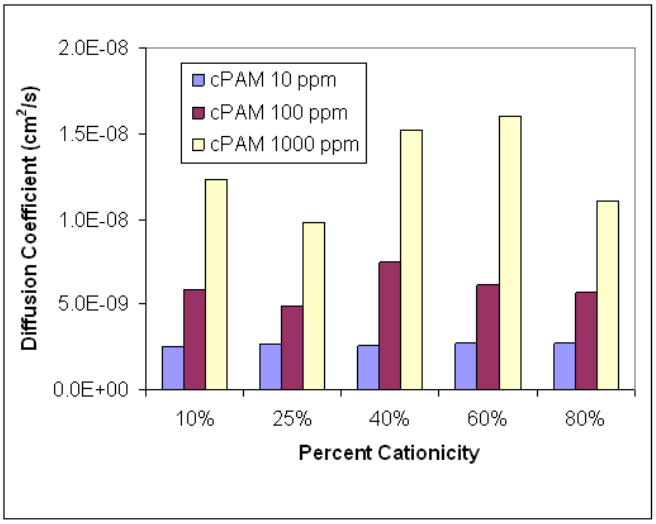

Figure 5.13. Diffusion coefficients for XP series L grade polyelectrolytes with varying cationicity; molecular weights of approximately 3 to 5 MDa.

At 10 ppm the diffusion coefficients are essentially constant. At 100 ppm, the medium 40% cationicity sample has the highest average diffusion coefficient. At 1000 ppm the 40% and 60% had the highest diffusion coefficients. Generally, it appears that polymers of low and high cationicity give rise to slightly lower molecular diffusion. It was expected that cationicity would be more of a factor affecting the polyelectrolyte diffusion coefficients. However, there was not a strong influence of cationicity on the diffusion coefficients. An analysis with ANOVA (Appendix D) concluded that differences in the diffusion coefficients were statistically significant between the three polyelectrolyte concentrations. The ANOVA analysis did confirm that the diffusion coefficients were not statistically significant with the varying cationicities. As a result, the hydration shell surrounding each polyelectrolyte would not be greatly influenced by changes in cationicity.

In addition to cationicity, the effect of molecular weight of the polyelectrolytes on diffusion was examined. Figure 5.14 reports diffusion coefficients for samples with varying high molecular weights and constant cationicity. The concentration of polyelectrolyte in solution has the largest effect on the diffusion coefficients. The effective diameter of a polyelectrolyte structure should be larger at low polyelectrolyte concentrations (i.e. 10 ppm) than at higher concentrations (i.e. 1000 ppm). The larger structure has a lower diffusion coefficient. At each concentration, the diffusion coefficients are approximately the same across the various molecular weights. Thus, according to the data, at very high molecular weights ranging in the millions, the polyelectrolyte diffusion coefficient (mobility) was essentially constant for these samples.

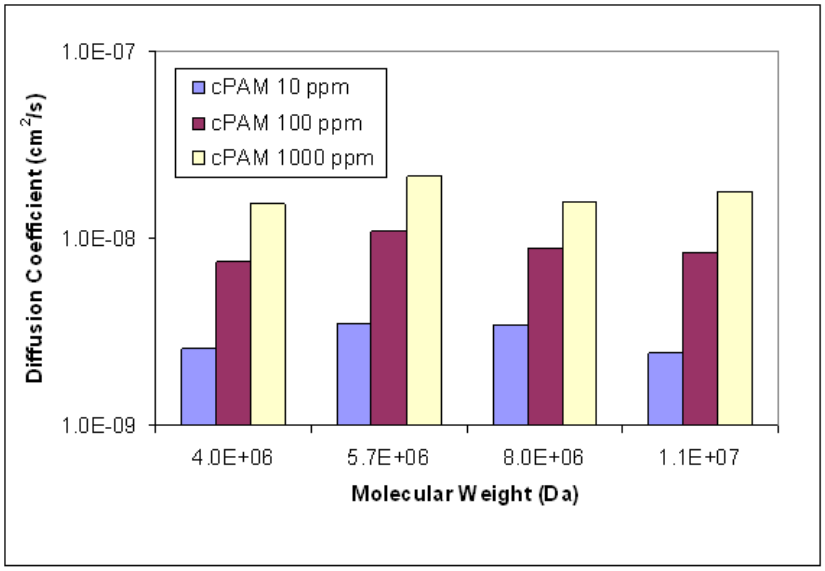

Figure 5.14. Diffusion coefficients for XP10025 polyelectrolytes with varying molecular weight grades; all samples have at 40% cationicity.

The ANOVA (Appendix D) confirmed that the diffusion coefficients were not statistically significant with the varying polyelectrolyte molecular weight. The ANOVA also concluded that the diffusion coefficients were again statistically significant across the three polyelectrolyte concentrations.

Empirical expressions have been developed, which relate a polymer's intrinsic viscosity or translational diffusion coefficient to its molecular weight. The Mark-Houwink-Sakurada (MHS) equation, a power law ($D = kM^{\alpha}$) fit expression, is such an expression. The empirical parameters (α and k) relate to the diffusion coefficient and the polymer molecular weight; from this equation the molecular weight of a polymer can be determined from data on the translational diffusion coefficient and vice versa. The empirically derived parameters depend on the macromolecule, the solvent, and the solution temperature. These parameters can be obtained only by using well characterized

polymer fractions. The Brookhaven 90Plus software contains a database of these parameters. For polyacrylamide (PAM) the parameters are α = -0.69 and k = 8.46x10^{-4} cm^2/s, which were used to generate the diffusion coefficient plot in Figure 5.15 as a function of polymer molecular weight. A value of α equal to 0.8 is typical for good solvents; for most flexible polymers, $0.5 \leq \alpha \leq 0.8$.

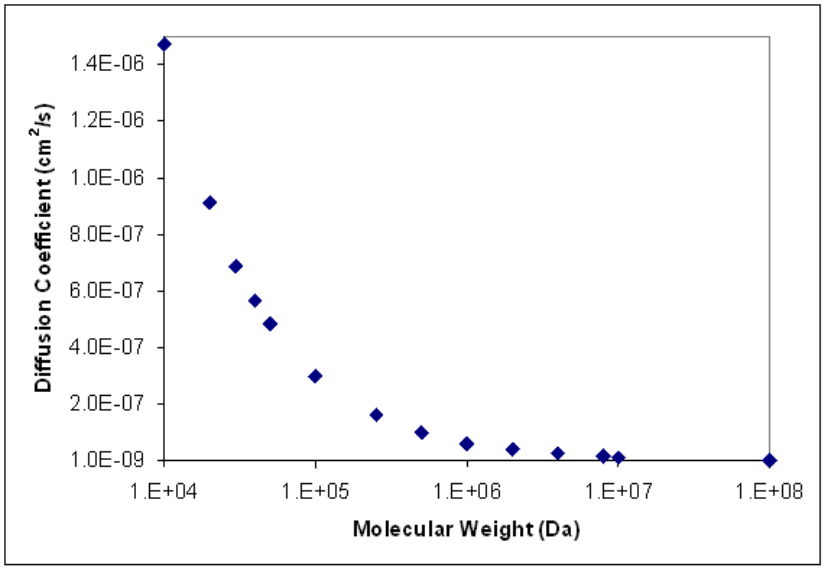

Figure 5.15. Mark-Houwink-Sakurada correlation for polyacrylamide. Parameters taken from database stored in Brookhaven 90Plus Particle Size Analyzer.

For molecular weights ranging from 3x10^6 Da to 12x10^6 Da the diffusion coefficient has a narrow range (1-3x10^{-8} cm^2/s), which explains why diffusion coefficients in Figure 5.14 at each constant concentration are essentially the same. Thus far, at 1000 ppm, the diffusion coefficients for the XP series polyelectrolytes are all of the order 10^{-8} cm^2/s and slightly smaller into the 10^{-8}-10^{-9} cm^2/s range for the lower concentration samples, which is appropriate for polyelectrolytes in the ~10^6 g/mole range.

Finally, diffusion coefficients were measured for polyelectrolyte-cellulase complexes. The diffusion coefficient of the cellulase preparation (1.2 mg/ml 50 mM citrate buffer) is $4.9x10^{-7} \pm 5.0x10^{-8}$ cm^2/s. Figure 5.16 shows a comparison of diffusion coefficients for various cationicity polymers at various concentrations with and without cellulase enzyme present. The diffusion coefficients with cellulase are on average over 10 times greater than the diffusion coefficients for the polyelectrolyte. With the addition of the cellulase, the polyelectrolyte-cellulase complex diffusion coefficient increased in every case.

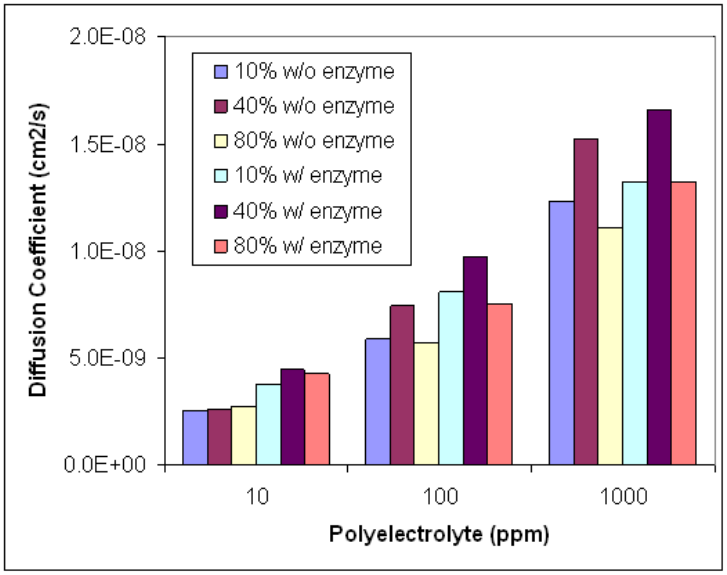

Figure 5.16. Diffusion coefficients for various cationicity polyelectrolyte-cellulase complexes using XP series polyelectrolytes.

The differences in diffusion coefficient were tested using an ANOVA analysis (Appendix D). There was not a statistically significant difference between diffusion coefficients with and without cellulase, and no statistical difference was found between the diffusion coefficients with and without cellulase, with different polyelectrolyte cationicities.

5.1.7 Discussion of Diffusion Coefficients

Typical diffusion coefficients for high molecular weight polymers are of the order 10^{-8} cm^2/s. Diffusion coefficients for varying molecular weights and cationicities were of that order at 1000 ppm. The diffusion coefficients were approximately the same with varying molecular weights. They decreased as polymer concentrations were reduced, which affects the size of the structure. It appeared that cationicity had a slight effect on diffusion but the differences were noticeable at the higher concentrations. When the cellulase was added, an increase in the diffusion coefficients was observed for all samples.

5.1.8 Polyelectrolyte Layer Thickness

Polyelectrolyte layer thickness will be investigated in this section and discussed in terms of how it may be used to minimize the effect of the repulsive double layer thickness on the substrate surface. A NIST traceable particle size standard was used to study polyelectrolyte layer thickness. Related studies reported by other investigators show that similar cationic polyelectrolytes adsorbed onto differing sorbents result in polyelectrolyte layer thicknesses that were found to be of the same length scale as the XP series polyelectrolytes on the NIST particle.

DLS measurements were performed to determine the polyelectrolyte layer thickness of cationic polyelectrolytes on an anionic absorbent. Ideally, it would be desirable to measure the polymer thickness on a cellulosic absorbent. Developing well-defined nano-cellulosic structures is not readily feasible and was beyond the scope of this project.

Fines from cellulose are approximately 70 microns long and are not in a useful geometry. As an alternative, a hard nanoparticle sphere served as a suitable surface. NIST Traceable Particle Size Standard (3090A) was chosen. The nanosphere size standard is made from general-purpose polystyrene having a particle density of 1.05 g/cm^3 and a nominal diameter of 90 nm. The mean diameter of the NIST traceable standard was given as 92 ± 4 nm, 7.6% CV. The NIST aqueous suspension standards were calibrated by Transmission Electron Microscopy (TEM). The solution contains approximately 1x10^8 particles/mL; the solutions contained 1% solids in water with a trace amount of surfactant added by the manufacturer. The zeta potential of the NIST particle averaged from ten measurements made in 25 mM buffer of pH 4.8 was -53.02 mV ± 2.03 mV. For particle size measurements the 1% solids NIST 90 nm nominal standard was diluted in ultra pure water at particle concentrations ranging from 0.25% to 0.66% by volume. High particle solution concentrations gave sampling count rates of approximately 2 to 4 million counts per second (Mcps). The effective diameter of the standard was 98 nm ± 4 nm. The standard was diluted to a count range from 300 to 500 thousand counts per second (kcps), approximately 0.05%, and the average effective diameter of the standard was 105 ± 2 nm. Ratios of polyelectrolyte and colloids were varied and measurements made under non-flocculating conditions.

5.1.9 PDADMAC Layer Thickness

Polyelectrolyte layer thickness was first measured using a 0.001 N analytical standard solution of cationic poly (diallydimethylammonium chloride) (PDADMAC). DLS results showed the PDADMAC (0.001 N) stock solution to have an effective diameter of 897 nm

± 75 nm. The low concentration allows the PDADMAC more space to expand in the solution likely due to low amount of repulsive charges.

The polyelectrolyte layer thickness was calculated by subtracting the effective diameter of the polyelectrolyte treated particles from the bare particle diameter. The resulting thickness was divided by two, resulting in an estimated polyelectrolyte layer thickness on the surface of the particle. The NIST standard stock solution comes concentrated as a white opaque solution. It was verified that the size distribution curve is unimodal over a concentration range of $7x10^4$ to $3x10^6$ particles per mL. Cuvettes were filled with 3 mL of ultra-pure water or 0.001N stock solution of PDADMAC. Varying amounts of NIST standard were pipetted into each respective cuvette and mixed. Samples were left to stand for 30 seconds before being run. The following Table 5.8 summarizes effective diameter results for varying particle amounts.

Table 5.8. Summary of PDADMAC layer thickness on NIST polystyrene standard.

Sample	A	B	C
Total # Particles	~$2x10^5$	~$1x10^6$	~$1x10^7$
NIST Stock (mL)	0.002	0.01	0.1
PDADMAC 0.001 N (mL)	3.0	3.0	3.0
Thickness (nm)	187 ± 15	71 ± 4	23 ± 2

There was an increase in the estimated polyelectrolyte layer thickness with decreasing number of particles. From inspection with the light scattering data in Figure 5.17, a bimodal distribution was observed for sample A with the first peak ranging 165-250 nm and the second peak spanning 1300-2200 nm. Both peaks are significant and the large

size would strongly indicate that the polystyrene particles were flocculated by PDADMAC.

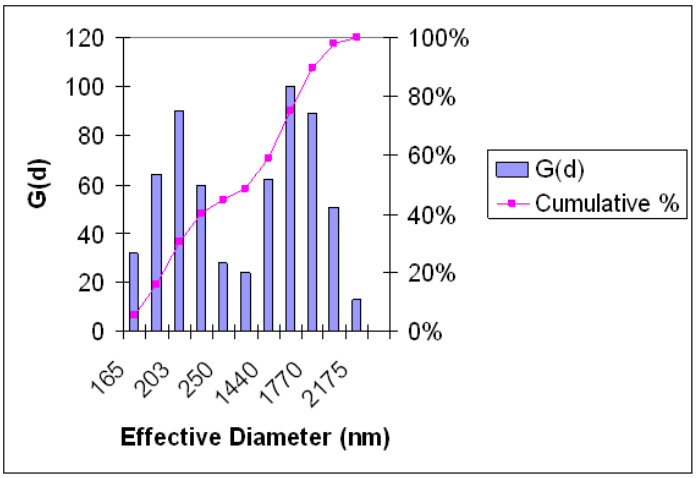

Figure 5.17. Size distribution sample A.

The maximum particle size of the first peak is 203 nm. This is either a particle with a layer thickness of approximately 44 nm or a discriminated complex made of two NIST particles. The overall effective diameter for sample A was approximately 488 nm resulting in the estimated layer thickness of 187 nm. This estimated thickness, being significantly larger than the particle itself, would therefore indicate a failure in this case to successfully discriminate the polyelectrolyte thickness layer, unless the first peak is truly a complex corresponding on average to individual NIST particles. Sample B was also found to be weakly bimodal with the first peak ranging 100-130 nm and the second peak spanning 400-521 nm as shown in Figure 5.18.

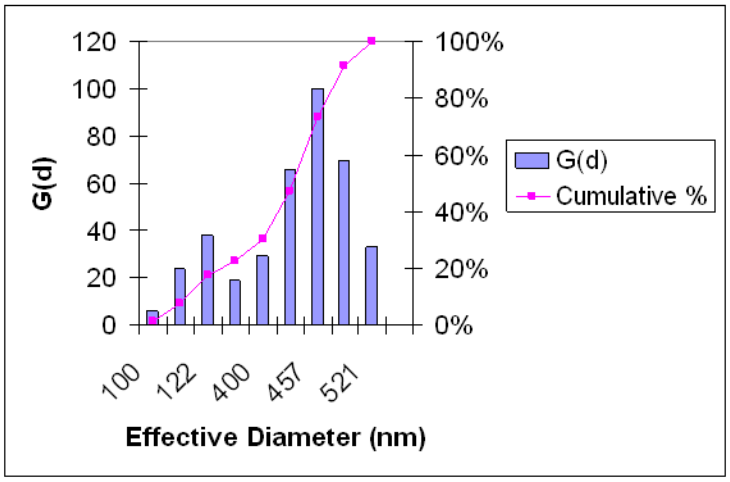

Figure 5.18. Size distribution sample B.

The two peaks in Figure 5.18 are obviously smaller than the two peaks found in sample A. The first peak would appear to be in the size range of the NIST particles with an estimated layer thickness of 2 nm. The second peak is most likely a flocculated structure of multiple particles. The floc structures, globular in nature, form by patching and bridging mechanisms (Eklund and Lindstrom, 1991; Scott, 1996). Shorter polymers are more suited for patching and longer polymers are more suited for bridging. From the data in Figure 5.18, the estimated polyelectrolyte layer thickness was 71 nm. A bimodal distribution is still present and thus an average thickness is still to some extent indeterminate. Finally, sample C resulted in a much weaker bimodal size distribution with the first peak ranging 42-48 nm and the second peak spanning 164-213 nm as shown in Figure 5.19. The small 50 nm peak does not appear in any other distribution, it was reproducible, and is an unclear artifact likely associated with the PDADMAC. The second peak seems to correspond to a particle size distribution of NIST particles. The maximum for the second peak is found at 187 nm. This would either be a particle with a layer thickness of approximately 39 nm or a discriminated complex again made of two

NIST particles. The overall effective diameter for sample C was approximately 156 nm resulting in the estimated average layer thickness of 23 nm.

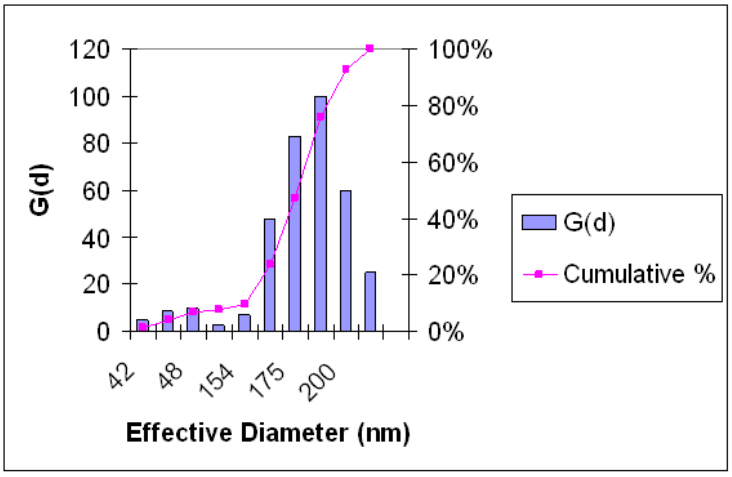

Figure 5.19. Size distribution sample C.

Sample C seems to exhibit the best size distribution accounting for a minimized flocculation but a layer thickness can still be estimated. A fourth sample with 0.2 ml of NIST standard was added to 3 ml of PDADMAC resulting in an effective diameter of 145 nm ± 2 nm corresponding to an estimated layer thickness of 18 nm, which is in agreement with the results from sample C. As the particle concentration increased, the effective diameter converged to the bare NIST particle diameter.

A globular structure with numerous particles would result in an effective diameter that represents multiple particles. This was observed with sample A where the NIST particles were complexed into large flocs. To help visually compare, Figure 5.20 was plotted to summarize the size estimates for floc diameter and polyelectrolyte layer thickness. The

flocs are the effective diameters of the raw data and the estimated polyelectrolyte thickness was estimated from that raw data.

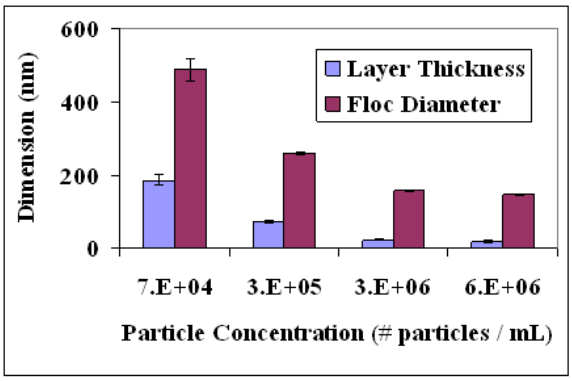

Figure 5.20. Summary of PDADMAC layer thickness on NIST particle.

A second series of PDADMAC – NIST particle data was generated where the particle density was held constant (~1x106 particles / 4 mL) for each sample and the concentration of PDADMAC varied from 0 to 1 mM. Figure 5.21 summarizes the effective diameter and layer thickness of these samples. The correlation coefficient for both was approximately 0.96. The results show an estimated layer thickness ranging between 30 nm to 78 nm. The estimated polyelectrolyte layer thickness linearly increased with increasing PDADMAC. The results in Figures 5.20 and 5.21 both support the feasibility of minimizing flocculation to estimate the polyelectrolyte layer thickness.

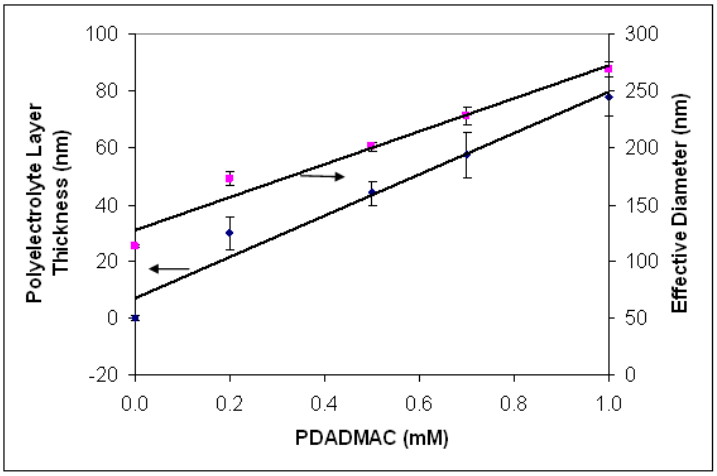

Figure 5.21. Summary of the average PDADMAC layer thickness on NIST particles.

5.1.10 XP Series Cationic Polyelectrolyte Layer Thickness

The estimates for PDADMAC layer thickness laid a foundation for estimating polyelectrolyte layer thickness for XP series samples. A working solution containing ~1x10^7 NIST particles was prepared in 25 mM citrate buffer with a pH 4.8. Stock solutions (100 mg/L) of XP10023L (10% cationicity), XP10025L (40% cationicity), XP1033L (80% cationicity), and XP10025H2 (40% cationicity, ultra-high molecular weight) were each prepared in ultra pure water. Solutions were prepared containing 5 mL of particle working solution (0.042% solids), varying polyelectrolyte (final concentrations 1-50 mg/L), and a balance of ultra pure water so that the solution totals 10 mL. It was verified that the signal intensity was approximately 300 kcps, which gives a desirable sampling rate. A summary for the effective diameter of the particles treated with varying polyelectrolytes is summarized in the following table.

Table 5.9. Summary of effective diameter of Eka polymers bound to NIST particles.

Sample	Range of Effective Diameter (nm)
XP10023L	225 – 255
XP10025L	173 – 216
XP10033L	196 – 228
XP10025H2	223 – 278

It is desirable to add the least amount of polyelectrolyte to each system to avoid the flocculation of individual particles. Polyelectrolyte layer thickness was estimated from the previous data and the results are summarized in Figure 5.22.

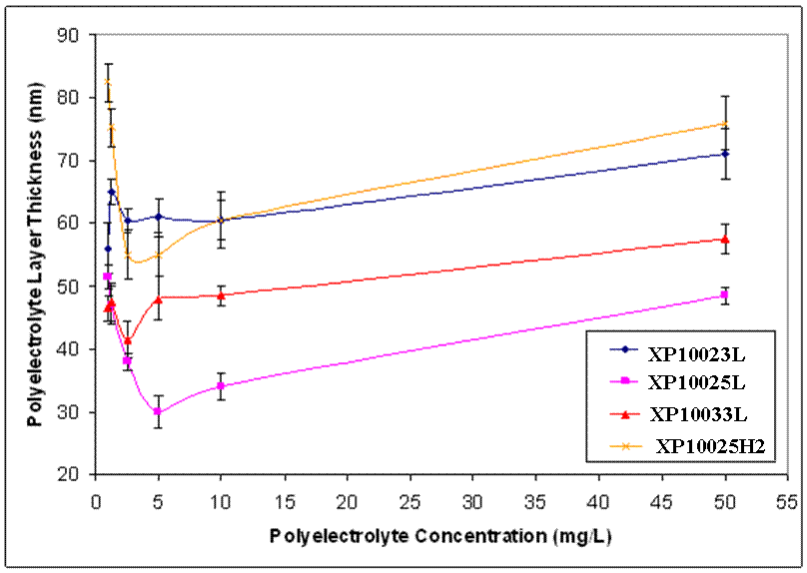

Figure 5.22. Estimated thickness of XP series polyelectrolyte layer thicknesses on NIST polystyrene colloids.

The reduction in layer thickness at low polyelectrolyte concentrations likely results from charge reversal. Under dilute concentrations there would be less charge repulsion, so the polymer is more extended. From 1 to 5 mg/L the decrease in thickness may be from an increase in the amount of polyelectrolyte on the surface, which reaches a minimum layer

thickness when the particle surface is charge neutral. Beyond approximately 5 mg/L, there is an increase in the polyelectrolyte layer thickness from charge repulsion. The 40% cationicity sample (XP10025L) produced the smallest overall layer thickness followed by the 80% cationicity (XP10033L). Over the entire polyelectrolyte concentration range, the XP10025H2 (40% cationicity, high M_n) sample shows a high layer thickness, which was similar to that of the XP10023L (10% cationicity) sample.

Polyelectrolyte layer thicknesses were averaged from Figure 5.22 and the following table reports a summary of the dimensional properties of the estimated layer thicknesses.

Table 5.10. Summary of average polyelectrolyte layer thickness.

	XP10023L	XP10025L	XP10033L	XP10025H2
Average Polyelectrolyte Layer Thickness (nm)	62	42	48	67
Thickness Standard Deviation ± (nm)	5	9	5	12
Minimum (nm)	56	30	42	55

In a related ellipsometric study, adsorbed layer thicknesses of high molecular weight polyacrylamides on silicon were reported (Ödberg et al., 1995). At 10 mM and 100 mM NaCl the cationic polyacrylamide layer thickness was measured to be 25 nm and 46 nm respectively, which is in agreement with results in Table 5.10. In another study, estimated polyacrylamide layer thicknesses on anionic latex spheres (0.24 micron) were in the tens of nanometers (Brotherson, 2007). In an AFM study on the binding of high molecular weight, low charge density cationic polyelectrolytes to mica surfaces, Brotherson and Deng (2008) found that the average polymer loop lengths ranged between 92 nm and 198 nm. A fully extended loop length would range from 46 nm to 99 nm, but

since polyelectrolytes adsorb by attaching at multiple sites, the layer thicknesses will be significantly less than the polyelectrolyte length. The approximate layer thicknesses reported in Figure 5.22 agree well with other investigators' reported layer thicknesses, which were approximately the same for a variety of different sorbents.

5.1.11 Discussion of Layer Thickness

It was demonstrated that by using the NIST Traceable Particle Size Standard (3090A) that polyelectrolyte layer thicknesses could be estimated using DLS. The method was first tested with PDADMAC and was then applied to a XP series of samples. The approximate average layer thicknesses on the NIST particles were found to range form 42 nm to 67 nm. Among samples of 10%, 40%, and 80% cationicity there was a minimum layer thickness associated with the 40% cationicity. A higher molecular weight 40% cationicity was also tested and the larger molecular weight resulted in a thicker layer thickness.

The polyelectrolyte layer thickness has been reported by other investigators where different surfaces, i.e. silicon wafer, latex particle, glass, and mica, were used. The length scale of the polyelectrolyte layer thickness was found to be in the same range for each of these different surfaces. Thus, as a best estimate, the polyelectrolyte layer thickness on the NIST polystyrene particle size standard (3090A) will serve as an estimate of what it may likely be on cellulose.

The electrical double layer thickness may range between 250 to 1000 nm in the presence of deionized water. However, at ionic strengths ranging at 10^{-5} M, 10^{-4} M, 10^{-3} M, and 10^{-2} M the electrical double layer thickness can range for each ionic strength from approximately 25 to 100 nm, 8 to 31 nm, 3 to 10, and 1 to 3 nm respectively (Brookhaven Instruments Corporation, 2002). By changing the ionic strength one can reduce the electrical double layer thickness. Additionally, if cellulases are adsorbed onto polyelectrolyte layer thicknesses, which have been measured to range around 40 to 70 nm, a patching mechanism is the likely mechanism because a bridging structure would require longer polymer structures. The layer thickness is hundreds of nanometers closer than the repulsive electrical double layer. The medium cationicity (e.g. 40%) polyelectrolyte has the thinnest polyelectrolyte layer thickness of the low, medium, and high cationicity samples, which may lead to improved enzyme-substrate interactions.

5.1.12 Protein Melting

Protein melting (or denaturing) can be detected by noting changes in the structure of the protein as it denatures from the rupturing of inter- and intra-molecular bonds.

By using DLS one can monitor the size of the protein. A protein has a native folded structure consisting of primary, secondary, and tertiary structures (Branden and Tooze, 1999). Proteins can be denatured by chemical, physical, or thermal means. A protein initially begins to unfold into a reversible conformation. Under aggressive conditions it irreversibly denatures. The denaturing process is illustrated in the following schematic.

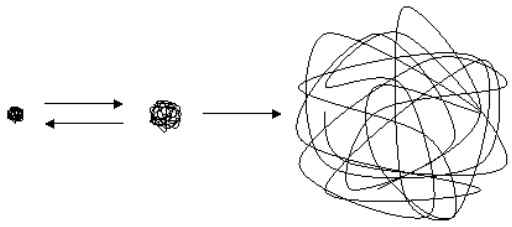

Figure 5.23. Schematic detailing the protein denaturing process and subsequent change in hydrodynamic size.

When the protein unfolds beyond a recoverable conformation, there is an exponential rate of change in the size of the protein from the rupturing of inter- and intra-molecular interactions. Protein denaturation is achieved by increasing temperature, which can cause significant solution evaporation. In order to seal off the test cell (cuvette), a cap was placed on top and wrapped with Parafilm to avoid loss of sample during heating. The samples were heated at 1^{o}C/minute from 25^{o}C to 70^{o}C. Debris free Pergalase 7547, which had been ultracentrifuged at 175,000 rcf for 1 minute at 10^{o}C was used at 1% (v/v). Four XP series D grade polyelectrolyte samples having 10%, 40%, 60%, and 80% cationicities were used. All polyelectrolytes were prepared at 1000 mg/L final concentration in 50 mM citrate buffer with pH 4.8. An overall summary of the DLS results are shown in Figure 5.24. First, the four polyelectrolytes were run; there was no change in size with increasing temperature. The cellulase was then run and showed a relatively stable baseline followed by a rapid change (denaturing) in the conformation size at 48^{o}C. Finally, the cellulase was added to the polyelectrolyte and the mixtures were run. The mixtures had relatively stable baselines followed by an increase in the size of polyelectrolyte-cellulase complex.

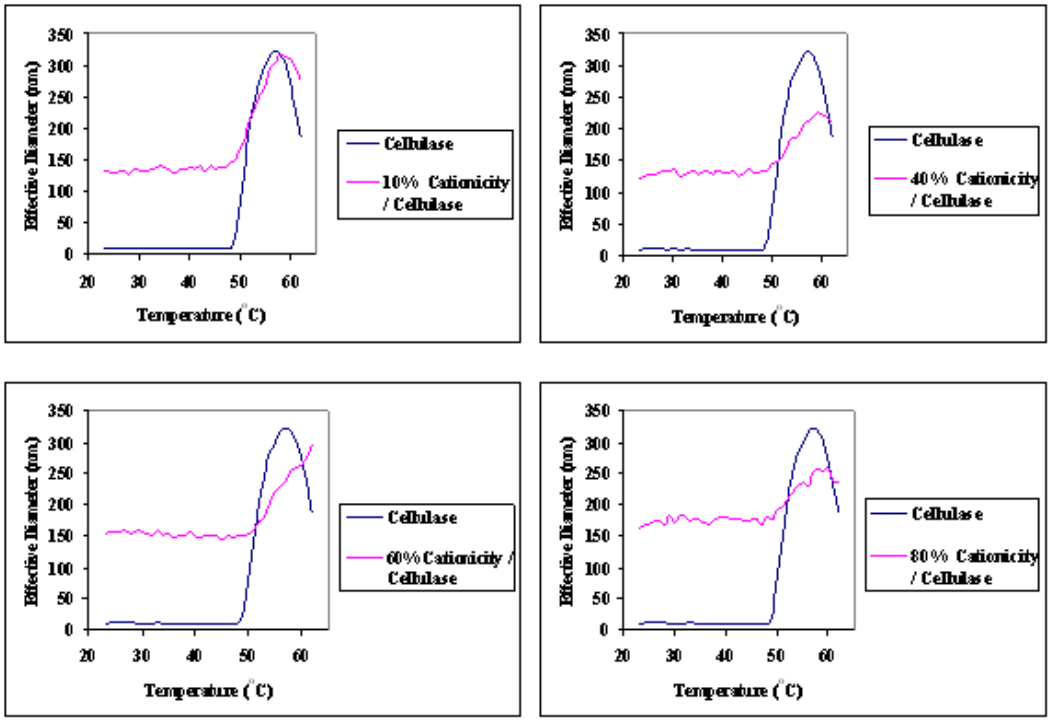

Figure 5.24. Results for the heating study for cellulase and cellulase-polyelectrolyte complexes.

The size of the denatured cellulase control increases from approximately 10 nm to more than 300 nm. The rate of denaturation is slower in the presence of the polyelectrolyte. In a related study, Stogov et al. (2010) report on the structural changes of a GAPDH protein bound to various polysulfoanions. Stable complexes with GAPDH were best formed with hydrophilic high-molecular-weight polyelectrolytes. Heat of adsorption curves showed that the interaction of polysulfoanions denatured the GAPDH. In a different study, Boeris et al. (2009) studied protein-polymer complex formation for the purpose of protein separation. The study found that the addition of a proper polyelectrolyte preserved the secondary and tertiary structure of the protein; the activation energy for thermal denaturation of BSA was increased with the addition of the polyelectrolytes. These two studies suggest that there may be positive or negative effects brought on by the

addition of polyelectrolytes. Application notes from DLS system vendors, i.e. from Malvern Instruments, promote DLS for monitoring protein melting; however, the literature, which does have extensive work examining protein denaturation has not reported the use of DLS for monitoring protein melting.

5.1.13 Discussion of Protein Melting

DLS provides a method to monitor protein denaturation. This was applied to polyelectrolyte-cellulase complexes as the solutions were heated. Figure 5.24 summarizes the DLS results. The polyelectrolytes show no conformational change from being heated. The cellulase showed changes in the protein conformation beginning at 48^{o}C.

5.1.14 Zeta Potential Used to Evaluate Cellulase – Polyelectrolyte Interactions

The zeta potential was used to further characterize the interactions of cellulase with cationic polyelectrolytes in solution. DLS was used as well to complement observations made from the data. First, in order to confirm that changes in the zeta potential correspond to protein changes in solution, a known bovine serum albumin (BSA) protein was tested to verify that isoelectric points could be determined. BSA solutions were prepared with 1 mg/mL at various pH values in citrate buffer. Results are reported in Figure 5.25.

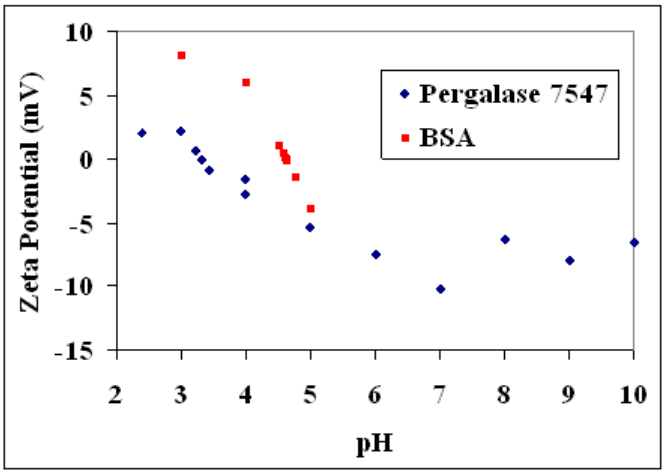

Figure 5.25. Zeta potential measurements of enzymes.

The isoelectric point (pI) was interpolated; the pI is defined as the pH at which a particular molecule or surface carries no net electrical charge (zeta potential equal to zero). The experimental pI for BSA was estimated to be 4.6 compared to 4.7 found in the literature (Ang and Elimelech, 2007). The pI was also measured for the cellulase solution (~ 1 mg/mL) and was interpolated to be 3.3. In the pH range 4 to 5, the zeta potential ranges from -1 to -3.3 mV.

Zeta potential measurements were made for varying ratios of cellulase-polyelectrolyte solutions made by adding varying amounts of 1% (v/v) Optimase CX 40L with corresponding amounts of 25mg/L (for 80% cationicity) or 50 mg/L (for 10% and 40% cationicity) polyelectrolyte solutions so that the total solution summed to 10 mL. Figure 5.26 shows the results of measuring zeta potential for the various solutions. The initial zeta potential ranged -2.2 mV to -3.1 mV.

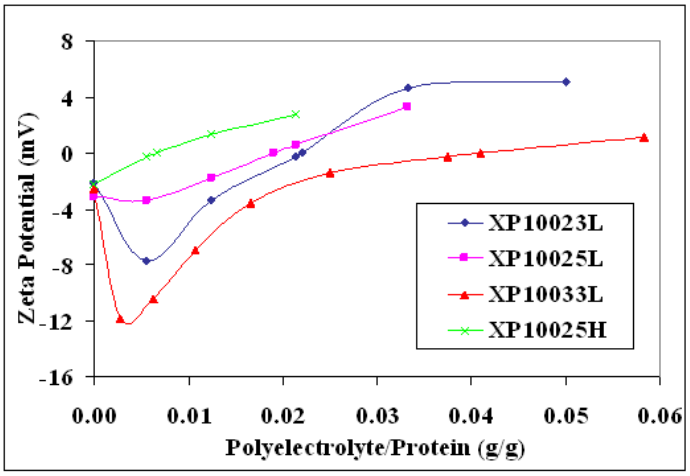

Figure 5.26. Zeta potential measurements for polyelectrolyte-cellulase complexes.

The first observation shows an unexpected initial dip in the data. Typically, if one starts off with a particle with a negative zeta potential and adds a positive counter polyion to the sample, an increase in the zeta potential results. If enough counter polyion is added, the zero point is reached. Figure 5.26 shows an unexpected initial dip followed by the expected increase in zeta potential. The solution ratio of polyelectrolyte to protein was increased until each sample crossed the zero point. The 40% cationicity H grade (higher molecular weight) sample did not show the initial dip. Group member, Kendra Maxwell, who did comparable work for solutions with varying amylase – polyelectrolyte ratios also observed this trend. To help explain these observations DLS was performed on the solutions to complement the zeta potential results. DLS analysis, as reported in Figure 5.27, shows that the average effective diameter and polydispersity of the solution complexes track each other when plotted against the polyelectrolyte/cellulase ratio.

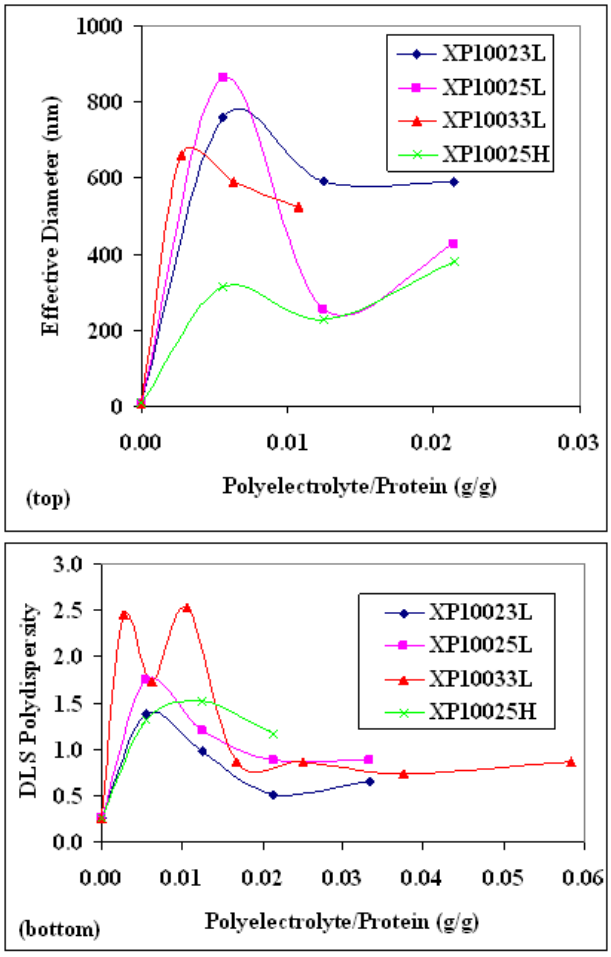

Figure 5.27. DLS measurement of the effective diameter for polyelectrolyte-cellulase complexes; average deviation 10% (top). DLS measurement of polydispersity polyelectrolyte-cellulase complexes (bottom).

The effective diameter and polydispersity at 0 g/g is for the cellulase with no polyelectrolyte. Overall, both figures show abrupt increases in effective diameter and polydispersity once the polyelectrolyte is first added. All samples seem to peak and then decay in size and polydispersity. With increasing polyelectrolyte the zeta potential abruptly drops initially becoming more negative and at the same time the complex size and polydispersity are at their maximum values. Between 0.005 and 0.02 g/g the zeta potential reverses and begins increasing in the positive mV direction which corresponds

to a decrease in complex size and polydispersity. A possible explanation for the dip in Figure 5.26 is as follows. The polyelectrolyte concentration is low in the region where the dip occurs. The negatively charged enzymes attach to the positively charged polymer and at low polymer concentrations the enzymes could cover the surface of the polyelectrolyte. The negative charge density of the enzyme surface would be relatively high, whereas the positive charge of the polyelectrolyte would be neutralized or held in the interior of the complex where it would be shielded and therefore subject to less repulsion and expand with greater complex size and polydispersity. The higher negative charge density of the complex would tend to make the zeta potential more negative. However, the size of the polyelectrolyte-enzyme complex would be much greater than that of the free enzyme, which if enough polyelectrolyte is present, the enzyme would not be able to shield the polyelectrolyte making the zeta potential more positive. If the effect of the negative charge outweighed that of the positive size, the zeta potential would turn more negative and the dip in Figure 5.26 would be accounted for. At higher polyelectrolyte concentrations, the enzyme would no longer shield the charge of the polyelectrolyte and the zeta potential would turns positive. Kitahara et al. (1971) may provide additional support for explaining the dip in zeta potential. Kitahara et al. showed that the zeta potential for increasingly large glass micro-particles became increasingly negative. If the enzymes bind and shield the polymer then the enzyme could appear as a larger negative particle resulting in a larger more negative zeta potential. Once enough polyelectrolyte is added as described, the enzyme would no longer shield the polyelectrolyte and the zeta potential would become more positive.

5.2 Effect of Cationic Polyelectrolytes on the Adsorption of Cellulase to Cellulosic Fiber

This section will examine the effect of cationic polyelectrolytes on the adsorption of cellulase on cellulosic fiber. First is an examination of how the cationic polyelectrolytes themselves adsorb onto the cellulosic fiber, followed by how the polyelectrolytes influence the adsorption of cellulase to the cellulosic fiber.

5.2.1 Fiber Sources Used in Adsorption Study

Bleached softwood kraft pulp was procured from Weyerhaeuser. The fiber length properties were measured for a fiber count sampling of 5000 fibers. The sample contained 1.29% length weighted fines and a length weighted fiber length was 2.20 mm.

5.2.2 Adsorption of Cationic Polyelectrolytes on to Cellulosic Fiber

Figure 5.29 shows the amount of PVSK titrant needed to titrate the filtrate of solutions of varying consistency treated with 10mg/L XP10025L (40% cationicity) polyelectrolyte. The PVSK binds with the unbound cationic polyelectrolyte and is a measure of how much cationic polyelectrolyte remains in solution. Figure 5.28 shows a monotonic decreasing trend with increasing consistency. With increasing amounts of fiber, more polyelectrolyte was removed from the liquid phase and adsorbed onto the fiber. At an extrapolated 1.4% consistency all the polyelectrolyte was adsorbed onto fiber. At this point the fibers were charge-neutralized with polyelectrolyte.

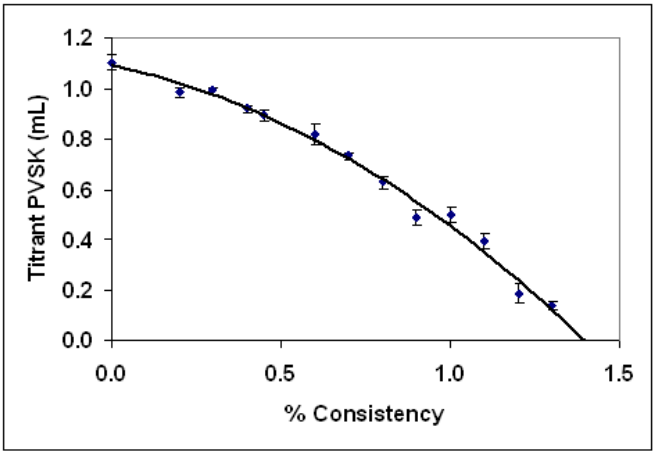

Figure 5.28. Plot of consistency vs. titrant for the adsorption of XP10025L (40% cationicity) polyelectrolyte onto bleached softwood kraft fiber.

The amount of XP 10025L polyelectrolyte adsorbed onto the cellulosic fiber was calculated from the charge titration data and is plotted for various consistencies in Figure 5.29.

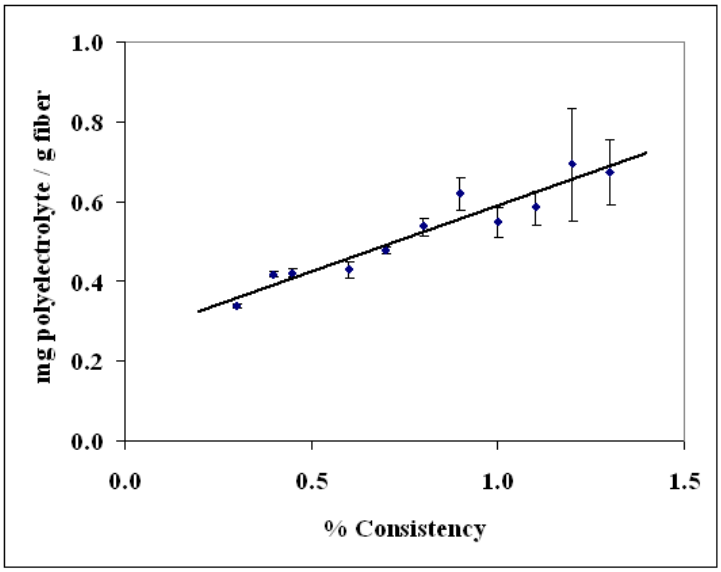

Figure 5.29. Adsorption of XP10025L at various fiber consistencies. The polyelectrolyte was loaded at 10 mg/L final concentration for each case.

The adsorption coefficients are linear with increasing fiber consistency and correspond to polymer dosages of 0.34 to 0.68 kg/mton fiber, which is consistent with other reported coefficients of 0.05 to 2.5 kg/mton OD fiber (Solberg, 2003; Petlicki and van de Ven, 1994).

A Freundlich adsorption isotherm:

$$\frac{x}{m} = Kc^{\frac{1}{n}} \tag{5.6}$$

was applied to the data in Figure 5.30 where *x* is the mass of adsorbate, m is the mass of adsorbent, c is the equilibrium concentration of adsorbate, and K and n are isotherm constants. According to Kadirvelu and Namasivayam (2000), n values between 1 and 10 represent beneficial adsorption. A linearized form of the Freundlich adsorption isotherm was used to evaluate the sorption data and is represented as:

$$\log\left(\frac{x}{m}\right) = \log K + \frac{1}{n}\log(c) \tag{5.7}$$

The constants were calculated from a linear regression, $R^2 = 0.97$, to be K = 0.34±0.021 and n = 3.2±0.45, thus inferring that there is strong adsorption between the polyelectrolyte and cellulose fiber.

Adsorption experiments were also performed for both XP10023L (10% cationicity) and XP10033L (80% cationicity) polyelectrolytes. Extrapolations similar to that made in Figure 5.28 were used to estimate the zero points, which correspond to the amount of polyelectrolyte needed to adsorb (charge neutralize) onto the fiber. Figure 5.30 summarizes the fraction of polyelectrolytes of varying cationicity that charge neutralize the fiber.

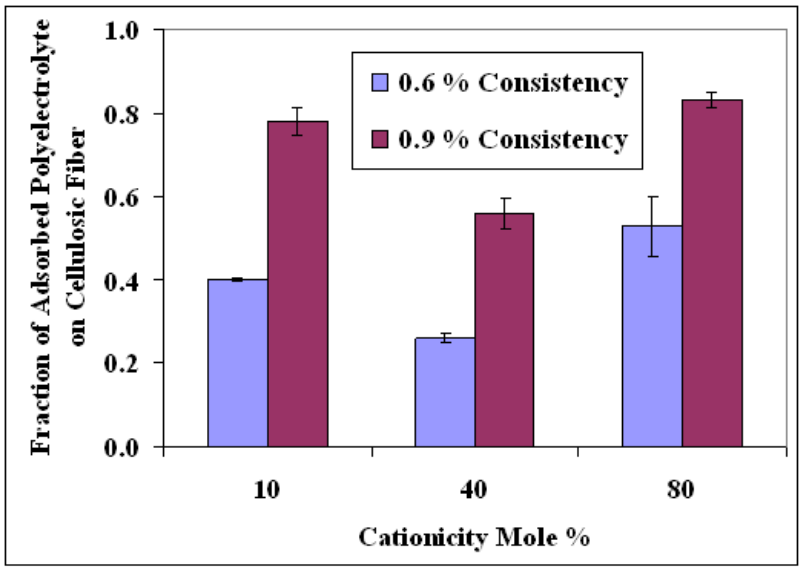

Figure 5.30. Fraction of adsorbed polyelectrolyte on cellulosic fiber for various polymer cationicity and fiber consistency.

The fractional amount of polyelectrolyte that adsorbed to the cellulosic fiber was greater at higher consistency. At 0.6% and 0.9% consistencies, the 40% cationicity sample had the lowest degree of adsorption. Hubbe and Rojas (2008), using X-ray photoelectron spectroscopy (XPS), found that the amount of adsorbed polyelectrolyte decreased with increasing charge density as shown in Figure 5.31.

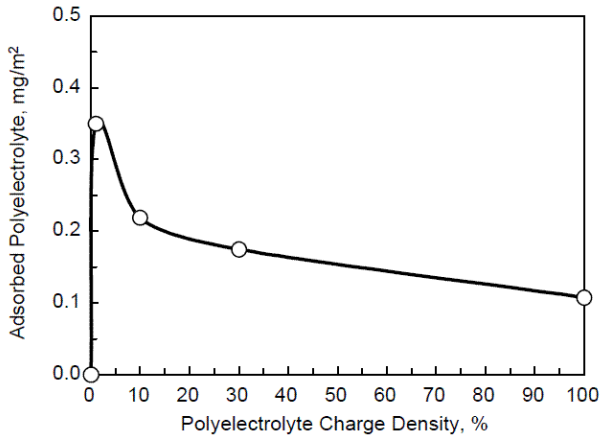

Figure 5.31. Effect of polyelectrolyte charge density on adsorption on cellulose surfaces as measured by an XPS method (Hubbe and Rojas, 2008).

An alternative adsorption procedure (section 4.6.2) was designed to attempt to mimic Hubbe and Rojas. The results in Figure 5.32 show the fractional amount of polyelectrolyte adsorbed to the cellulose fiber as a function of polyelectrolyte concentration for samples with varying cationicity.

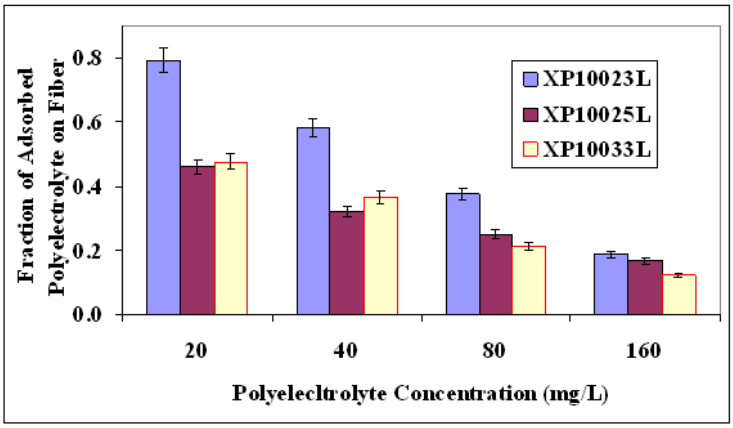

Figure 5.32. Adsorption of polyelectrolyte on cellulosic fiber as a function of polyelectrolyte cationicity and polyelectrolyte concentration. Cationicities: XP10023L (10%), XP10025L (40%), and XP10033L (80%).

At all concentrations, the sorption of the 10% fraction (XP10023L) is greater than that of the other polyelectrolytes. The trends begin to agree with Hubbe and Rojas at 80 mg/L. However, at 40 mg/L the trend is in accord with that shown in Figure 5.30 in that the 40% cationicity polyelectrolyte has the lowest adsorption coefficient. The basis of these differences is outside the scope of this study. The overall adsorption trends in Figure 5.32 for varying cationicity polyelectrolytes are in agreement with the results of other investigators (Wang et al., 1988; Van de Steeg et al., 1992; Hubbe and Rojas, 2008). The adsorption of colloidal particles onto various adsorbents has been known to satisfy a Langmuir isotherm model (Petlicki and van de Ven, 1994). The association constant for the adsorption of a polyelectrolyte onto cellulose is described by the following reactions and expression:

$$\begin{gathered} \text{Free surface} + \text{Polyion} \xleftrightarrow{K_e} \text{Complex} \\ \text{Cellulose fiber} + \text{Polyelectrolyte} \xleftrightarrow{K_e} \text{Complex} \\ K_e = \left(\frac{\theta}{1-\theta}\right)\left(\frac{1}{x}\right) = -\frac{\Delta G}{kT} \end{gathered} \tag{5.8}$$

where θ is the fraction of surface covered by polyelectrolyte, x is the molar fraction of polymer in solution, K_e is the association constant for the surface reaction, ΔG is the apparent free energy of adsorption per polyion molecule, k is the Boltzmann constant, and T is the absolute temperature (Petlicki and van de Ven, 1994). In cases where the differences in molecular size between polymers and solvents are large, it is more appropriate to use weight fractions instead of mole fractions (Song et al., 2003). Apparent free energies of adsorption were estimated using equation 5.2 for 10%, 40%,

and 80% cationicity polyelectrolytes. Table 5.11 summarizes the polyelectrolyte free energy of adsorption coefficients (# kT) onto bleached softwood kraft fiber.

Table 5.11. Free energy of adsorption for cationic Polyelectrolyte to cellulose fiber (# kT / molecule).

Cationicity	10%	40%	80%
mg/L	XP10023L	XP10025L	XP10033L
20	80 ± 4	46 ± 5	48 ± 4
40	59 ± 3	32 ± 3	37 ± 3
80	38 ± 2	25 ± 3	21 ± 2
160	19 ± 2	17 ± 2	12 ± 1
* All samples 1% consistency bleached softwood kraft pulp			

The higher the kT value the more strongly adsorbed the polyelectrolyte is to the surface. In Table 5.11 the apparent energy of adsorption dropped with increasing polyelectrolyte concentration as the fiber was held at a constant 1% consistency; the apparent energy of adsorption decreased with increasing cationicity. At low polyelectrolyte concentrations when the fiber surface is substantially free of polymer the polymer is able to attach at multiple sites thereby increasing the adsorption coefficient and the associated free energy. At higher concentrations, the number of available sites decreases, the polymer attaches to the surface at fewer locations and the distribution coefficient decreases.

Comparative data was found for polyethylenimine (PEI) adsorption onto cellulosic fiber. The free energy for the adsorption of low (M_w=8,000) and high molecular (M_w=600,000) weight polyethylenimine (PEI) onto bleached cellulose fiber (0.2% consistency solution) was 22 kT and 26 kT respectively (Petlicki and van de Ven, 1994). The PEIs contained primary, secondary, and tertiary amine groups in the ratio of 1:2:1. The primary and secondary amines are pH sensitive, while the tertiary amines function well across the

widest pH range. The adsorption energies are similar for the two different molecular weight PEI polymers. The higher molecular weight PEI contains more sites to bind to the fiber but that did not lead to proportionately higher adsorption energy. The XP series polyelectrolytes being compared are composed of only tertiary amine groups making them more effective polyelectrolytes at varying cationicities. At 0.30% consistency, the free energy of adsorption was 33 kT for the XP10025L polyelectrolyte. The energies of adsorption for the XP series polyelectrolytes are not significantly different inferring that their binding is not that different from each other.

5.2.3 Adsorption of Cellulase on Polyelectrolytes Treated Cellulosic Fiber

The sorption of cellulase on polyelectrolyte-treated fiber (1% consistency) dispersed in water was measured at two enzyme levels, 0.25% and 0.5%, and were used along with polymers of 10, 40%, and 80% cationicity. The measurements were made at 4^{o}C to minimize hydrolysis. The polyelectrolyte increased cellulase binding to fiber across all cationicities (~40% increase). Dissociation constants were calculated using equation 5.4 and the results are provided in Figure 5.33. Values for the amount of cellulase bound to the polyelectrolyte-treated fiber were corrected by subtracting the amount of bound enzyme to the fiber alone. For the 40% cationicity polymer, the K_d results in Figure 5.33 compares reasonably well with the value of 5 nM obtained from the light scattering experiments, given that the two were estimated from two completely different methods; both infer strong binding. The smaller binding at 80% cationicity was comparable to the 40% cationicity sample. The 10% cationicity samples resulted with the largest K_d of the

three polyelectrolytes meaning that the binding is significant but less relative to the 40% and 80% cationicity containing samples.

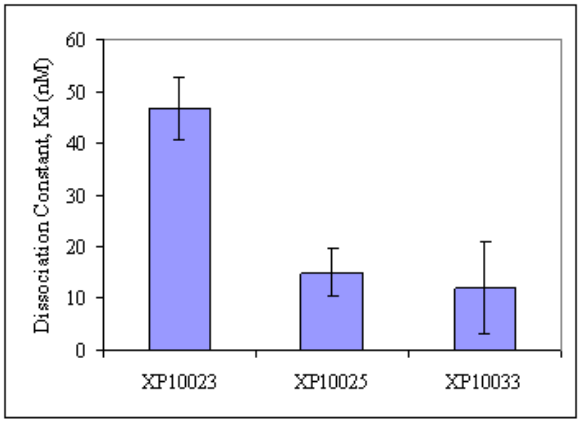

Figure 5.33. Summary of the dissociation constants for cellulase adsorbed onto the polyelectrolyte-fiber dispersions.

It was found through an unpaired t-test (Appendix D) that there was a positive statistical significance between all polyelectrolyte-treated samples with a control containing no polyelectrolyte.

In addition to the dispersed fiber experiments, the cellulose fiber was processed into handsheets. Measurements of the adsorption of cellulase to fiber were made with and without polyelectrolyte. Because polyelectrolytes are known to adsorb differently to fiber fines and long fiber (Hartley and Banerjee, 2008), the fines and short fiber were removed from a sample of bleached softwood kraft pulp. Table 5.12 summarizes the fines and fiber content of bleached softwood kraft pulp in its initial state and after being fractionated.

Table 5.12. Properties of pulp fibers and fines.

	Before Fractionating	After Fractionating
Fiber count	5000	5000
Percent length weighted fines	1.29% (18.64%)	0.27% (5.12%)
Mean length weighted length	2.20 (1.04) mm	2.20 (1.35) mm
* Arithmetic averages in parentheses		

The pulp fiber was made into handsheets according to TAPPI test method T 205 at a basis weight of 53 ± 3 gsm. They were air dried overnight; air drying instead of oven drying was done in an attempt to minimize hornification (Diniz et al., 2004; Brancato et al., 2007). Half the handsheets were treated with XP10031H and the reference handsheets were treated with water and again air dried overnight. Handsheets were soaking in a 0.1% - 0.5% (v/v) solutions of cellulase at 4°C. The enzyme remaining in the supernatant was measured with the BCA protein assay, and the amount of enzyme bound to the sheet determined by difference. Figure 5.34 summarizes the results.

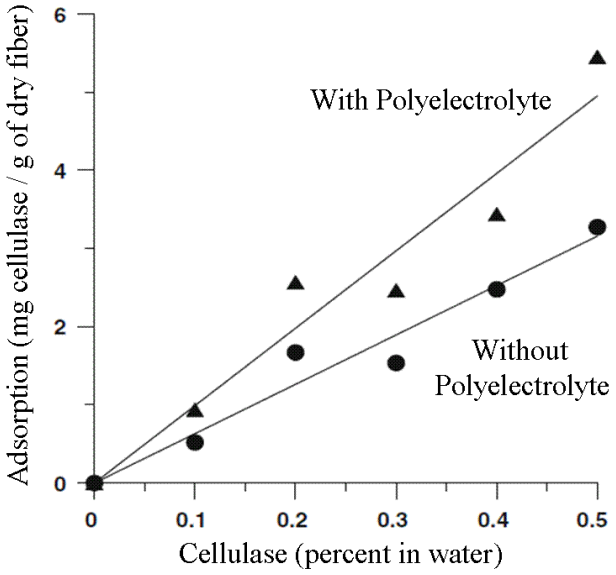

Figure 5.34. Adsorption of cellulase to kraft softwood fiber handsheets. Handsheets were dipped in XP10035 polyelectrolyte; average percent error is 12%.

As with the dispersed fiber, the addition of the polyelectrolyte increased the adsorption of cellulase onto the handsheets. A dissociation constant was also estimated for the data in Figure 5.34 using equation 5.4. Again, values for the amount of cellulase bound to the polyelectrolyte-treated fiber were corrected by subtracting the amount of bound enzyme to the fiber alone. The polyelectrolyte equilibrium concentration was estimated from Figure 5.32 for a 100 ppm dosage to be approximately 20% of the polyelectrolyte bound. The estimated K_d was 4±1 nM, which suggests the binding of cellulase to polyelectrolyte treated fiber is significant. Recall that Goldstein et al. (1993) reported the cellulase carbohydrate binding domain (CBD) dissociation constant was in the 1 μM range.

Up to this point it is claimed that the polyelectrolyte enhances the adsorption of cellulase to the substrate. An experiment was conducted where a handsheet was added to a solution of cellulase (0.5%) and either 0 mg/L, 100 mg/L, or 1000 mg/L XP10035 (35% cationicity) polyelectrolyte. The handsheet was present at 1% consistency. All solutions were maintained at 4^{o}C and the adsorption measured after 20 minutes. Figure 5.35 summarizes the results.

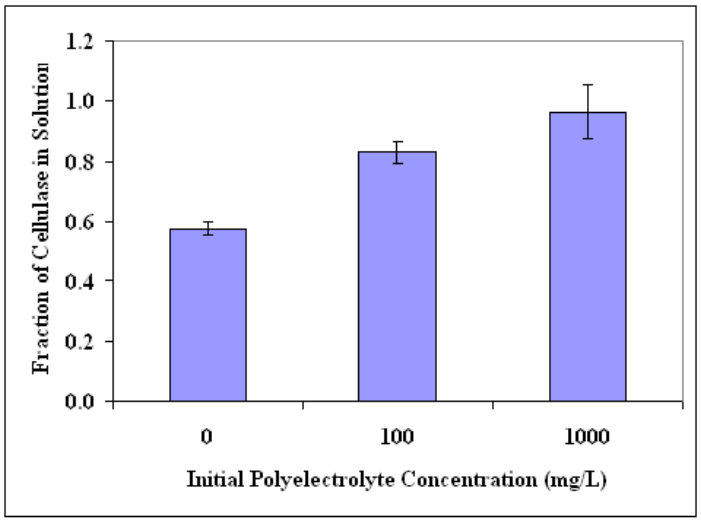

Figure 5.35. Fractional amount of cellulase remaining in solution with varying polyelectrolyte concentration in the presence of a handsheet.

The Figure 5.35 shows that the adsorption of cellulase decreased with increasing polyelectrolyte. The conclusion from Figure 5.35 is that the cellulase is attracted by and associates with the polyelectrolyte. With increasing polyelectrolyte, the cellulase stays in solution and less is bound to the substrate. Instead of treating a fiber with the cationic polyelectrolyte and then trying to adsorb cellulase to the modified surface, here the cellulase is interacting with the polyelectrolyte and when that solution was added to a handsheet in solution, the cellulase stays with the polyelectrolyte. Finally, the effect of cationicity and molecular weight was tested on the adsorption of cellulase to the modified cellulose fiber (procedure found in section 4.6.3). Figure 5.36 summarizes the adsorption of cellulase for varying cationicity and molecular weight polyelectrolytes.

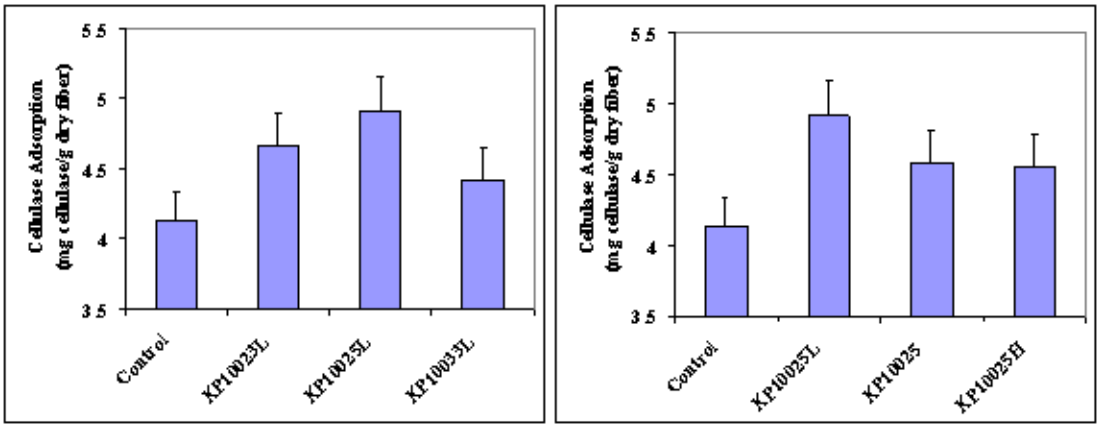

Figure 5.36. Summary for adsorption of cellulase for varying cationicity (left) and varying molecular weight (right) polyelectrolytes.

In the left figure, the samples show that low, medium, and high cationicity (10%, 40%, and 80% cationicities) resulted in higher adsorption than the control. Unpaired t-test results (Appendix D) suggest that there is a statistical significance between the control and both 10% and 40% cationicity samples. There was not a statistical difference between the control and the 80% cationicity sample where adsorption falls off for the high cationicity polymer. As for varying molecular weight, all samples resulted in higher adsorption than the control. It was seen that cellulase adsorption decreased slightly with increasing molecular weight from 3 to 12 MDa. The differences observed with changing cationicity and molecular weight are significant but small. Unpaired t-test results (Appendix D) suggest that for varying molecular weight, there was statistical significance between the control and the XP10025L sample but the higher molecular weight samples (each 40% cationicity) did not show a statistical difference compared with the control or between themselves. Interpretation of these differences is not warranted with the data at hand. However, it is safe to conclude that adsorption is relatively insensitive to polyelectrolyte charge and molecular weight. Results from an analysis with atomic force

microscopy (AFM) show insensitivity of an AC240TS probe to the fiber surface treated with the same polyelectrolytes (see Appendix C). The adhesive pull-off force between the fiber treated with various cationic polyelectrolytes and concentration did not show significant differences with respect to the surface properties of the fiber.

5.2.4 Discussion of Polyelectrolyte and Cellulase Adsorption to Cellulose Fiber

With a constant polyelectrolyte loading and increasing cellulase loading it was shown that the XP series polyelectrolytes were strongly bound to the cellulose fiber. At low polyelectrolyte dosages of 80 to 160 mg/L, the lower charge density polymers adsorbed slightly better than high charge density samples.

The differences observed with changing cationicity and molecular weight are significant but small where the adsorption was found to be relatively insensitive to polyelectrolyte charge and molecular weight. The fractional amount of cellulase that adsorbed went up approximately 30% to 40% in the presence of the polyelectrolyte. Two different types of cellulase adsorption strategies were tried; one was combining cellulase with the polyelectrolyte and then adding it to the fiber suspension. The second strategy was first treating the fiber with polyelectrolyte and then the treated fiber with cellulase. It was found that the cellulase followed the polyelectrolyte. When the polyelectrolyte was in excess and in free solution then the cellulase stayed in solution, whereas there was an increase in the cellulase adsorption where the fiber was previously treated with the polyelectrolyte. Polyelectrolytes of low and medium cationicity were more efficient in

adsorbing cellulase to fiber, but even high cationicity polymers showed greater binding than a control without any polyelectrolyte

In section 5.1.11 it was mentioned that the repulsive electrical double layer thickness may be as high as 1000 nm. The addition of electrolytes (increasing ionic strength) can cause a screening of coulombic repulsion decreasing the double layer thickness, which is illustrated in Figure 5.37. This screening decreases the double layer by a depletion mechanism (Delgado et al., 2005).

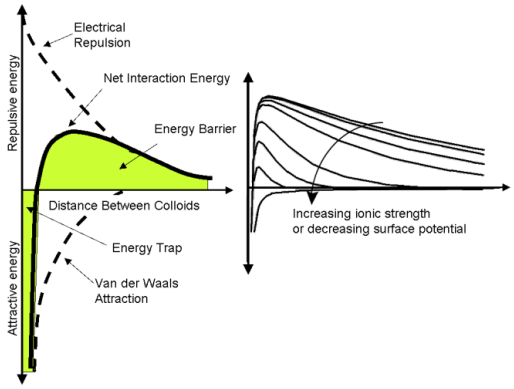

Figure 5.37. Schematic of a net interaction curve; produced by subtracting the attractive curve from the repulsion curve (left) and energy barrier curves with increasing ionic strength or decreasing surface potential (right).

Bridging and patching mechanisms can be used to reduce the repulsive electrical double layer by reducing surface potential; Figure 5.38 shows a schematic of both patching and bridging mechanisms for negatively charged fibers and enzymes, which are either patched or bridged together by an oppositely charged polyelectrolyte.

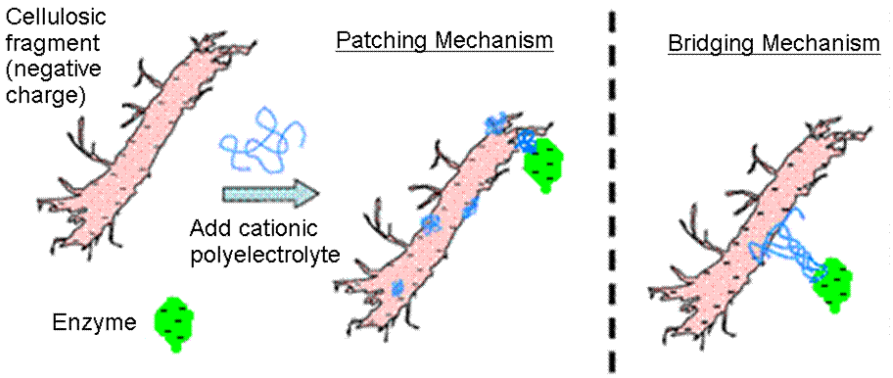

Figure 5.38. An example of flocculation mechanisms.

Once the polyelectrolyte anchors, it can extend out into the solution and act as a bridge as it absorbs to an oppositely charged surface (Eklund and Lindstrom, 1991). Since the polyelectrolyte chain can extend beyond the electrical double layer of the fiber, the extended chain increases the possible area for flocs to form (Neimo, 1999). Typically, the charge patch mechanism occurs with highly charged cationic polyelectrolytes having molecular masses ranging from approximately $1x10^5$ to $2x10^6$ g/mole, which are on the low end of the XP series samples. Bridging polyelectrolytes typically are high molecular weight, greater than $1x10^6$ g/mole and up to approximately $20x10^6$ g/mole (Eklund and Lindstrom, 1991; Neimo, 1999). The adsorbed conformations of the polyelectrolytes contain tail, loop, and train structures, which overcome the repulsive electrical double layer. Thus, a reduction in the thickness of the double layer can be achieved to increase the adsorption of enzyme, which may be advantageous for increasing enzymatic hydrolysis. The polyelectrolyte layer thickness is consistent with a patching mechanism. Adsorption experiments indicate that there is a significant (~40%) increase in the amount of cellulase absorbed to the fiber with the addition of the polyelectrolyte.

5.3 Effect of Cationic Polyelectrolytes on the Rate of Enzymatic Hydrolysis

In the previous sections, the results focused on how cationic polyelectrolytes and enzymes interact in solution and how polyelectrolytes and cellulase adsorb onto cellulosic fiber. It was shown that the presence of the polyelectrolyte increases the amount of cellulase adsorbed onto the fiber complex. In this section, the results and discussion will focus on the kinetics, which will demonstrate that the addition of the cationic polyelectrolytes can increase the rate of enzymatic hydrolysis of cellulose.

5.3.1 Effect of Varying Conditions on Cellulase Activity

Cellulase activity was measured with Novozymes 22CG; the charge and protein concentrations were -7 ± 1 C/g and 153 ± 1 mg/mL, respectively. First, activity was tested for temperature ranging from 4^{o}C to 60^{o}C. The temperature profile in Figure 5.39 shows an optimal activity at 50^{o}C, which is the reported optimum temperature for cellulase from *T. reesei*. From 4^{o}C to 22^{o}C the relative activity ranged from 3.3% to 9.2%. At 60^{o}C the relative activity dropped to 6.6% of the optimum value.

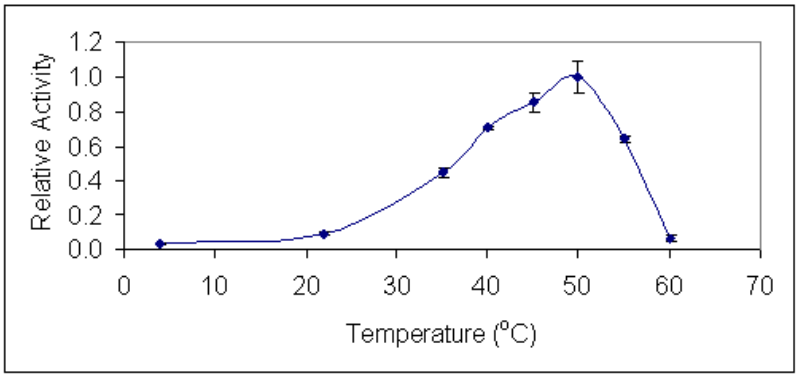

Figure 5.39. Relative activity as a function of temperature.

Next, the effect of pH on the activity was tested, which is summarized in Figure 5.40. Activity is optimal around pH 4.8 to 5.0. The cellulase has broad pH stability. This is advantageous in that the inherent pH of cationic polyelectrolytes solutions ranging from low to high concentrations (10 mg/L to 1000 mg/L) range between 3.8 to 5.0.

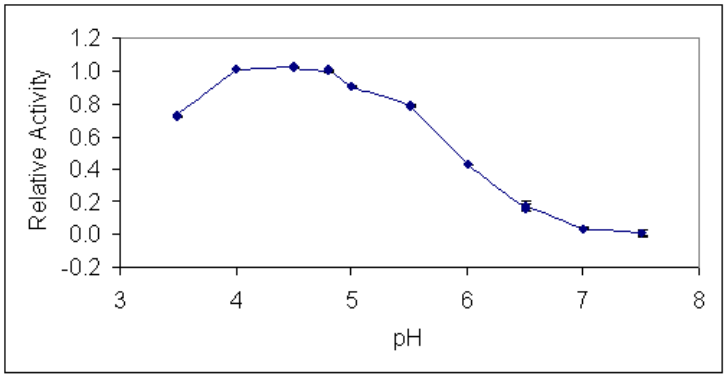

Figure 5.40. Relative activity as a function of pH.

The cellulase and XP series polyelectrolytes operate around the same pH domain. The cellulase activity declines with pH values greater than 5.0 and at a pH of 7.5 the relative activity is approximately zero. The cellulase activity was also tested at varying ionic strengths which affect both cellulase binding and activity. Surface repulsion from the

electric double layer, which affects binding, is also affected by ionic strength. Figure 5.41 shows 50 mM citrate buffer at the optimal ionic strength for the cellulase activity that corresponds to the optimal conditions from NREL.

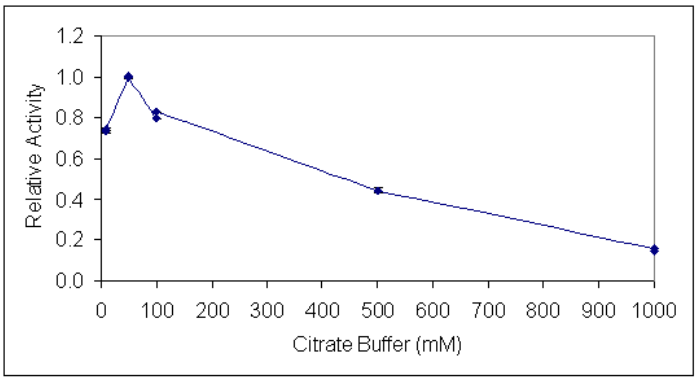

Figure 5.41. Relative activity vs. ionic strength; all solutions prepared at pH 5.0.

5.3.2 Temperature Dependence on Cellulase Hydrolysis of Cellulosic Fiber

If was found that there is a temperature dependence on the enzymatic hydrolysis of cellulosic fiber. Three general types of cellulosic fiber were used: bleached kraft softwood pulp, bleached kraft hardwood pulp, and Whatman grade 1 filter paper. A summary of fiber properties is summarized in the following Table 5.13; uncertainty in fiber length was less than 1%. The Whatman #1 filter paper was used for measurement of enzyme activity. Variations of these substrates were used, for example, with fines removed or with only fines.

Table 5.13. Fiber properties measured by fiber quality analysis (FQA).

	Fines (%)	Length Weighted Fiber length (mm)	
		Initially	After 1 hour hydrolysis
Whatman Fiber	9.70	0.94	
Hardwood Fiber	24.5	1.04	
Hardwood Fiber 48 mesh	0.47	1.02	1.01
Softwood Fiber	9.12	2.12	2.06
Softwood Fiber 28 mesh	0.73	2.60	2.39
Softwood Fines	56.5	0.155	

Hydrolysis experiments were conducted using Novozymes Cellic CTec. Fiber fractions (28 mesh and 48 mesh) were prepared using the TAPPI T233 standard method. Relative glucose generation over 1 hour (initial rate) with the dispersed and handsheet fibers are provided in Table 5.14 with average values plotted in Figure 5.42 (Lu et al., 2010). These measurements are akin to activity measurements. The results are normalized to the value obtained at 50^{o}C for the Whatman filter paper. Results from an ANOVA analysis (Appendix D) supported that the relative glucose production at different temperatures appeared not to be different for both handsheet and dispersed fiber samples. Results from the ANOVA analysis for both handsheets and dispersed fiber samples also concluded that the relative glucose production for the different fiber furnishes (cellulosic fiber slurries) for both handsheet and dispersed samples were not the same.

Table 5.14. Relative glucose generation for various furnishes and temperatures.

	Relative glucose generation %[1]					
T (^{o}C)	Whatman # 1 Filter Paper	HWD[2]	HWD (48 mesh)	SWD[2]	SWD (28 mesh)	SWD Fines
Handsheet						
30	29 ± 1	19 ± 1	20 ± 3	24 ± 3	32 ± 4	35 ± 11
40	60 ± 1	23 ± 1	27 ± 5	32 ± 1	44 ± 4	66 ± 15
50	100 ± 7	35 ± 3	31 ± 6	36 ± 3	44 ± 22	94 ± 31
Dispersed						
30	86 ± 1	42 ± 4	29 ± 2	72 ± 1	70 ± 6	106 ± 3
40	168 ± 5	45 ± 1	38 ± 1	82 ± 1	78 ± 10	174 ± 5
50	218 ± 2	50 ± 1	48 ± 7	77 ± 1	83 ± 14	233 ± 8
[1]average deviation obtained from 2 or 3 measurements; [2]unfractionated						

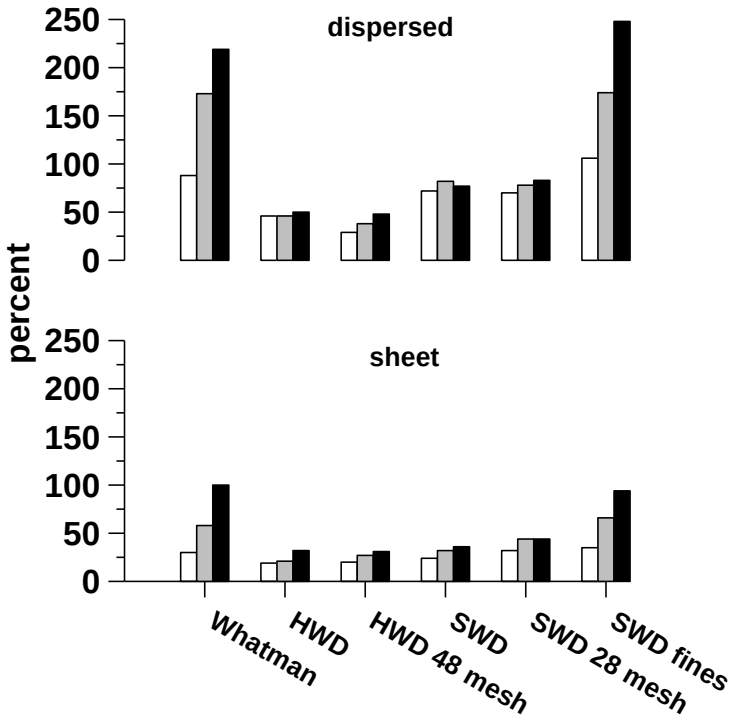

Figure 5.42. Dependence of enzyme activity on furnish type and temperature. The clear, gray, and bold bars represent 30, 40 and 50^{o}C, respectively. HWD and SWD refer to unfractionated hardwood and softwood fiber, respectively. The results are normalized to the Whatman sheet, which is assigned a value of 100%.

The fiber distribution in each subsample taken for replicate measurements can differ appreciably, which is a common problem in the measurement of properties of fiber suspensions. The dispersed fibers are about twice as reactive as those present in the handsheet. This is to be expected because inter-fiber bonding in the handsheet reduces the surface area accessible to the enzymes. The fines are also up to six times more reactive than the longer fibers due to their higher surface area. The crystallinity index of the fines and the 28-mesh fiber was measured by IR spectroscopy and was found to be 1.4 and 0.9, respectively. Crystallinity imparts recalcitrance towards hydrolysis (Harris et al., 2009); evidently, the higher surface area of the fines more than compensates for the loss of reactivity from the higher crystallinity.

The temperature dependence of the activity shown in Figure 5.42 demonstrates that the trends for the handsheet and the dispersed fiber are similar. The most striking feature is that the hydrolysis of the fines is strongly temperature dependent whereas that of the longer softwood fractions is much less so. It is known that the adsorption of the enzyme to cellulosic fiber is inversely dependent on temperature. For example, Ooshima et al. (1983) found that the adsorption of endoglucanase obtained from *Trichoderma viride* on the surface of pure cellulose increased with temperature from 5^{o}C up to 28^{o}C and then decreased as it was measured up to 50^{o}C. The slope of the increase depended on the degree of crystallinity of the cellulose, while above 28^{o}C the adsorption decreased the same rate regardless of crystallinity. Palonen et al. (1999) reported that the partition coefficient (between solid and liquid phases) for the adsorption of exoglucanase from *Trichoderma reesei* and its catalytic and carbohydrate binding domain (CBD) is

temperature dependent, falling two- to four-fold as the temperature was increased from 4°C to 40°C. Linder and Teeri (1996) showed that adsorption of the CBD of *T. reesei* to the surface of crystalline cellulose is inversely dependent on temperature between 4°C and 30°C. Ong et al. (1993) demonstrated that the adsorption of the CBD of an exoglucanase from *Cellulomonas fimi* dropped by a factor of 2.7 between 4°C and 50°C. Kim and Hong (2000) showed that the adsorption processes of CBH I and II from *T. reesei* were exothermic.

The catalytic step should be directly temperature dependent, which must mean that the inverse temperature dependence of the adsorption step can offset that of the catalytic step. If the cellulase is limiting most of it will adsorb to the substrate and the rate will increase with temperature. However, if this is not the case then increasing temperature will decrease the degree of adsorption on the one hand and increase the rate on the other; the two effects would tend to cancel. The adsorption of the cellulase to the 28-mesh fraction was 1.28 ± 0.03 mg protein/g fiber; the corresponding value for the fines was 3.70 ± 0.02. Clearly, proportionately much more of the cellulase adsorbed to the fines. Because a higher fraction of the cellulase remains free for the longer fiber its adsorption behavior is more likely to be affected by temperature leading to an overall insensitivity in the rate of hydrolysis.

Activation energies calculated from first order kinetic parameters were calculated from both handsheet data and dispersed fiber. A first order kinetic model was assumed for the initial rate kinetics. The activation energies for the handsheet data were found to be

greater than for those calculated from the dispersed fiber data summarized in the following table.

Table 5.15. Activation energy for various furnishes from data in Table 5.14.

Activation Energy (kcal/mol)					
Whatman	HWD	HWD (48 mesh)	SWD	SWD (28 mesh)	Fines
Handsheet					
12 ± 2	5.4 ± 0.9	4.3 ± 0.7	6.2 ± 1	3.1 ± 0.5	9.5 ± 1.5
Dispersed					
8.9 ± 2	0.8 ± 0.2	4.9 ± 0.8	0.5 + 0.1	1.7 ± 0.3	7.6 ± 1.2

The higher relative surface area with the dispersed fiber results in a lower relative activation energy of hydrolysis. Fines and shorter fiber, i.e. filter paper, resulted with higher activation energies compared to the longer fiber furnishes; those two samples showed the greatest temperature dependency compared to the rest of the samples. Samples with lower temperature dependency resulted with lower activation energies. The relative activation energies reported for handsheets agree with a related study where an apparent activation energy for the hydrolysis of a cellulose film was reported to be 8.8 kcal/mol (Hu et al., 2009).

5.3.3 Comparison of the Effect of Polyelectrolytes on Cellulosic Fiber and Cornstarch Hydrolysis

A study was performed to determine the effect various cationic polyelectrolytes have on the enzymatic hydrolysis of both cellulose fiber and cornstarch. It will be shown that cornstarch can also benefit from the addition of polyelectrolyte accelerant. Ashland-Hercules Water Technologies, Wilmington, DE, supplied the polyelectrolytes for this

study. A screening of various polyelectrolyte properties was done with the Ashland samples; however, the great majority of the work done in this thesis has been with polyelectrolytes (XP series) supplied by Eka Chemicals (a subsidiary of AkzoNobel).

The charge of enzyme, polyelectrolyte, and substrate are important in the adsorption and flocculation of the hydrolytic complexes. A charge characterization was performed on both the bleached softwood kraft pulp and the cornstarch. The results are summarized in Table 5.16. Back titration was performed using either PDADMAC, a low molecular weight polyelectrolyte, or XP10023L polyelectrolyte.

Table 5.16. Summary of cellulosic fiber and cornstarch charge densities.

Samples	C/g	± C/g
10% Cationicity XP10023L Polyelectrolyte	+113	6
Softwood bleached Kraft fiber using XP10023L	-0.04	0.01
Softwood bleached Kraft fiber using PDADMAC	-0.13	0.05
Cornstarch using XP10023L	-0.004	0.001
Cornstarch using PDADMAC	-0.07	0.02

The cellulose substrate has a relatively small charge density per unit mass. The charge estimate is approximately 3 times greater if PDADMAC is used instead of XP10023L. The PDADMAC molecular weight is at least 10 times lower and thus may adsorb in a more packed manner and give a better estimate of the fiber surface charge. Surface charge measurements have been reported for kraft (pine) to be -0.42 C/g (Rao and Kuys,

1995), which is in general agreement with the above measured value. In another study, the surface charge density for bleached softwood kraft pulp (a mixture of Norway spruce and Scots pine), was reported to be equivalent to -0.21 C/g (Enarsson et al., 2009). Cellulosic fibers produced from the pulping process have been likened to polyelectrolytic gels because of their anionic charge (Lindstrom and Carlsson, 1978; Scallan and Grignon, 1979). The charges within the cellulosic gel cause electrostatic repulsions that result in swelling of the fiber. Therefore, the degree of fiber swelling is dependent on the amount of charge, ionic strength, and the type of counter-ion (Lindstrom, 1992).

Back charge titration results for cornstarch are summarized in Table 5.16. As with cellulose, it was confirmed that cornstarch also has a net negative charge. The same polyelectrolyte solutions were used to back titrate for the cornstarch charge density. For both polyelectrolytes the active cornstarch substrate was found to have a relatively small charge density per unit mass, less than that of fiber. The charge density for raw cornstarch was reported to be less than -2 μeq/g (Song et al., 2009) and from Table 5.16 the -0.07 C/g converts to -0.73 μeq/g, showing that the charge density is in reasonable agreement. These two substrates were used in a screening of polyelectrolytes.

Ashland provided a variety of cationic polyelectrolyte samples based on their Praestol® product line. Specific molecular weights were not made available but were higher than those obtained from Eka Chemicals. These Ashland samples were used for early kinetic screening. Details of each sample series were obtained through correspondence with

Ashland. The BS series are linear AM/Q-9 dry polyelectrolytes in the order of increasing cationic charge. The labels for the type of co-polymers used are short for: [2-(acryloyloxy)ethyl] trimethylammonium chloride (Q-9), (3-acrylamidopropyl) trimethylammonium chloride (APTAC), and acrylamide (AM); molecular structures are summarized in the following Figure 5.43. A second series (K-#-L and K-#-FL) consisted of linear AM/Q-9 emulsions also listed with increasing cationic charge. The K-295-FL sample is a linear Q-9 homopolymer emulsion with high cationic charge. The BC series consist of linear AM/APTAC dry copolymers with increasing cationic charge. The last Praestol® series K-#-FLX consisted of branched AM/Q-9 emulsions ranked by increasing cationic charge.

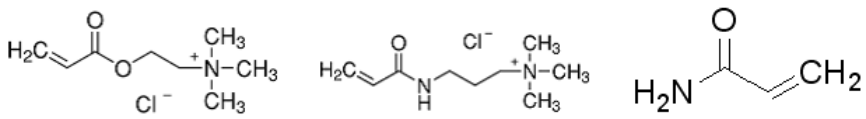

Figure 5.43. Monomer units constituting cationic polyacrylamide co-polymers. (left) [2-(acryloyloxy)ethyl]trimethylammonium chloride (Q-9), (middle) (3-acryl amidopropyl)trimethylammonium chloride (APTAC), (right) acrylamide (AM).

Properties of the polymer sets are summarized in Table 5.17 showing the diverseness of polymer properties represented. Through charge titration a total charge of the cationic polyelectrolytes was measured for each sample. Some of the samples were supplied as either a dry solid or an emulsion; the percent of active substance in the emulsions is also summarized in Table 5.17. The total charge per unit mass ranges from 43 to 420 C/g or approximately 1 to 56% cationicity. The estimated percent cationicity came from the charge verses cationicity regression in equation 5.1. Some viscosity information is

provided for these samples. For the BS series there is an observed increase in viscosity with increasing cationicity.

Table 5.17. Summary of Ashland polymer set.

Sample	Dry solid or Emulsion	Type of co-polymer	Total Charge Amount (C/g)	Viscosity 0.5% wt (mPa-s)	Viscosity 0.1% wt (mPa-s)	Estimated Cationicity %	Expected Ionic Charge
K226FLX	Emulsion	AM/Q-9	58			1	weakly
K274FLX	Emulsion	AM/Q-9	60			1	weakly
K275FLX	Emulsion	AM/Q-9	130			12	medium
K279FLX	Emulsion	AM/Q-9	119			10	medium
K290FLX	Emulsion	AM/Q-9	169			18	medium
K111L	Emulsion	AM/Q-9	58			1	weakly
K122L	Emulsion	AM/Q-9	89	4500	1000	6	medium
K133L	Emulsion	AM/Q-9	105	4500	900	8	medium
K136L	Emulsion	AM/Q-9	127			11	medium
K148L	Emulsion	AM/Q-9	127			11	medium
K260FL	Emulsion	AM/Q-9	123			11	medium
K290FL	Emulsion	AM/Q-9	123			11	medium
K295FL	Emulsion	Q-9	188			21	strongly
835BS	Dry solids	AM/Q-9	160	3500	100	17	medium
855BS	Dry solids	AM/Q-9	315	4000	150	40	medium
857BS	Dry solids	AM/Q-9	312	6000	200	40	strongly
858BS	Dry solids	AM/Q-9	420	6500	200	56	very strongly
859BS	Dry solids	AM/Q-9	391	6500	200	52	very strongly
610BC	Dry solids	AM/APTAC	43	450	35	1	weakly
611BC	Dry solids	AM/APTAC	109	450	35	9	weakly
644BC	Dry solids	AM/APTAC	262	700	70	32	medium
650 BC	Dry solids	AM/APTAC	189	700	65	21	medium

Samples were prepared with either fiber or corn starch, each at 1% consistency, dosed with 500 and 100 mg polyelectrolyte/L, respectively and reacted for six hours at 50^{o}C in a shaking water bath at 150 rpm. The results for the hydrolysis screening are reported in Figure 5.44. The set of commercial polyelectrolytes were screened for their effect on the performance of α-amylase on corn starch and of cellulose on fiber for a 6 h reaction time. Glucose yields from cornstarch and fiber were each normalized to the maximum yield for each case. The controls are at the point (0,0) where no polyelectrolyte is present; the best overall polyelectrolyte would have a coordinate of (1,1).

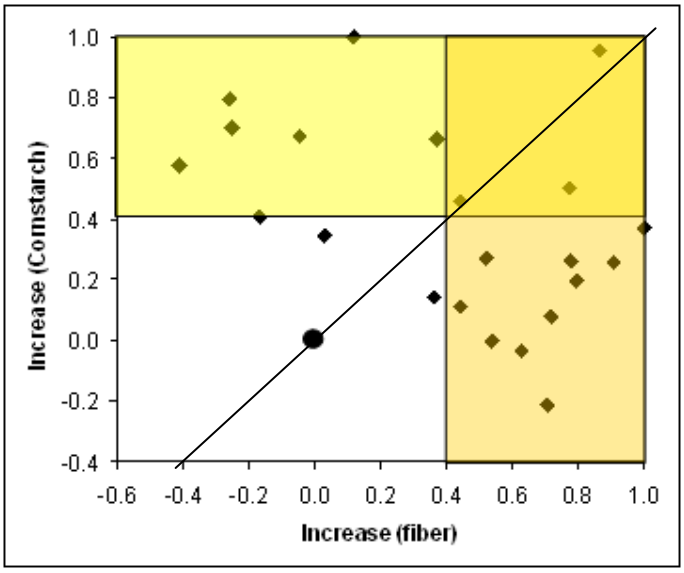

Figure 5.44. Hydrolysis results from screening of varying cationic polyelectrolytes supplied from Ashland Water Technologies.

Rate measurements made in some cases showed that 6 h is at the high end of the linear part of the curve, so the glucose yields correspond approximately to the initial rates. Several polymers were found to be effective in enhancing both the cornstarch and fiber applications albeit to varying degrees. It is striking that except for three instances where there was no effect; the polyelectrolytes provide a clear benefit for the cornstarch application. Results from an unpaired t-test for the cornstarch screening resulted with 19 of 22 sample means being greater than the control (no polyelectrolyte added) and 14 of the 22 samples were found to be positively statistically significant. For the fiber work, five of the polyelectrolytes tested were inhibitory; they have negative values on the abscissa. The main conclusion is that the effect of the cationic polyelectrolytes is non-specific in that it boosts the performance of two completely different systems. Results from an unpaired t-test for the fiber screening resulted with 17 of 22 sample means being greater then the control (no polyelectrolyte added) and 9 of the 22 samples were found to

be positively statistically significant. The negative responses for cornstarch and fiber seemed to be a result of samples with the lowest cationicities.

5.3.4 Effect of Polyelectrolyte from Eka Chemicals on the Hydrolysis of Cellulosic Fiber

First, cellulase activity was tested in the presence of various polyelectrolytes using the NREL assay.

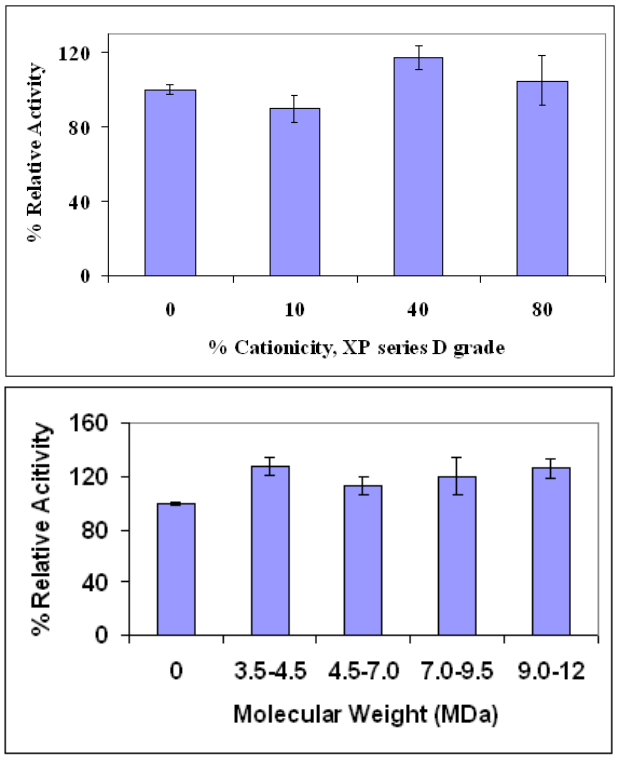

Figure 5.45. Relative Activity for varying cationicity and molecular weight XP series polyelectrolytes (1000 mg/L). Relative activity screening for various, (Top) XP series L grade polyelectrolytes of various cationicity and (Bottom) XP series of various grade polyelectrolytes at 40% cationicity.

The results in Figure 5.45 show that relative activity is not significantly different from the reference control with no polyelectrolyte. The NREL activity assay does not include agitation. The assay tests performance of the enzyme in a static solution. Reaction rates typically increase in the presence of agitation, which is the case here. To verify that agitation makes a difference the four samples in Figure 5.45(top) were run and compared against each other.

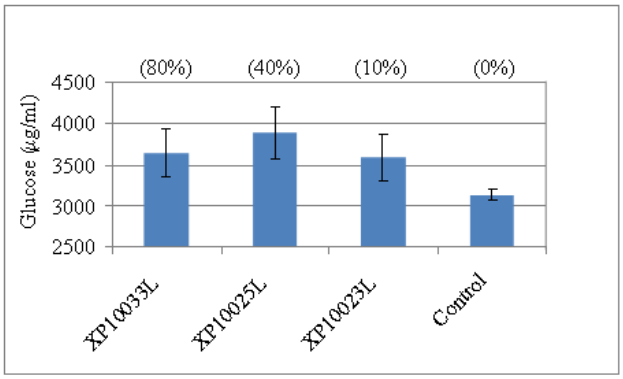

Figure 5.46. Effect of varying polyelectrolyte cationicity; 1000 ppm (XP series L grade) after 6 hours with samples being agitated in a 50^{o}C, 150 rpm shaking water bath. Samples were loaded with 1 g cellulase (Pergalase 7547)/L on bleached softwood fiber.

The results in Figure 5.46 show that there is an improvement in the hydrolysis by having the added agitation. While all three polyelectrolytes increase the rate of hydrolysis, there are no major differences among them, indicating that the rate is independent of polyelectrolyte cationicity.

In an enzymatic saccharification study regarding the biodegradability of soybean-hulls, Enayati et al. (1995) reported on the difference between a stirred system and a water bath agitated system. Stirring and shaking did not have the same effect; stirring in fact had a

significantly positive greater effect on the saccharification kinetics. In a related study, it was shown that the amount of stirring matters on the saccharification kinetics (Ingesson et al., 2001).

To achieve better mixing a bioreactor, BioFlo 3000 from New Brunswick Scientific, was used for its ability to control temperature and agitation; reactions were conducted at 50°C. Figure 5.47 shows that agitation increases the hydrolytic rate.

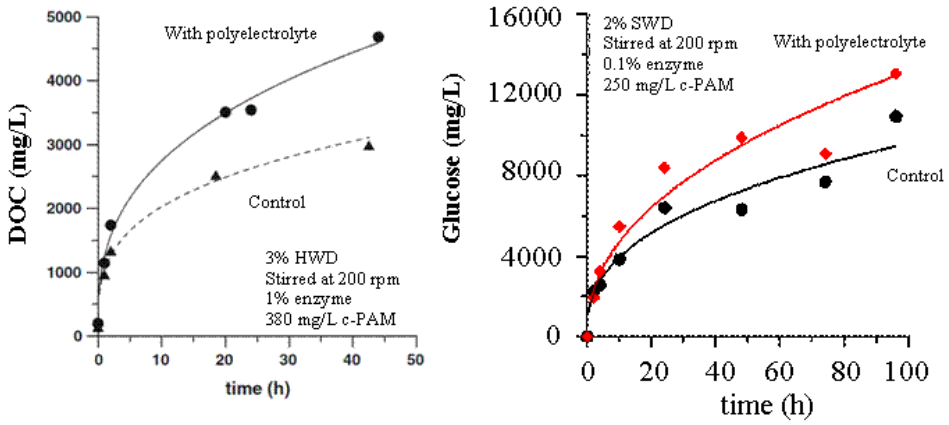

Figure 5.47. Effect of cationic polyelectrolyte on different furnish types with agitation. (Left) Effect of cationic polyelectrolyte, 1000 ppm (XP10024, 38% active ingredient, ~6.7 MDa), on the efficiency of 1 g cellulase (Optimase CX 40L)/L on bleached hardwood fiber. (Right) Effect of cationic polyelectrolyte, 250 ppm (XP10035), on the efficiency of 0.1 g cellulase (Cellis CTec)/L on bleached softwood kraft fiber.

Figure 5.47(left) shows the accumulation of dissolved organic carbon (DOC) over time. Figure 5.47(right) shows the accumulation of glucose over time. Without agitation (i.e. activity assays) the hydrolysis rates in the presence of cationic polyelectrolytes change only slightly. With agitation the enzymatic hydrolysis rates increase substantially. Cationic polyelectrolytes are flocculants. Without agitation the fibers floc, thereby

reducing surface area, which offsets the benefit of the polyelectrolyte. As the hydrolysis proceeds more cellulose ends are produced increasing the DOC. At the end of the time course reactions there was a ~70% increase in DOC yield in the left figure and a ~44% increase in glucose yield in the right figure; glucose and DOC do track each other. First order kinetic parameters were estimated for both sets of data in Figure 5.47; k_C = 0.005±0.005 hr^{-1} and k_{WP} = 0.008±0.004 hr^{-1} (left) and k_C = 0.005±0.004 hr^{-1} and k_{WP} = 0.009±0.005 hr^{-1} (right). Addition of the polyelectrolyte for the experiments in Figure 5.47 increased the first order rate constant by approximately 1.7 times in both cases.

To quantify agitation, mixing Reynold's numbers were calculated from mixing speed in order to determine the mixing regime. The flow is laminar when Re<10, turbulent for Re>10^4, and in transition for a range between 10 and 10^4. In a cylindrical stirred tank vessel the agitator characteristic diameter is denoted by D, the velocity is ND where N is the rotational speed (revolutions per second). The mixing Reynold's number is defined as (Brodkey and Hershey, 1988):

$$\mathrm{Re} = \frac{\rho N D^2}{\mu} \tag{5.9}$$

where ρ is fluid density in kg/m^3 and μ is viscosity in kg/m*s. The mixing system used an agitator with *D* equal to 0.052 m, ρ is fluid suspension density of approximately 10^3 kg/m^3. The viscosity for 2% bleached softwood kraft pulp fiber solution was estimated from extrapolation of viscosity data for aqueous suspensions of bleached kraft pine pulp fiber ranging from 0.2 to 1.0% consistency at temperature ranging from 15°C to 75°C (Ferreira AG et al., 2003). The extrapolation was made from a linear relationship

between viscosity and fiber consistency at 50°C. The extrapolated viscosity of 2% suspension is approximately 54.5 mPa.s. The mixing Reynolds's number was then estimated for different levels of agitation.

Hydrolysis experiments were run at varying agitation for 2% SWD consistency solution, 0.1% (v/v) Ctec Cellic 2, and 250 mg (XP10035)/L initially added to a stirred glass flask held at 50°C by a water bath. The results are reported in Table 18 and illustrated in Figure 48 (Reye et al., 2010).

Table 5.18. Summary of varying agitation for hydrolysis of cellulosic fiber.

Time (hour)	Glucose (ppm)				
	Re/rpm 113/137	Re/rpm 203/245	Re/rpm 294/356	Re/rpm 380/460	Re/rpm 458/554
0	0	0	0	0	0
2	770	1138	1488	1354	1098
4	1139	1488	2320	1452	1460
6	1153	1669	2731	1615	1789
12	1576	2091	3055	2397	2314
k (hr^{-1})	0.005±0.005	0.007±0.007	0.01±0.01	0.007±0.007	0.008±0.006

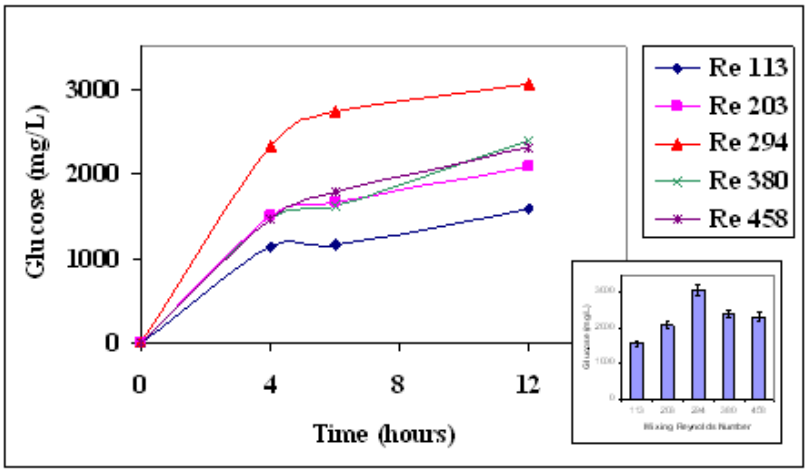

Figure 5.48. Varying agitation for hydrolysis of cellulosic fiber. The right corner graph shows a bar graph of the glucose yields after 12 hours with an optimal Re equal to 294.

The agitation regimes were all in the lower transition range. With lower agitation, there is less of an effect on hydrolysis. The polyelectrolyte ties up (flocs) the fines under low shear conditions not allowing the cellulase to have as much access to the fines. It was found that an agitation speed of 356 rpm showed the best result. At 356 rpm, the floc structure experience optimal agitation freeing fines and fibers without shearing and breakup of the desirable complexes. At the higher end of the agitation range, the enzyme/polyelectrolyte/fiber floc complex is likely sheared by the agitation speed, losing the benefit from the beneficial binding complexes. At 356 rpm, the floc structure experiences an optimal agitation. Coagulation and flocculation mixing processes are commonly designed also using G-values (Park et al., 2006).

5.3.5 Proposed Mechanism for the Effect of Polyelectrolyte on Hydrolysis of Cellulosic Fiber

The mixture of hydrolytic enzymes, in a cellulase cocktail, works synergistically to convert macro cellulose fibers into glucose monomers. Figure 5.49 summarizes this synergism.

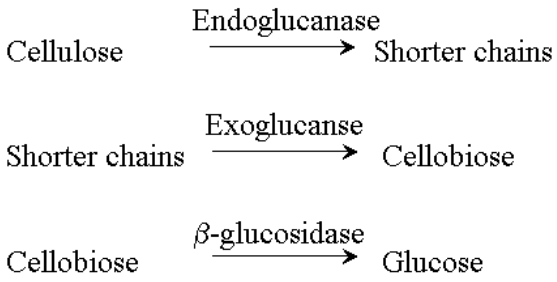

Figure 5.49. Synergism of the major hydrolytic enzymes for cellulose degradation.

The reduction in fiber length is caused by endoglucanase. As the number of shorter chains increases the number of cellulose chain ends begins to increase. Exoglucanase processively hydrolyzes a cellulose chain into cellobiose units. As cellobiose is released, β-glucosidase hydrolyzes the cellobiose into glucose. The question arises as to what enzymatic steps are enhanced by the addition of the polyelectrolyte. First, in Figure 5.50, hydrolysis was monitored by measuring fiber length with and without polyelectrolyte addition.

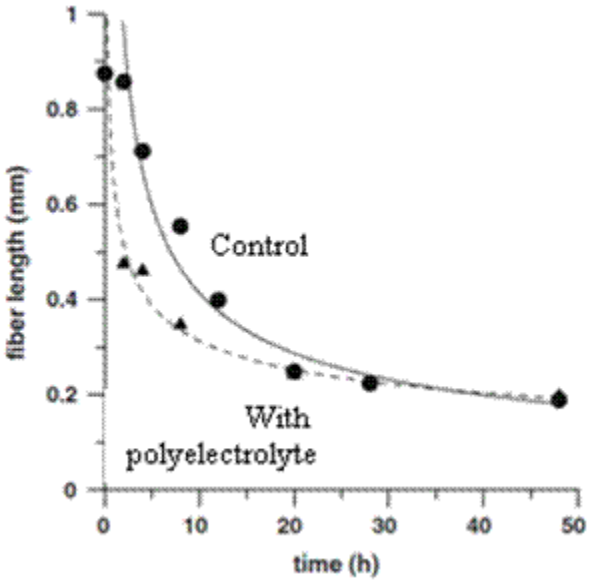

Figure 5.50. Effect of 500 mg (XP10033H) / L on the degradation of 1% (w/v) bleached hardwood by 1% (v/v) Pergalase 7547 (Reye et al., 2009).

The addition of the cationic polyelectrolyte accelerates the rate of fiber length reduction as shown in Figure 5.50. The cationic polyelectrolyte therefore boosts the endoglucanase activity. The effect is small but significant. As expected, the cationic polyelectrolyte did not break down the fiber in the absence of the enzyme. If fines were initially present they would react faster as the fines data in Figure 5.42 confirm.

The generation of soluble carbon (cellobiose and glucose) is controlled by exoglucanase. As the processive exoglucanases release cellobiose an increase in DOC was observed and accelerated with the addition of cationic polyelectrolyte Figure 5.47(left). This increase likely arises from patching of the polyelectrolyte between the cellulase and fiber because the magnitude of both the reaction rate and binding increase are similar suggesting that binding is responsible. Once cellobiose is produced, β-glucosidase rapidly hydrolyzes it into glucose. It was found that DOC and glucose track, which implies that the endoglucanase is likely rate limiting. Otherwise the fiber would disappear and there would be a build-up of DOC. The β-glucosidase hydrolysis occurs fast; otherwise, DOC would not track the glucose as illustrated in Figure 5.51.

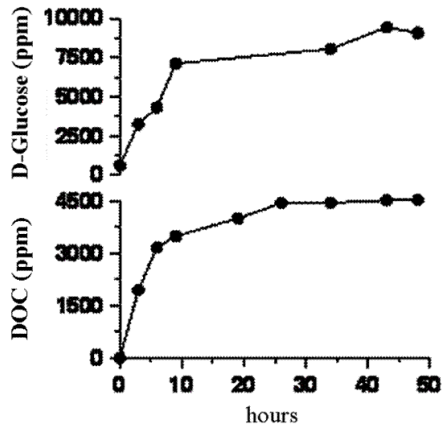

Figure 5.51. Glucose and DOC data from Figure 5.50.

The effect of cationic polyelectrolyte addition was also determined for cellobiose hydrolysis. Figure 5.52 shows the effect of varying amounts of cationic polyelectrolyte on the reaction.

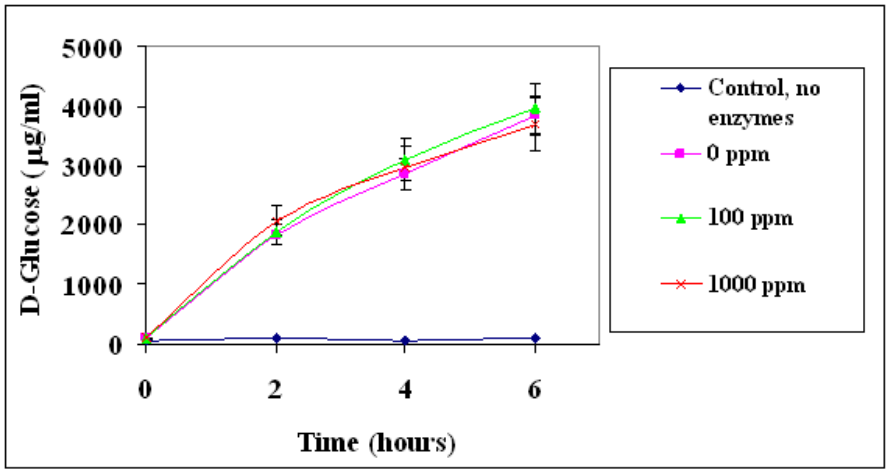

Figure 5.52. Effect of cationic polyelectrolyte on cellobiose hydrolysis; used XP10035 polymer, 1 g Pergalase 7547/L, 1% (w/v) cellobiose (EMD Bioscience, ≥98% purity), and 50 mL total initial volumes.

There was no noticeable difference in the rate of cellobiose hydrolysis with varying polyelectrolyte addition; first-order reaction rate constants were all the same 0.06±0.04 hr^{-1}. In a patching mechanism, disaccharides of glucose are not likely to floc with the addition of a polyelectrolyte. Nam et al. (2010) report from computational analysis of various β-glucosidase crystal structural states of pre-reaction (native), intermediate (cellobiose cleavage), and post-reaction (glucose binding) that the configuration of cellobiose in the catalytic pocket of the enzyme will affect the enzyme kinetics. Since no inhibitory or enhancement affect is observed with the addition of the polyelectrolyte, it is likely that the cellobiose is not bound to the cationic polyelectrolyte when being hydrolyzed in the catalytic pocket of the enzyme.

Endoglucanase activity was boosted by the addition of cationic polyelectrolyte reducing the fiber length faster than without accelerant addition. The exoglucanase, which most affects DOC, was enhanced with the addition of the accelerant. This was observed with

both glucose and DOC monitoring of softwood and hardwood respectively. The polyelectrolyte did not have any measureable effect on the β-glucosidase hydrolysis of cellobiose.

The cationic polyelectrolytes, acting as accelerants, are likely functioning conventionally as flocculants through a patching mechanism. Since both fiber and enzymes are slightly negative, there is a charge barrier (repulsive electrical double layer) to enzyme/fiber adsorption, which must be overcome. Patching, which aids in reducing and overcoming the electrical double layer, may increase the probability of interaction between the cellulase and fiber by reducing the repulsive barrier.

To support this mechanism, an experiment was devised to first allow a static incubation for 48 hours at 4^{o}C where the hydrolysis generated fines, shorter fibers, and overall more cellulose chain ends. The samples were then moved to a shaking water bath where typical reaction conditions were used to continue the hydrolysis. Hydrolysis experiments were prepared with 1% consistency bleached softwood kraft fiber, 1% (v/v) Pergalase 7547, and varying polyelectrolyte were combined; the pH range for the samples was between 4 to 5. Reactions were then placed into a shaking water bath at 50^{o}C and 150 rpm. The results of the time course are shown in Figure 5.54. The initial cold incubation led to glucose yields of 1329 μg/mL to 1759 μg/mL. The values in the figure were corrected for the initial conversion.

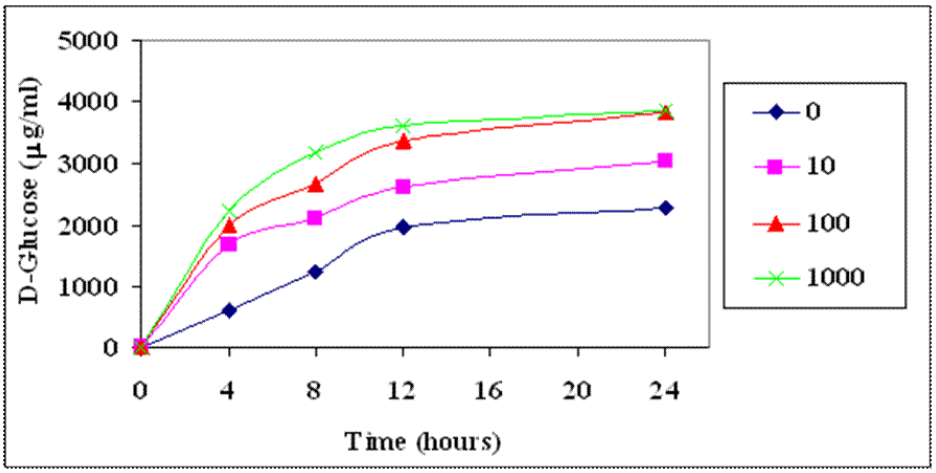

Figure 5.53. Time course of enzymatic hydrolysis of bleached softwood kraft pulp. The polyelectrolyte dosages in the key are in mg XP10035/L. Standard errors of the glucose measurements are within 5%.

The data illustrate that polyelectrolyte progressively increased the rate of hydrolysis. At 24 hours the final yields ranged from 36% to 56%. This type of experiment had been performed previously, but without an initial incubation. In such cases lower polyelectrolyte dosages (10 and 100 mg/L) appeared more like the control and higher values (1000 mg/L) showed greater differences compared to the control. The extent of the reaction was the same for 100 and 1000 mg/L. If the enzyme and polyelectrolyte don't degrade it could be assumed that all the experimental cases would reach the same conversion; however, with polymer and enzyme degrading some cases many vary.

The acidic nature of the cationic polyelectrolyte could also be a reason for the increase in the rate of hydrolysis. Reactions were conducted with 1% (v/v) Pergalase 7547, 1% consistency fiber, run at 50^{o}C in a shaking water (150 rpm). Conducted at the same time and following the procedure for the experiments in Figure 5.54 a comparison of pH where one sample pH was adjusted with HCl and the other was a result of the addition of

cationic polyelectrolyte (1000 mg XP10035/L); both with pH 4.0. Figure 5.54 shows the results of a pH comparison. The results show that the accelerant effect is not a pH driven effect since both samples were prepared with the same initial pH. The pH did not change over time by more than a couple tenths, thus dropping final pH values to just under 4. It was also observed that there is a change of slope after 8 hours. The pH of the top curve was created with a cationic polymer whereas the bottom curve was changed directly with HCl. The enzymes might possibly be more stable in the presence of the polyelectrolyte and be more prone to degradation in the presence of the HCl. From Figure 5.54 it can be observed that the increase in hydrolysis is not from pH. Thus, a patching mechanism still stands as the most likely reason for the enhancement.

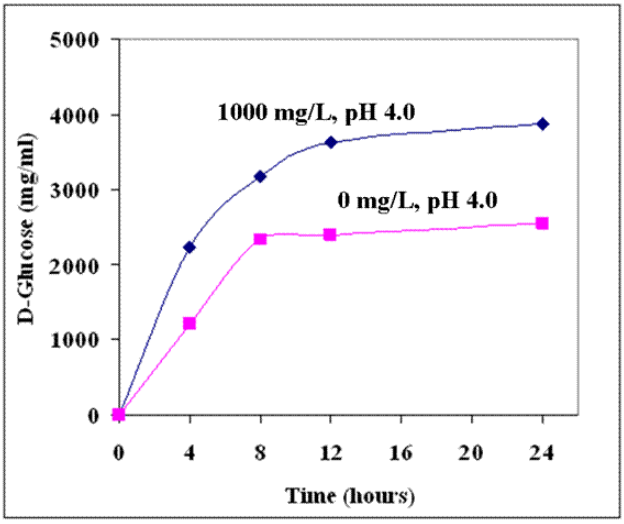

Figure 5.54. Time course of enzymatic hydrolysis of bleached softwood kraft pulp with pH 4.0. Standard errors of the glucose measurements are within 5%.

In another experiment, polyelectrolyte was systematically added to hydrolysis reactions which were initially started without any polyelectrolyte addition. The hydrolysis experiments were run for 2% bleached kraft softwood solution, 0.1% (v/v) Ctec Cellic 2,

and 250 mg (XP10035)/L added at various times to a stirred (220 rpm) glass flasks held at 50^{o}C in a water bath. The results are as follows.

Table 5.19. Bleached softwood fiber hydrolysis in stirred system with polyelectrolyte addition at different times (Reye et al., 2010).

Time, h	[1]Glucose, ppm				
	No c-PAM	1 hour	2 hours	4 hours	6 hour
0	0	0	0	0	0
1		1454		1580	1499
2	2243	1830	1944	2299	1819
4	2574	2462	3235	2680	2454
6	3045	2962	3950	3916	2802
12	4053	4345	5712	5401	4125
24	6411	6182	8394	9306	7636
[1]Glucose measurements are contain <5% error					

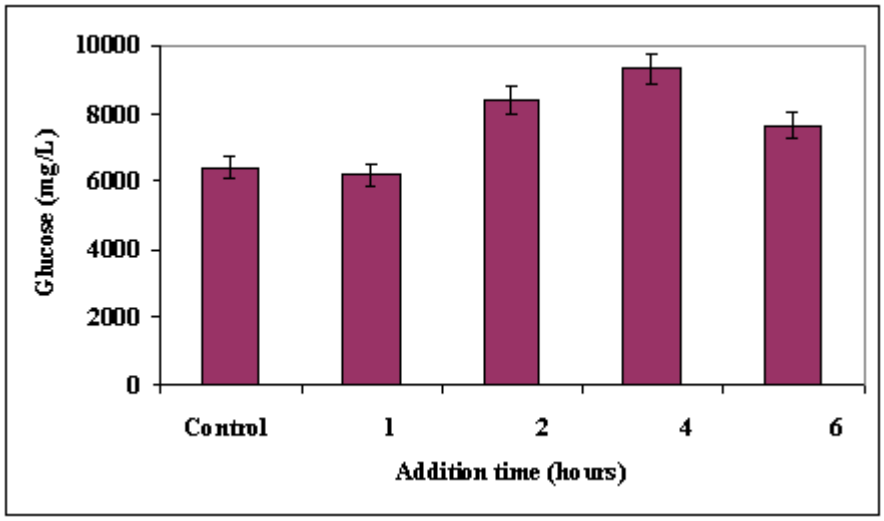

Figure 5.55. Glucose released after polyelectrolyte addition at different periods.

In Table 5.19 the data shows time course results for cellulose hydrolysis. Five time courses were conducted. A control with no polyelectrolyte was compared to equivalent parallel hydrolysis samples, which were each dosed with polyelectrolyte at different times during the enzymatic hydrolysis. The hydrolysis activity would be over time

producing more degraded cellulose and more cellulose chain ends. With a polyelectrolyte addition at one hour there was no hydrolysis enhancement. However after 2, 4, and 6 hours there was increased hydrolysis. Recalling the results in Figure 5.53, where each sample was incubated for an initial hydrolysis. After an initial hydrolysis the results show an increase in hydrolysis over time with increasing polyelectrolyte load. These experiments also began with an initial hydrolysis. In Figure 5.55, the addition of the polyelectrolyte after four hours was most effective at improving the hydrolysis, and the final hydrolysis yields in Figure 5.55 were greater for reactions where there was initial degradation prior to the addition of the polyelectrolyte. If only long fibers are present in the beginning, the initial addition of polyelectrolyte would result in either an inhibitory or no improved yield gain. With the long softwood fiber initially broken down the later addition of polyelectrolyte resulted in final yields greater than those where the polyelectrolyte was initially or early added. Thus, the polyelectrolyte appears to work best with shorter fibers and fines; the longer the fibers the lower the benefit gained from the polyelectrolyte. An initial hydrolysis treatment of long fibers before polyelectrolyte addition is an appropriate strategy. This definitely applies to softwood but may also be applicable for hardwood fibers as well. In related work from visiting group member Jian Lu (from the State Key Laboratory of Pulp and Paper Engineering, South China University of Technology, Guangzhou 510640, China), the enzymatic hydrolysis of pulp mill sludge was enhanced by the addition of polyelectrolyte (data not shown). The spent fibers in sludge are already short and more ideal for hydrolysis. Experiments where the polyelectrolyte was added at the beginning of the reaction showed rate and yield enhancement.

5.3.6 Discussion of Kinetic Results

It was learned that the temperature dependence of wood pulp hydrolysis by hydrolytic enzymes can depend on the length and surface area of the fiber involved. Glucose generation increases with temperature for fines and for short fiber but was relatively temperature-independent for the longer fiber. The adsorption step is inversely temperature dependent whereas the catalytic step should have a direct dependence on temperature. The two effects tend to offset for the longer fiber, which adsorbs the cellulase to a proportionately smaller extent.

It was found that the addition of a cationic polyelectrolyte into the cellulosic hydrolysis system can increase the hydrolysis rate. A polyelectrolyte screening showed that the process may be general because the polyelectrolytes enhanced the hydrolysis of both cellulase/cellulose and amylase/cornstarch hydrolytic systems. A mechanism was proposed suggesting that patching is the likely reason for the hydrolytic rate enhancement. The polyelectrolyte addition had a synergistic effect with the endoglucanase and exoglucanase as the cellulose was hydrolyzed. The endoglucanase activity was boosted by the addition of cationic polyelectrolyte, which decreased the fiber length faster than without addition of the accelerant. As fiber ends were produced exoglucanase would release dissolved carbon, solubilizing the fiber in the form of cellobiose. The polyelectrolyte did not have any effect on the β-glucosidase hydrolysis of cellobiose. These three types of cellulase work synergistically in the hydrolysis of cellulosic fiber.

CHAPTER 6

FINAL DISCUSSION AND FUTURE WORK

6.1 Final Discussion and Conclusions of Project

This dissertation reports a new method for enhancing rates of enzymatic hydrolysis. To do this, experimental methods were used to directly determine how cationic polyelectrolytes and cellulase interact with each other and how they both adsorb onto cellulosic fiber. Kinetic experiments were conducted to determine how a polyelectrolyte affects the enzymatic hydrolysis of the substrate. A mechanism was proposed based on the experimental results.

DLS results generally showed non-specificity for cellulase-polyelectrolyte interactions. Absorption of cellulase increased with the addition of polyelectrolytes. The magnitude of the binding of cellulase and rate of hydrolysis were similar suggesting that binding is responsible. Shorter fibers and fines have higher surface area than longer fibers. An adsorption coefficient for fines was found to be three times greater than for long fibers. Long fibers having a lower surface area proportionally bind enzymes resulting in a greater amount of free enzymes not bound. Cellulase binding is a function of temperature but given the negative charge of the both cellulase and cellulose fibers there is also a resistance to adsorption. The polyelectrolyte layer thicknesses (40-70 nm) were found to be significantly lower than the repulsive double layer thickness (250-1000 nm). The polyelectrolyte adsorption may reduce the negative surface charge of the fiber thus reducing the repulsive layer thickness. Additionally, the binding of cellulase to the

polyelectrolyte layer through a flocculation mechanism brings the cellulase and cellulose closer for binding and reaction to occur. Without agitation, the fiber flocs and the surface area accessible to the enzyme are reduced offsetting the benefit of the polyelectrolyte flocculation.

The increase in binding cellulase to fiber in the presence of a cationic polyelectrolyte is believed to be the main reason for the increase in enzymatic hydrolysis. This process works for a variety of different cationic polyelectrolytes thus demonstrating the generalized process. The process has been found to work with wood pulp fiber and cornstarch. Thus, the effect of the cationic polyelectrolyte is non-specific in that it can boost the performance of two completely different systems.

6.2 Future Outlook

The reported method for improving the saccharification of biomass has the potential of improving both first generation (i.e. sugar, corn and vegetable oil) and second generation (i.e. cellulosic and non-food crops) biofuel production. Back of the envelope calculations estimate that a 100 million gallon per year corn ethanol plant (36 million bushels of corn) may use as much as 5000 metric tons of dry cationic polyelectrolyte. A pending patent has been licensed to Akzo Nobel who is presently pursuing commercialization (Banerjee and Reye, 2009).

6.3 Future Work and Suggestions

This thesis work focused on the use of clean model substrates, mainly woody bleached cellulosic fiber, and refined raw cornstarch. Besides these model substrates, more unrefined, renewable feedstocks may be used to produce precursors for chemical and energy production. Table 6.1 summarizes the composition of some widely studied biomass sources reported in % dry weight; samples were analyzed at the National Renewable Energy Laboratory. Corn stover, switchgrass, bagasse, and wheat straw make up some renewable biomass sources that do not conflict with human consumption. Other than straw for livestock consumption, these biomasses may be considered waste. These and other agricultural wastes may eventually be more effectively utilized in producing value added products.

Table 6.1. Composition of Pine, Herbaceous species, and paper samples.

Lignocellulosic Materials	Glucan	Xylan	Mannan	Arabinan	Galactan	Lignin	Extractives	Ash
Pine[d]	42.37	5.94	11.02	1.28	2.29	27.1	3,71	0.3
Corn Stover[a,e]	36.4	18	0.6	3	1	16.6	7.3	9.7
Switchgrass[e]	31	20.4	0.3	2.8	0.9	17.6	17	5.8
Bagasse[b,e]	40.2	21.1	0.3	1.9	0.5	25.2	4.4	4
Wheat straw[e]	38.2	21.2	0.3	2.5	0.7	23.4	13	10.3
Office paper[e]	68.6	12.4	7.8	-	-	11.3[c]	-	-

a - Corn stover includes cornstalks and cobs as they come out of the combine
b - Bagasse is the residue after the juice is extracted from sugar cane
c – Includes ash
d - (Saddler, 1993)
e - (Wyman, 1996)

Additionally, other polyelectrolytes could be tried such as polydiallyl dimethyl ammonium chloride (PDADMAC), polyethyleneimine (PEI), or poly aluminum chloride

(PAC). These options offer alternatives to c-PAM in cases that concern may exist regarding human contact or consumption. PDADMAC, PEI, and PAC provide alternatives that are more health and environmentally conscious. However, if c-PAM was produced and certified to be under an acceptable limit of acrylamide then there should be no problem.

APPENDIX A

DYNAMIC LIGHT SCATTERING (DLS)

Photon correlation spectroscopy (PCS), sometimes referred to as dynamic light scattering (DLS) or quasi-elastic light scattering (QELS), is a technique which can be used to determine the size distribution of particles in a suspension or polymers in solution (Bohren and Huffman, 1998; Chu, 1974). When light hits small particles moving through a suspension the light scatters in all direction (Rayleigh scattering) as long as the particles are smaller compared to the wavelength of the striking light. If the light source is a monochromatic laser, then the light scattering generates a time-dependent fluctuation in the light scattering intensity. The fluctuations are due to small particles undergoing Brownian motion (also called "random walk") and so the distance between the particles in solution is constantly changing with time. The scattered light can then undergo either constructive or destructive interference depending on the distance traveled to the detector. The simplest measurement that can be made using a light scattering instrument is that of light scattering intensity. The detector measures an average intensity with superimposed fluctuations as illustrated in the following figure, where τ is a time delay**.**

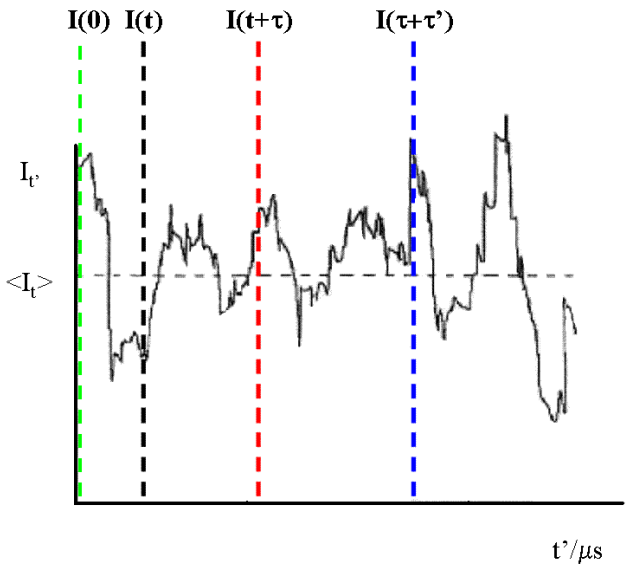

Figure A.1. Fluctuations about the average scattered light intensity.

Within the intensity of light scattering fluctuations, dynamic information of the particles is contained about the time scale movement of the particle. The PCS theory is only valid for light being scattered once. Multiple scattered light leads to erroneous PCS results and misinterpretations. As a result, PCS necessitates highly diluted suspensions in order to avoid multiple scattering. On the other side, low concentrations of particles make this method sensitive to impurities in the liquid; algorithms for "dust filters" have been used in control software.

As described, the random motion of small particles in the liquid medium gives rise to fluctuations in the time intensity of the scattered light. The basic principle of PCS is the detection of concentration fluctuations as a function of spatial position r and time t by a Doppler broadening of the scattered light; the Doppler shift, which is to say there is a very slight change in the scattered light compared to unscattered. Larger particles will move slowly exhibiting a small Doppler shift, whereas small particles will move quickly

and exhibit a large Doppler shift. The dynamic information of the particles is derived from an autocorrelation of the intensity trace recorded during the experiment. A second order autocorrelation curve $g^2(\tau)$ is generated from the intensity trace by equation (4.1), which is then used to regress out parameters A and B in equation (A.2) (Min et al., 2002).

$$g^{(2)}(\tau) = \frac{\langle I(\tau) I(0) \rangle}{\langle I(0) \rangle^2} \tag{A.1}$$

$$g^{(2)}(\tau) = B + A\left(g^{(1)}(\tau)\right)^2 \tag{A.2}$$

$$g^{(1)}(\tau) = e^{(-\Gamma \tau)} \tag{A.3}$$

In the above set of equations, I is the light signal intensity, τ is the time delay between measurements, A is an optical constant, B is the background constant, and Γ is related to the relaxation of the fluctuations. The $g^2(\tau)$ intensity correlation function describes particle motion while the $g^1(\tau)$ electrical field correlation function describes the measured fluctuations which are related to connect the measurement and motion. The autocorrelation function $g^2(\tau)$ when plotted in a log-log plot with respect to τ results in the following figure.

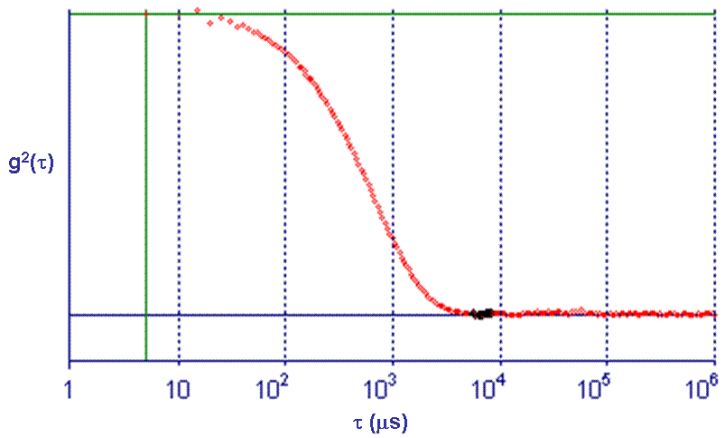

Figure A.2. Example of an autocorrelation function.

It is important for the quality of the measurement for the signal to decay smoothly to the baseline. The fitted $g^2(\tau)$ is used to estimate Γ, which with θ and n is then used to estimate D. The Γ and q variables are defined as,

$$\Gamma = Dq^2, [rad/\sec] \tag{A.4}$$

$$q = \frac{2\pi n}{\lambda_o} 2\sin\left(\frac{\theta}{2}\right) \tag{A.5}$$

where D is the translational diffusion coefficient, q is the magnitude of the scattering wave vector and is calculated from the scattering angle (e.g. 90^o), π is the number pi, n is the index of refraction, λ_o is wavelength of the laser light (0.635 micron), and θ is the scattering angle in radians. The translational diffusion coefficient is the principle quantity measured by DLS and is useful for probing interactions between macromolecules. At this point, a translational diffusion coefficient has been estimated for a particle of an assumed generally globular shape. Particle size can be related to the translational diffusion coefficient for simple common shapes like spheres, ellipsoids,

cylinders and random coils. Of these, the sphere has traditionally been the most widely assumed. Using the Stokes-Einstein equation, the diameter for a spherical particle moving through a liquid with a low Reynolds's number is related to the translational diffusion coefficient as shown in equation (A.6),

$$D = \frac{k_B T}{3\pi\eta d}, \left[cm^2 / \sec\right] \tag{A.6}$$

where k_B is Boltzmann's constant, T is the temperature of the medium in K, η is the viscosity of the liquid medium (in centi poise) in which the particle is moving, and d is the particle diameter. DLS was used to investigate how enzyme and polyelectrolytes interact together under various conditions.

APPENDIX B

DLVO THEORY

Polyelectrolytes have been used in commercial applications as adhesives, dispersion stabilizers, and flocculating agents. The paper industry, for many decades, has used polyelectrolytes as retention aids with fines and/or added fillers in the formed paper, or to improve the mechanical properties of the paper. The polyelectrolytes used in these types of applications can vary in their molecular weight, molecular structure, and reactive groups. These retention aids require the action of colloidal forces such as steric forces, entropic forces, van der Waals forces, and electrostatic forces. Steric forces arise when atoms or molecules are brought too close together. The result is an unfavorable associated cost in energy from overlapping electron clouds, which can influence a preferred conformation and reactivity of a molecule. In the case of chain crossing, a polymer coiled in a random conformation cannot change from one conformation to another closely related structure by a small displacement if it required one polymer chain to pass through another or through itself. Next, entropic forces are produced according to the second law of thermodynamics where a system will progress to a state in which the entropy is maximized. In the case of van der Waals forces, they are produced from interactions between two dipoles that are either permanent or induced. When a particle does not have a permanent dipole, fluctuations in the electron density can generate a temporary dipole in a given particle. As a result, the temporary dipole can then induce a dipole in neighboring particles. The temporary dipole and the induced dipoles are attracted to each other. This attractive interaction is known as van der Waals forces. Finally, electrostatic forces are attractive or repulsive interactions between colloidal

particles, which carry an electrical charge. Cationic polyelectrolytes can experience each of these forces; the most obvious of these may be the electrostatic forces due to the cationic moieties attached to the chains. These forces control the types of interactions with polyelectrolytes, particle fines, and colloids. In the 1940s Derjaguin, Landau, Verway, and Overbeek (DLVO) developed a theory describing colloidal stability. The stability of a colloidal system is determined by the sum of repulsive and attractive energies that particles experience as they approach one another. In this theory, repulsive and attractive energies are added together. Repulsive interactions are a result of the electrical double layer forces, while attractive interactions are a result of van der Waals forces as two particles come closer together. The DLVO Theory is the classic explanation of how particles interact, which is illustrated in Figure B.1.

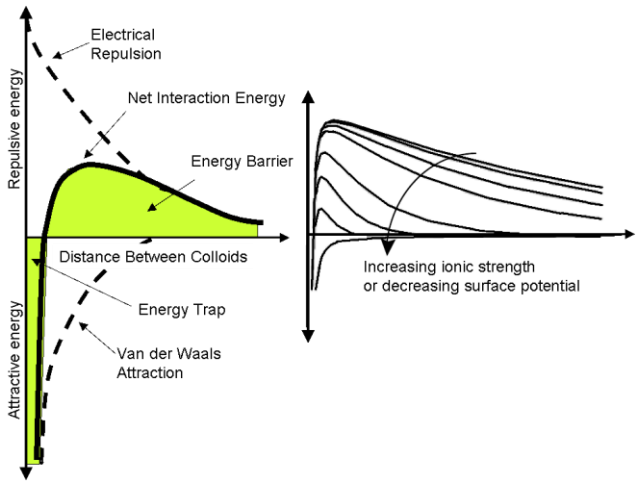

Figure B.1. Schematic of a net interaction curve produced by subtracting the attractive curve from the repulsion curve (left) and energy barrier curves with increasing ionic strength or decreasing surface potential (right).

DLVO theory can account for why some colloids agglomerate and flocculate while others do not. Electrostatic repulsion between two particles becomes significant when they approach each other and their electrical double layers begin to overlap. In order to overcome this repulsive interaction, energy is required to force the particles together. The amount of energy required increases considerably as the particles are moved closer together. In Figure B.1 the schematic includes an electrostatic repulsion curve (above dotted line), which indicates the energy which must be overcome in order to force particles together. A van der Waals attraction curve is also illustrated (bottom dotted line) between two colloids and is the result of forces between a pair of individual colloids. Recall that temporary dipole and the induced dipoles produce attraction between colloids and this effect is additive. An attractive energy curve is used to indicate the variation in attractive force with distance between particles. A net interaction curve is produced by subtracting the attractive curve from the repulsion curve. Figure B.1 shows the result of combining the repulsive and attractive energies to form a net interaction energy-distance profile. If the particles have a sufficiently high repulsion then the dispersion will resist flocculation; this will be a colloidally stable system. If there is no repulsion mechanism then flocculation can occur and eventually turn to coagulation, resulting in an unstable system. In this case, the particles have aggregated to some extent but the system is reversible, and with some mechanical energy from mixing can be brought back to a stable system.

For colloidal stability, the repulsive forces must be dominant. There are two fundamental mechanisms that affect dispersion stability: steric repulsion and electrostatic (charge)

repulsion, which is illustrated in Figure B.2. Steric stability includes the adsorption of surface active components. This adsorption is irreversible. It can affect the final properties of your system because of the layers that are adsorbed onto the particle do remain with the particle. Steric stabilization is a simple system requiring just the adsorption of a surface active polymer, oligomer, or processing aid. Once adsorption of a polymer has occurred, it can be difficult to subsequently flocculate the system.

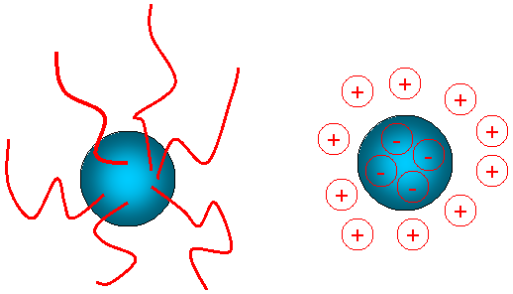

Figure B.2. Steric (left) verses electrostatic (right) stabilization.

Electrostatic stabilization refers to the charge on the surface of the particle and the effectiveness of that charge to influence the electric double layer around the surface of the particle. These electrostatic effects are easy to assess because they are directly measurable by zeta potential. Electrostatic interactions are reversible. Changes to ion concentration, pH, or changes to the ionization of the surface charge groups can affect the electrostatic conditions around the surface of the particle and in the medium. Electrostatic stabilization or flocculation of the system occurs simply by altering the concentration of ions in the system. This can be achieved by changing the pH or by the addition of salt ions or polyelectrolytes. Either way, electrostatic stabilization is a reversible process and generally an inexpensive process. Zeta potential is a useful index for the magnitude of the interaction between colloidal particles, and zeta potential measurements are used to asses the stability of colloidal systems.

In order for two particles to agglomerate, the two particles must approach each other and collide with sufficient kinetic energy to overcome an energy barrier. Once the energy barrier is cleared, the net interaction energy becomes all-attractive. With attractive forces dominating, the particles then agglomerate. This attractive region in Figure B.1 is an energy trap because the colloids are considered trapped together by the attractive van der Waals forces. The right side of Figure B.1 illustrates how increasing the ionic strength or decreasing the surface potential changes the DLVO energy barrier.

For effective coagulation, the energy barrier needs to be lowered so that the net interaction is always attractive. That can be done by two different strategies: the first, compressing the double layer, and the second, reducing the surface charge. Flocculation by double layer compression can be achieved by the addition of significant amounts of salt, referred to as salting out the colloid (Kam and Gregory, 1999). This is by no means a practical strategy when using fresh water. However, for an application to treat brackish wastewater, the salt content may be used to help flocculate waste particles. The second strategy, reducing surface charge to lower the energy barrier, can be achieved by the addition of a coagulant to reduce the surface charge and consequently, the zeta potential. The energy barrier concept helps explain why larger particles will sometimes flocculate while smaller ones in the same suspension escape. At equal velocity, a larger particle with greater mass and therefore more energy can overcome the energy barrier, whereas the smaller particle may not overcome the barrier and therefore not flocculate. In water treatment, the terms coagulation and flocculation are used interchangeably and ambiguously. It is therefore essential to distinguish the two in terms of purpose.

Coagulation occurs when the DLVO energy barrier is reduced and effectively eliminated; this lowering of the DLVO energy barrier is a destabilization of the system. On the other hand, flocculation refers to the successful collisions that occur when destabilized particles come out of suspension and are driven toward each other through processes of contact and adhesion by hydraulic shear forces. As a result, agglomerates of colloids floc together forming microflocs that continue to draw together into visible floc masses. The difference between coagulation and flocculation can be blurry; coagulants can perform both functions at once; their primary function is charge neutralization.

There are two kinds of fiber flocs, soft flocs caused by both flow and inter-fiber friction, and hard flocs caused by polyelectrolyte interactions (Britt and Unbehend, 1976). Synthetic polyelectrolyte flocculants have been used to improve the efficiency of sold/liquid separation in such industries as wastewater treatment and paper manufacture. The use of cationic polyelectrolytes, as coagulants, can aid in the flocculation of not only fibers, but also various types of particles, and colloids in aqueous suspensions. The use of flocculating agents continues to be an ongoing area of study with economic importance, notably for the pulp and paper industry. Several mechanisms for polyelectrolyte-induced flocculation exist, which include charge neutralization, charge patching, and polymer bridging flocculation (Eklund and Lindstrom, 1991; Scott, 1996).

An example of a charge neutralization mechanism would involve reducing the negative charge of fibers and fines in order to reduce the electrical repulsion so that van der Waals attractions can exist (Neimo, 1999). The following figure illustrates a generic example of

charge neutralization, where a positively charged particle is added to a negatively charged particle resulting in charge neutralization.

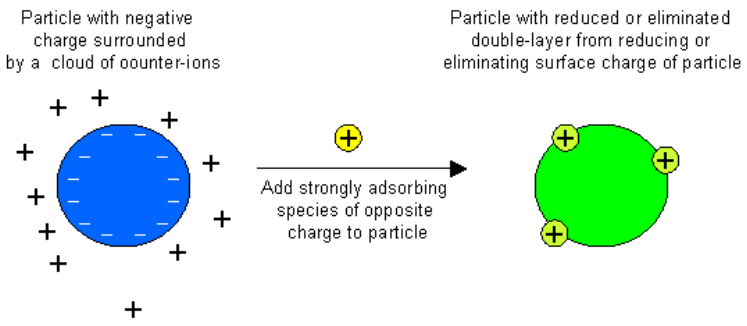

Figure B.3. Example of charge neutralization between a negative particle with a strongly adsorbing cationic specie resulting in a neutralized particle with a reduced or eliminated double-layer.

Flocculation by charge neutralization obeys DLVO theory, which describes the reduction of the energy barrier responsible for electrical repulsion by compression of the electrostatic double-layer (Eklund and Lindstrom, 1991). By adding an electrolyte to the solution, the number of counter ions increases, which reduces the difference in charge. When the charge difference is significantly reduced and approaches zero, flocculation will occur (Scott, 1996). Flocs can also be broken up if too much electrolyte is added. An example of a charge neutralizing polyelectrolyte would be one that is highly cationic with a low molecular weight (Neimo, 1999).

A second type of flocculation mechanism is that of a charge patch model. An example of the patch mechanism would be a cationic polyelectrolyte adsorbing onto a negatively

charged surface to create sites of positive charge (Eklund and Lindstrom, 1991; Neimo, 1999). A schematic for a charge patch mechanism is shown in the following figure.

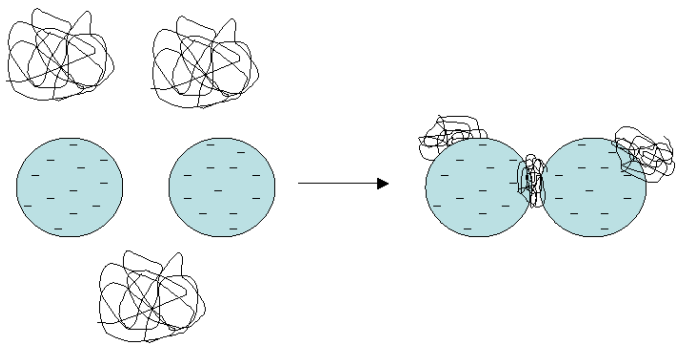

Figure B.4. Example of a charge patch model between negative particles with a strongly adsorbing cationic specie resulting in reducing or neutralizing of the surface charge of the particles.

The schematic shows negatively charged particles (e.g. negative charged fibers) are not charge neutralized but have open areas of bare negatively charged surface. Cationic polyelectrolytes are absorbed over the negative surface in the form of small patches. The polyelectrolyte is anchored to the surface allowing the free surface of the patch to bind to another negative bare surface. The patch must be thicker than the electrostatic double-layer in order for flocculation to occur (Eklund and Lindstrom, 1991). Typically, the charge patch mechanism occurs when highly charged cationic polyelectrolytes have molecular masses ranging from approximately 100,000 to 2 million grams per mole. The charged-patch mechanism may be partially reversible. If enough hydrodynamic shear force is applied, a patch linking two surfaces can break detaching bound surfaces; however, in a charge patch mechanism, the surfaces may effectively reflocculate (Neimo, 1999).

The third flocculation mechanism follows a bridging model. With cellulosic fiber flocculation serving as an example, the first step in a bridging mechanism involves a polyelectrolyte partially absorbing to the surface of a fiber (Eklund and Lindstrom, 1991; Neimo, 1999). Once the polyelectrolyte is anchored, it extends out into solution and acts as a bridge as it absorbs to an oppositely charged surface (Eklund and Lindstrom, 1991). Since the polyelectrolyte chain can extend beyond the electrical double layer of the fiber, the extended chain increases the possible area for flocs to form (Neimo, 1999). The following schematics in Figure B.5 show how a bridge mechanism can link two negative particles together with a cationic polyelectrolyte.

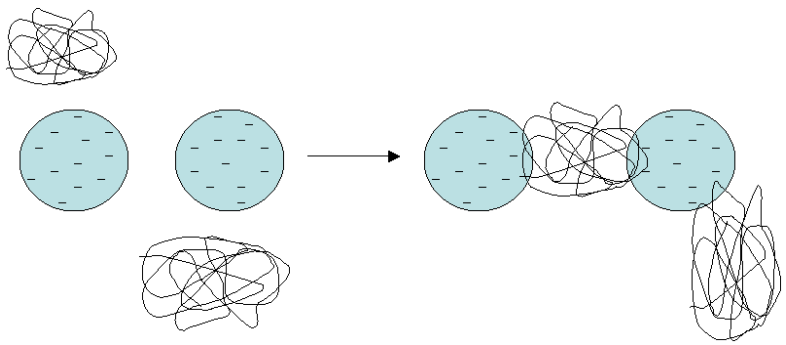

Figure B.5. Example of bridge model where two particles of a negative charge are bridged together by a polyelectrolyte of an opposite positive charge.

The bridging polyelectrolytes have characteristic structural features such as loops, trains, and tails. In addition to variations in structural features, polyelectrolytes vary in the types of structural conformations they can form such as mushrooms, pancakes, and brushes, which are illustrated in Figure B.6.

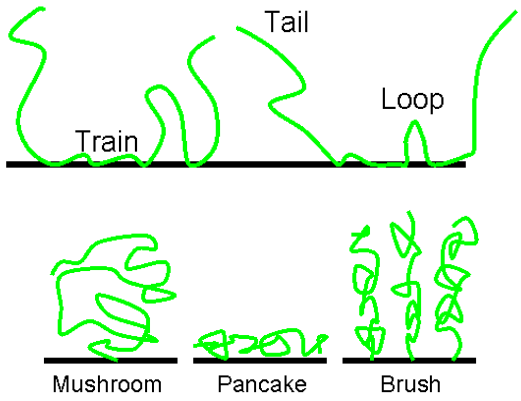

Figure B.6. Schematic of structural and conformational types of features of adsorbed polyelectrolytes. Structural features of an adsorbed polyelectrolyte (top). From left to right tail, loop, and train (Jenkel and Rumbach, 1951). Conformational structures of adsorbed polyelectrolytes (bottom). From left to right mushroom, pancake, and brush (Jenkel and Rumbach, 1951).

Polymer brush layers are created by either polymer adsorption or grafting. The brush conformation regime is more favorable when there is a high level of adsorption and $s < R_g$, where s is the distance between anchoring points for the polymer on the surface. The mushroom conformation regime favors a low level of adsorption and $s > R_g$. Polymer layers are normally neither a brush nor mushroom; loops, tails, and trails are more the norm. More often, the polyelectrolyte adopts some version of a pancake conformation. If the interaction between the polymer and the surface is weak or even repulsive the chain may form a random coil linked to the surface, and based on the distance between anchoring points would conform to a mushroom or brush. However, if the segments of the surface attached polymer are strongly absorbed, then the favorable interactions between the polymer and surface obtain a flat pancake like conformation. Dissolved polyelectrolytes are long and have molecular weights of at least 2 million grams per mole in order to work effectively by this mechanism. If enough hydrodynamic shear force is applied to bridge fibers, the bridge can break between the fibers, and the bridge is

irreversibly damaged. This prevents reflocculation from occurring (Neimo, 1999). The types of polymers vary in a wide range of properties depending on the different retention strategies (SNF, 2010).

The electrical double layer has been mentioned above but has not yet been discussed. The development of charge at the particle surface affects the distribution of ions surrounding the interfacial region, resulting in an increased concentration of counter ions close to the surface. Thus, an electrical double later exists around each particle. Figure B.7 illustrates a double layer for a particle with a negatively charged surface surrounded by an electrical double layer.

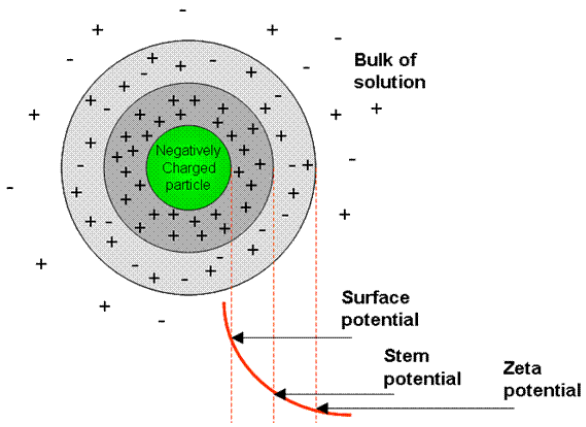

Figure B.7. Schematic of the Surface, Stern, and Zeta Potentials for a negatively charged particle. A rigidly adsorbed layer of positive ions (Stern layer) surrounds the charged particle. Outside the Stern layer is a diffuse boundary layer where positive ions outnumber negative ions and balance the excess in the Stern layer. The electrostatic potential at the particle surface decreases through the Stern and diffuse layers and reaches zero charge at the outer boundary of the diffuse layer. The diffuse layer can shift under changes in potential, which introduces a slipping plane that separates the mobile bulk fluid from the fluid that remains attached to the surface. The zeta potential is the electrical potential at this plane.

The liquid layer surrounding the particle exists as two parts; an inner region (Stern layer) and an outer region (diffuse layer). In the Stern layer, ions are strongly bound with a net cationic or counter ion layer. Within the diffuse layer is a notional boundary within which the particle acts as a single entity. The zeta potential is the electrical potential at the notional boundary between the charge at the edge of the Stern layer and the shifting plane with the bulk of the suspending liquid. When zeta potential is reported, the measuring devise is actually measuring electrophoretic mobility, which is defined as the velocity of the particle / electric field strength. Zeta potential is an indication regarding the effectiveness of the surface charge. The magnitude of the zeta potential gives an indication of the potential stability of the colloidal system, as shown in Table B.1.

Table B.1. ASTM stability behavior of colloids (ASTM 1985).

Zeta potential [mV]	Stability behavior of the colloid
from 0 to ±5,	Rapid coagulation or flocculation
from ±10 to ±30	Incipient instability
From ±30 to ±40	Moderate stability
From ±40 to ±60	Good stability
more than ±61	Excellent stability

The zeta potential (z) is related to the electrophoretic mobility (U_E) by the Henry function f(ka) in the following equation.

$$U_E = \frac{2 \times \varepsilon \times z \times f(ka)}{3\eta} [=] 10^{-8} \mathrm{m^2 s^{-1} V^{-1}} \quad \text{(B.1)}$$

The dynamic viscosity (η) units are (Pa s). The dielectric constant (ε) is the dielectric constant and defined as the permittivity of a substance / permittivity of free space. The

larger the dielectric constant, the more charge that can be stored. The Henry function contains the reciprocal length (k) and the particle radius (a), where 1/k is the thickness of the electrical double layer (the Debye length). The ratio of the particle radius to double layer thickness is (ka). A summary of ka and Henry function is reported in Table B.2.

Table B.2. Summary of ka and corresponding Henry function.

ka	0	1	2	3	4	5	10	25	100	infinity
f(ka)	1.000	1.027	1.066	1.101	1.330	1.160	1.239	1.370	1.460	1.500

For particles in polar media the f(ka) is equal to 1.5 (Smoluchowski approximation) and for particles in a non-polar media the f(ka) is equal to 1.0 (Huckel approximation). The thickness of the electrical double layer (1/k) is calculated using equation B.2.

$$\frac{1}{k} = \left(\frac{\varepsilon_o \varepsilon_r k_B T}{2000 e^2 I N} \right)^{1/2} \tag{B.2}$$

where ε_o is the permittivity of free space, ε_r is the relative permittivity of liquid (or dielectric constant), k_B = Boltzmann's constant, T = temperature in Kelvin, e = electronic charge in coulombs, I = ionic concentration (in mol/L), and N = Avogadro's number. In cases for water at 298K the equation simplifies to:

$$\frac{1}{k} = \frac{0.304}{I^{1/2}} \tag{B.3}$$

Where 1/k is calculated in nanometers (nm) and I is the ionic strength. The ionic strength is calculated by $I = \frac{1}{2} \Sigma C_i Z_i^2$, where C_i is the concentration of the particular electrolyte

species and Z_i is the valency of the species. An example would be as followed, NaCl is 1:1 electrolyte and $AlCl_3$ is 3:1 electrolyte. The calculation of I is shown in Table B.3.

Table B.3. Summary of ionic strength for different electrolytes.

Electrolyte	Ionic Strength
1:1	$I = 1/2[C_1^2 + C_1^2] = C$
1:2 or 2:1	$I = 1/2[2C_1^2 + C_2^2] = 3C$
2:2	$I = 1/2[C_2^2 + C_2^2] = 4C$
1:3 or 3:1	$I = 1/2[3C_1^2 + C_3^2] = 6C$
3:3	$I = 1/2[C_3^2 + C_3^2] = 9C$
2:3 or 3:2	$I = ½[3C_2^2 + 2C_3^2] = 15C$

By knowing the ionic strength of a given electrolyte estimates for the double layer thickness can be made. Table B.4 is a summary of double layer thickness and ionic strength for various general electrolytes.

Table B.4. Summary of double layer thickness and ionic strength.

Double Layer Thickness (nm)							
		Electrolyte					
Ionic Strength (mol/L)	Ionic Strength mM	1:1	1:2, 2:1	2:2	1:3,3:1	3:3	2:3,3:2
10^0	1000	0.30	0.18	0.15	0.12	0.10	0.08
10^{-1}	100	0.96	0.55	0.48	0.39	0.32	0.25
10^{-2}	10	3.04	1.76	1.52	1.24	1.02	0.78
10^{-3}	1	9.61	5.55	4.81	3.92	3.2	2.48
10^{-4}	0.1	30.4	17.6	15.2	12.4	10.2	7.85
10^{-5}	0.01	96.1	55.5	48.1	39.2	32	24.8
10^{-6}	0.001	304	176	152	124	102	78.5
10^{-7}	0.0001	961	555	481	392	320	248

APPENDIX C

ATOMIC FORCE MICROSCOPY (AFM)

C.1 Atomic Force Microscopy

Scanning Probe Microscopy (Binnig et al., 1982) encompasses several related technologies, the two primary forms being scanning tunneling microscopy (STM) and atomic force microscopy (AFM) (Magonov and Whangbo, 1996). The invention of the AFM in 1986 by Binnig et al. (Binnig et al., 1986) has emerged as a powerful tool for investigating nanoscale surface topography and chemistry in various applications (Magonov, 1993). SPM technologies share the concept of scanning an extremely sharp tip (3-50 nm radius of curvature) across an object surface. The tip is mounted on a flexible cantilever, allowing the tip to follow the surface profile.

Atomic Force Microscopy operates by scanning a tip with an average radius <50nm, supported on a 60-300 μm long force-sensing cantilever, over the sample and thus generating a three-dimensional image of the surface. Probe-sample interactions induce bending of the cantilever typically measured through a laser deflection signal change that is recorded on a photodetector. A feedback control system responds to those changes by adjusting the tip-sample distance in order to maintain a constant deflection distance to the sample surface. This vertical movement translates into a topographical image of the surface, with an accuracy of a few nm or less. A schematic of the AFM is shown in the following figure.

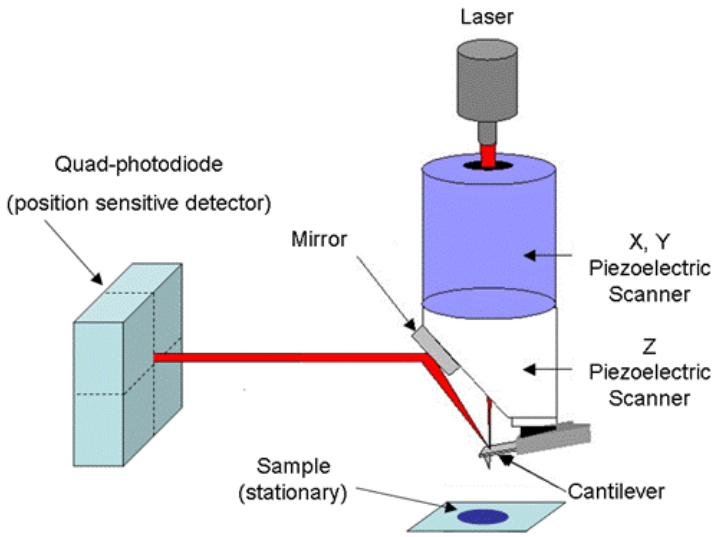

Figure C.1. Schematic of atomic force microscopy (AFM).

The AFM is generally operated in three types of imagining modes, a contact mode where the tip is moved directly over the surface, a non-contact mode which is only achievable in a vacuum system, and thirdly, the tip can be oscillated at a given frequency, thereby having only intermittent contact with the sample, known as tapping mode. Scans can cover a distance of over tens of microns in the x and y directions. In addition to imaging, measuring the interaction between the cantilever tip and a sample is becoming an increasingly common method for characterizing chemical nature and surface chemistry of the sample (Gurnagul et al., 1993; Jung and Bhushan ,2006). An example of a typical deflection/force trace is shown in Figure C.2. A schematic of the tip and cantilever positions is also superimposed.

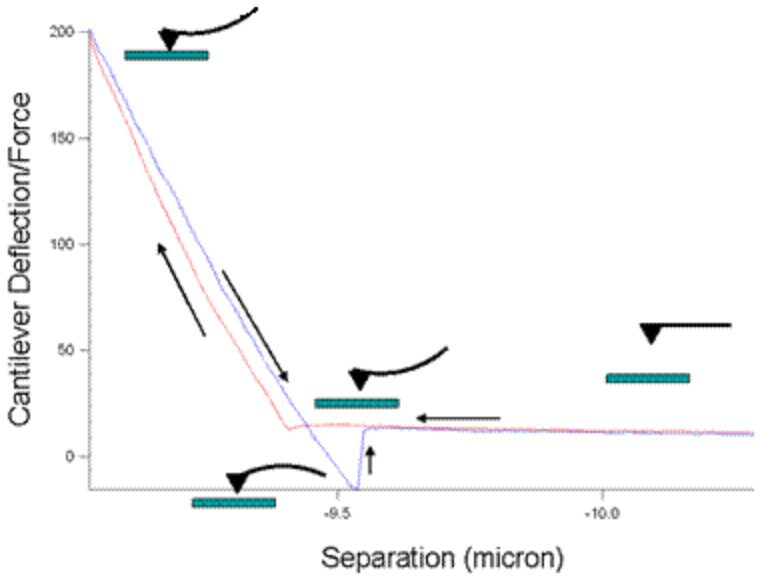

Figure C.2. Force curve of AC240TS cantilever with cellulosic fiber at 90% RH.

The arrows illustrate the path of the force curve trace where the red line is the approach and the blue line is the retraction. The force measurement is initiated by the cantilever's approach to the surface. Once the tip is close enough to the surface it begins to interact and eventually engages the surface of the sample. Once the tip and sample are in contact the cantilever begins deflecting, which increases linearly until the tip stops its approach; this approach distance would be a system input. The tip is then retracted, where it is pulled off the surface. An adhesive attraction between the tip and sample would create a downward deflection of the cantilever until the force exerted by the cantilever exceeds the adhesive force, causing the tip to release, which is illustrated by the vertical deflection at then end of the force deflection trace in Figure C.2.

C.2 Materials and Methods Used in AFM Study

Softwood handsheets were prepared at a 50 gsm basis weight and allowed to air dry overnight. Handsheets were laid on brass screens and dipped into polyelectrolyte solutions for five minutes, removed, excess solution was dripped off, and the samples were allowed to dry overnight. Samples were then stored in a desiccator.

When ready, samples were cut to size, ranging from 0.5 cm^2 to 2 cm^2, and placed on a piece of double sided sticky tape, which was adhered to a round glass wafer. The wafer was placed into an environmental chamber, where environmental humidity could be controlled.

The AFM based study was performed using an Asylum Research MFP-3D™ atomic force microscope with a MFP-3D Closed Fluid Cell and BioHeater. Ultra pure nitrogen gas was plumbed to the fluid cell through two parallel AALBORG mass flow meters flowing at most 10 mL/min and a 20 kPa gauge pressure; one line was bubbled through and air-stone submerged in ultra pure water. Humidity in the closed fluid cell was controlled by changing the ratio between the dry and wet gas lines. The MFP-3D system is housed in an acoustic enclosure to minimize noise and vibrations. Images of the AFM system are in the following Figure C.3. The (left) image shows the basic AFM base, scanner and head. The (middle left) schematic highlights the mechanics and laser path of the AFM head. The (middle right) schematic shows the parts that make up the closed fluid cell. A tutorial video is available from Asylum to assemble and maintain the fluid cell. Finally, the (right) image shows an SEM image of an AFM probe where the

cantilever is mounted to a chip base shown on the far left of the image. The tip is at the very end of the cantilever.

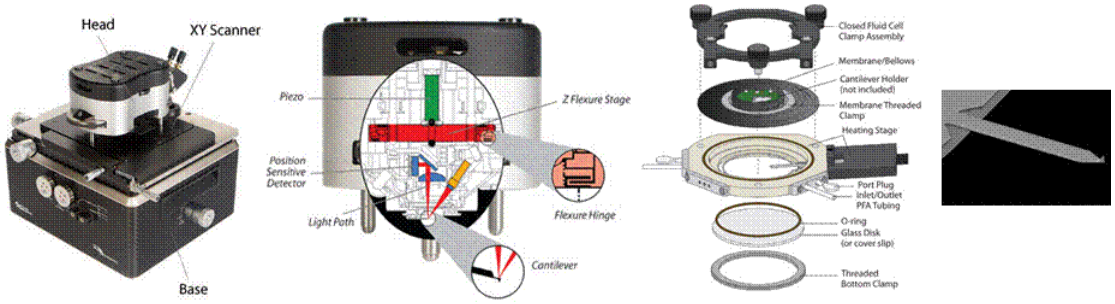

Figure C.3. Images of AFM equipment. (Left) Image of a basic MFP-3D AFM head, base, and scanner system. (Middle left) Schematic of MFP-3D head. (Middle right) Image of a MFP-3D Closed Fluid Cell and BioHeater. (Right) SEM image of an AC240TS cantilever and tip, which is mounted onto the AFM head. Images are taken from Asylum Research website.

The AFM probe, AC240TS, is manufactured by Olympus. This general application probe is made from silicon and has a reflective backside coating made from aluminum (approximately 100 nm thick). The cantilever nominal spring constant is 2 N/m with a resonant frequency ranging from 50 kHz to 90 kHz. The cantilever has a rectangular shape with the width, length, and thickness of 30 ± 2 μm, 240 ± 10 μm, and 2.7 ± 1 μm respectably. The tip has a 3-sided triangular spike shape with the tip height of 14 ± 4 μm and an apex radius 9 ± 2 nm. The AC240TS probe is meant to be used in air and is commonly used in a tapping mode and in forces traces. Si tips have a native SiO_2 layer, which make the tip surface hydrophilic**.**

C.3 AFM Imaging

Scanning probe microscopy methods have been applied to studying wood fiber and paper research (Niemi et al., 2002). Some investigation has gone into studying morphological changes of cellulose treated with cellulase. For example, Lee et al. reported AFM micrographs showing CBH I tracking action along the surface of a cellulose fiber.

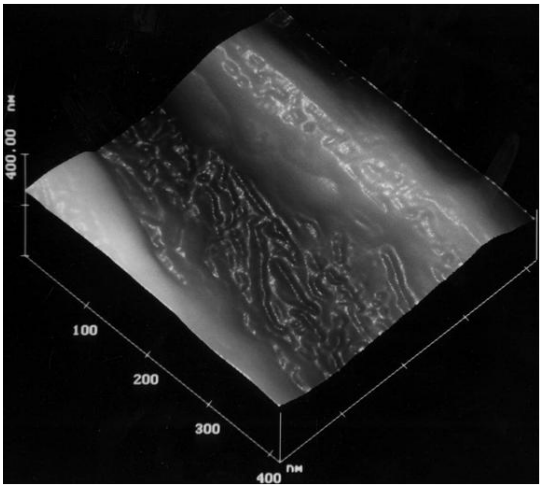

Figure C.4. Cotton fibers incubated with CBH I for 6 hours, dried, and imaged with AFM. The surface of the macrofibrils appears to show indentations and paths caused by the tracking action of the CBH I (Lee et al., 2000).

An example micrograph showed the dented track made by the CBH I as the fiber was treated. This creates a rough surface. In another AFM study, Calvimontes and Stamm (2009) showed that at lower cellulase concentrations a random surface roughening of the cellulose resulted; with increasing enzyme concentration, the cellulose surface became smoother. The focus of literature related to polyelectrolyte treated cellulose is on cellulosic beads immobilizing onto the tip of a cantilever probe, treating the bead with a polyelectrolyte, and performing force measurements (Salmi et al., 2007). Salmi et al. examined how forces between cellulose surfaces changed when treated with different

polyelectrolytes. The results correlated with flocculation observations for fiber flocs in papermaking suspensions.

C.4 Cellulose Fiber Imaging

Handsheets of bleached softwood kraft pulp were treated with 1% (v/v) cellulase. The surface topography in Figure C.5 shows a roughening of the surface. The fiber at time equal to zero shows the untreated surface, and after 10 and 20 minutes, there was noticeable change topography to the surface. This series of reactions was performed at a high cellulase dosage. The roughness, as calculated by the image software, decreases from 263 nm, to 194 nm, to 130 nm respectively. From left to right the height scales show decreasing variation. The rms roughness is a function of the variation in the surface features. As the surface appears more chewed up, the height scale is narrowning. This experiment confirms observations made by Calvimontes and Stamm who reported that with high cellulase loads the roughness decreased.

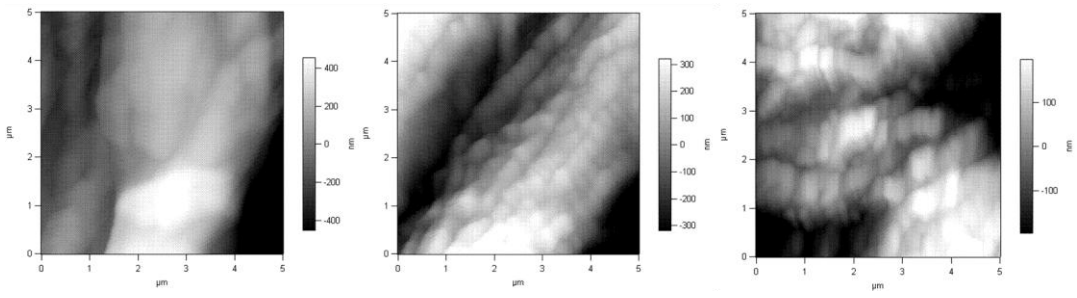

Figure C.5. AFM micrographs of enzymatic hydrolysis of cellulose. The image domains are 5 μm x 5 μm for each image. From left to right are reaction times corresponding to 0, 10, and 20 minutes. Reactions were conducted at room temperature using AC240TS probes (nominal force constant 2 N/m).

Imaging of polyelectrolyte treated samples using the AC240TS probe produced images with sliver and spike like features that were clearly erroneous (images not shown). Imaging with a probe with such a low force constant was not achievable. A new probe, NANOSENSORS™ PPP-NCHR (nominal force constant of 42 N/m and tip radius of curvature < 10 nm) was used to image polyelectrolyte treated systems. The PPP-NCHR probe is much stiffer than the AC240TS probe, which has a nominal force constant of 2 N/m. Treatment of the cellulose fibers did not produce any noticeable change in the surface topology. Thus, the imaging experiments were not as fruitful as anticipated.

C.5 Humidity Control

To best determine how to operate the closed fluid cell a test was performed to monitor moisture adsorption in a handsheet. Three handsheets were dried in an oven at 105^{o}C for 2 hours. The samples were taken out, placed onto a mass balance, and the weight was measured as a function of time. The ambient conditions were 37% relative humidity and the room temperature was 70^{o}C. The results of this test are shown in Figure C.6.

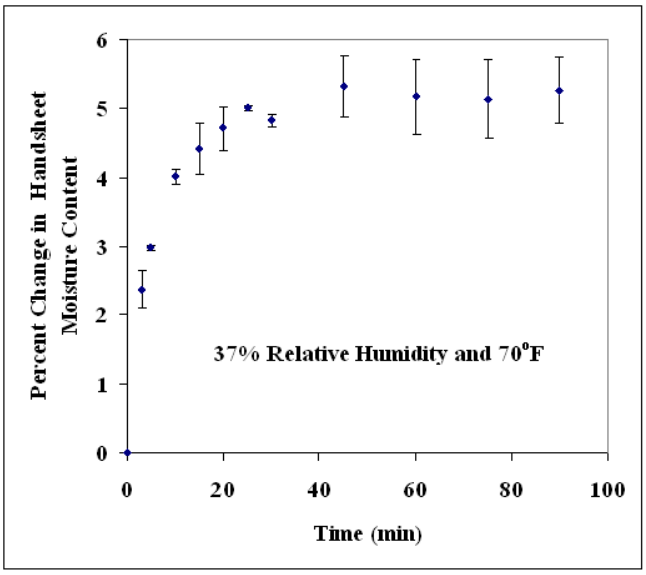

Figure C.6. Time course for change in moisture content in handsheet.

After approximately 50 minutes, the handsheet went from oven dried to reaching equilibrium with the ambient air; it took almost an hour for the cellulose fiber to reach equilibrium. From this test, it was decided that the closed fluid cell would be flushed with ultra pure nitrogen for two hours (a safety factor of two) in order to equilibrate the fiber sample with the gas purging the fluid cell. In a related AFM study, Lee et al. allowed two hours for cellulose samples to equilibrate in a humidity-controlled cell (Lee et al., 2007).

The fluid cell relative humidity was varied by changing the ratios of the mass flow meters supplying ultra pure nitrogen so that a dry line and a wet air line mix to achieve 0%, 20%, 50%, and 90% relative humidity. Force measurements between bleached kraft softwood pulp fiber and an AC240TS probe at varying relative humidity are reported in Figure C.7.

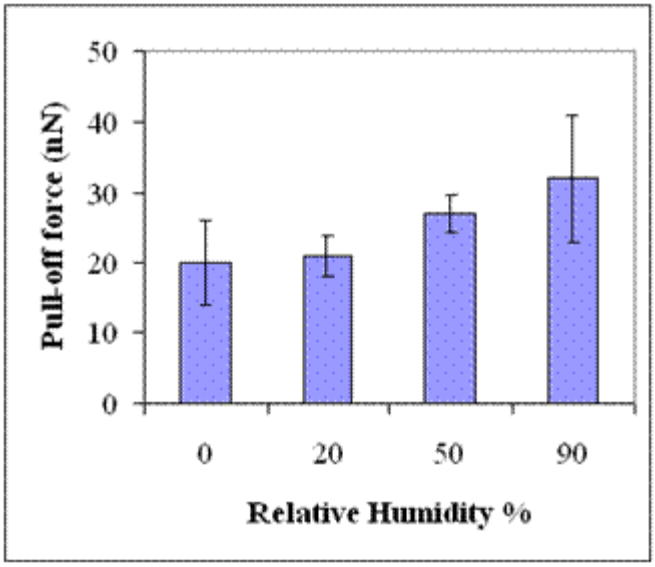

Figure C.7. Pull-off force as a function of relative humidity percent using AC240TS probe and softwood bleached kraft pulp. Each pull-off force is an average of 30 individually measured points from different areas of the handsheet.

From Figure C.7 there is an increase in the pull-off force with increasing relative humidity. With increasing relative humidity, there is an increasing water layer on the surface of both the fiber and the probe. As the probe is approached and retracted a water bridge is formed between the surface water on both the fiber sample and the probe. Under wet air conditions, the water bridge can influence the pull-off force. If the fluid cell was filled with water then the water bridge would no longer be an issue. However, new methods for measuring forces in a liquid fluid would then need to be followed. The pull-off forces show strong adhesive forces, which increase with increasing humidity. In order to avoid the water bridging effects the rest of the experiments were performed under dry conditions with only dry ultrapure nitrogen purging the fluid cell.

C.6 Effect of Cationic Polyelectrolyte on Fiber

Force measurements were made for varying surface treated handsheets made from softwood bleached kraft pulp. Solutions of XP 4409 D grade polyelectrolyte at 0, 1, 10, 100, and 1000 mg/L concentrations were prepared. As described in section 4.6.3, handsheets were dipped into the solutions and allowed to air dry. Samples were stored in a desiccator until needed. Additional handsheets were also treated with various XP series D grade polyelectrolytes, 10%, 40%, and 80%, each prepared at 1000 mg/L, allowed to dry, and stored in a desiccator. Samples were mounted inside the closed fluid cell and the cell was equilibriated with dry ultrapure nitrogen for 2 hours. The effect of varying polyelectrolyte cationicity on fiber surface was analyzed with results in the following figure.

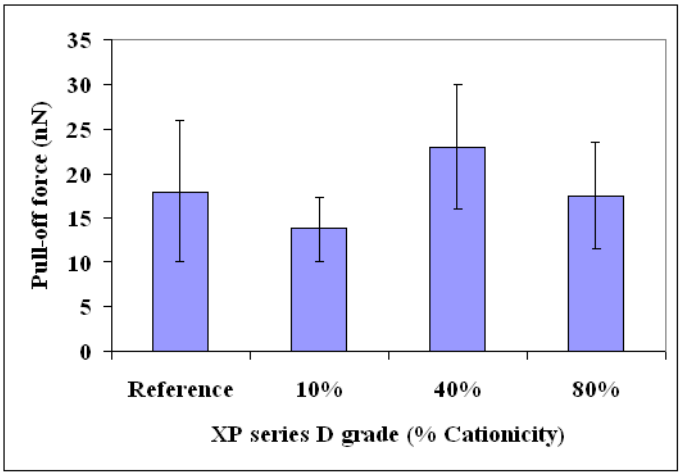

Figure C.8. Effect of varying cationicity on fiber surface.

The data in Figure C.8 were generated using a method called force mapping. Each measurement is an average of 500 data points. All the values are the same within experimental error. There is no difference and the AC240TS tip does not mimic the enzyme. Using XP 4409 D grade polyelectrolyte, the effect of polyelectrolyte concentration on fiber surface was tested, with results reported in the following Figure C.9.

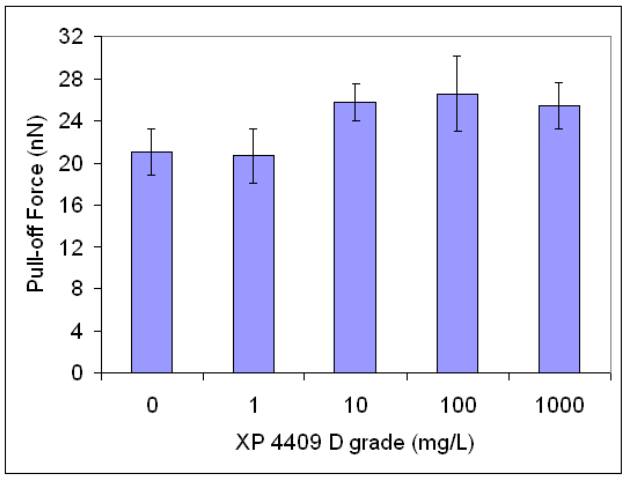

Figure C.9. Effect of polyelectrolyte concentration on fiber surface. Each measurement is an average of 50 data points.

The pull-off force for 0 and 1 mg/L were essentially the same. At 10, 100, and 1000 mg/L the presence of the polyelectrolyte showed an increase in the adhesion force. Therefore, at high concentrations, 10 mg/L $\leq$, polyelectrolyte surface coverage appears the same as measured by a silicon AFM probe. The estimated tip surface area could potentially be as low as 255 nm^2; depending on the tip penetration as much as 9 μm^2 of the tip could make contact with the fiber surface. This is a problem working with a soft material. The average softwood fiber diameter is 40 μm, tip radius 9 nm, tip height 14

micron, and a typical cantilever deflection of 2 μm, (Smook, 1989). At this scale, the polyelectrolyte is most certainly making contact with more than just the top surface and would thus make it difficult to estimate surface coverage by force measurement; another AFM method or another method outright might be better. TEM studies by Nanko et al. (2003) imaged cationic polyacrylamides on cellulose and starch using gold nanoparticles that bound to the polyelectrolyte in order to image fine structures of the polyelectrolyte bound on a given material.

APPENDIX D

ANOVA AND T-TEST STATISTICS

An unpaired (two sample) *t*-test compares the means of two groups. It tests the null hypothesis that the population mean related to two independent, random samples from an approximately normal distribution are equal. The alternative hypothesis is that the means are different.

Table D.1. Interpretation of unpaired t-test results.

If	Then
p value < α	Reject the null hypothesis
p value > α	Accept the null hypothesis

Analysis of variance (ANOVA) compares three or more groups. Two factor ANOVA is used to determine if two factors have the same mean value. The null hypothesis is that the means are equal (i.e. factor 1's mean = factor 2's mean), the alternative hypothesis is that the means are different. The goal is to accept or reject the null hypothesis at a confidence level of 95%.

Table D.2. Interpretation of ANOVA two-way without replication results.

If	Then
test statistic > critical value (i.e. F> Fcrit)	Reject the null hypothesis
test statistic < critical value (i.e. F< Fcrit)	Accept the null hypothesis
p value < α	Reject the null hypothesis
p value > α	Accept the null hypothesis

D.1 Dynamic Light Scattering Analysis

ANOVA was used for comparing the difference between diffusion coefficients by three polyelectrolyte concentrations for five different cationicity polyelectrolytes. ANOVA Two-Factor Without Replication (alpha=0.05 for a 95% confidence) was run to compare samples.

Table D.3. Raw cationicity data used for ANOVA analysis.

% Cationicity	10 ppm	100 ppm	1000 ppm
10%	2.53E-09	5.84E-09	1.23E-08
25%	2.65E-09	4.86E-09	9.84E-09
40%	2.58E-09	7.44E-09	1.52E-08
60%	2.70E-09	6.12E-09	1.60E-08
80%	2.74E-09	5.70E-09	1.11E-08

Table D.4. ANOVA cationicity calculation summary.

Anova: Two-Factor Without Replication	Alpha	0.05		
SUMMARY	*Count*	*Sum*	*Average*	*Variance*
2.65E-09	2	1.47E-08	7.35E-09	1.24E-17
2.58E-09	2	2.26E-08	1.13E-08	3.01E-17
2.7E-09	2	2.21E-08	1.11E-08	4.88E-17
2.74E-09	2	1.68E-08	8.4E-09	1.46E-17
5.84E-09	4	2.41E-08	6.03E-09	1.16E-18
1.23E-08	4	5.21E-08	1.3E-08	9.14E-18

Table D.5. ANOVA results for cationicity.

Source of Variation	*SS*	*df*	*MS*	*F*	*P-value*	*F crit*
Row (Cationicity)	2.31E-17	3	7.72E-18	2.984541	0.196571	9.276628
Column (Concentration)	9.81E-17	1	9.81E-17	37.95957	0.008605	10.12796
Error	7.76E-18	3	2.59E-18			
Total	1.29E-16	7				

Here the P-values for the rows (i.e., all diffusion coefficients of different cationicity) is not less than alpha (0.05), so we can accept the hypothesis that all of the diffusion coefficients with different cationicities are the same. The P-value for columns (i.e., polyelectrolyte concentration) is less than alpha, so we can reject the hypothesis that all of the diffusion coefficients with different polyelectrolyte concentrations are the same.

ANOVA was used for comparing the difference between diffusion coefficients by three polyelectrolyte concentrations for four different molecular weight polyelectrolytes. ANOVA Two-Factor Without Replication (alpha=0.05 for a 95% confidence) was run to compare samples.

Table D.6. Raw molecular weight data used for ANOVA analysis.

MW (MDa)	10 ppm	100 ppm	1000 ppm
Std	2.6E-09	7.4E-09	1.5E-08
SH	3.5E-09	1.1E-08	2.1E-08
SSH	3.4E-09	8.8E-09	1.5E-08
VHM	2.5E-09	8.5E-09	1.8E-08

Table D.7. ANOVA molecular weight calculation summary.

Anova: Two-Factor Without Replication	Alpha	0.05		
SUMMARY	*Count*	*Sum*	*Average*	*Variance*
3.48E-09	2	3.21E-08	1.61E-08	5.51E-17
3.43E-09	2	2.42E-08	1.21E-08	2.16E-17
2.45E-09	2	2.64E-08	1.32E-08	4.44E-17
7.44E-09	3	2.81E-08	9.37E-09	1.56E-18
1.52E-08	3	5.46E-08	1.82E-08	8.77E-18

Table D.8. ANOVA results for molecular weight.

Source of Variation	*SS*	*df*	*MS*	*F*	*P-value*	*F crit*
Rows	1.65E-17	2	8.27E-18	4.013851	0.199447	19
Columns	1.17E-16	1	1.17E-16	56.74179	0.017171	18.51282
Error	4.12E-18	2	2.06E-18			
Total	1.38E-16	5				

Here the P-values for the rows (i.e., all diffusion coefficients with different molecular weights) are not less than alpha (0.05), so we can accept the hypothesis that all of the diffusion coefficients with different molecular weight are the same. The P-value for columns (i.e., polyelectrolyte concentration) is less than alpha, so we can reject the hypothesis that all of the diffusion coefficients with different polyelectrolyte concentrations are the same.

ANOVA was used for comparing the difference between diffusion coefficients by three polyelectrolyte concentrations in five different ionic strengths (citrate buffered) solutions. ANOVA Two-Factor Without Replication (alpha=0.05 for a 95% confidence) was run to compare samples.

Table D.9. Raw ionic strength data used for ANOVA analysis.

mM	10 ppm	100 ppm	1000 ppm
5	8.64E-09	1.29E-08	3.3E-08
10	9.43E-09	1.24E-08	3.4E-08
50	1.79E-08	4.45E-08	3.1E-08
100	9.44E-08	4.72E-08	3.5E-08
500	2.65E-07	4.66E-08	2.9E-08

Table D.10. ANOVA ionic strength calculation summary.

Anova: Two-Factor Without Replication	Alpha	0.05		
SUMMARY	*Count*	*Sum*	*Average*	*Variance*
9.43E-09	2	4.63E-08	2.32E-08	2.31E-16
1.79E-08	2	7.53E-08	3.77E-08	9.38E-17
9.44E-08	2	8.2E-08	4.1E-08	7.69E-17
2.65E-07	2	7.51E-08	3.76E-08	1.64E-16
1.29E-08	4	1.51E-07	3.77E-08	2.85E-16
3.32E-08	4	1.28E-07	3.2E-08	8.38E-18

Table D.11. ANOVA results for varying ionic strength.

Source of Variation	*SS*	*df*	*MS*	*F*	*P-value*	*F crit*
Rows	3.8E-16	3	1.27E-16	0.757483	0.587568	9.276628
Columns	6.44E-17	1	6.44E-17	0.385509	0.578649	10.12796
Error	5.01E-16	3	1.67E-16			
Total	9.45E-16	7				

Here the P-values for the rows (i.e., all diffusion coefficients with different citrate concentration) is not less than alpha (0.05), so we can accept the hypothesis that all of the diffusion coefficients in solutions with different ionic strengths are the same. The P-value for columns (i.e., polyelectrolyte concentration) is not less than alpha, so we can accept the hypothesis that all of the diffusion coefficients with different citrate concentrations are the same.

ANOVA was used for comparing the difference between three polyelectrolyte concentrations with and without cellulase in solution. The rows in Table D.12 correspond to 10, 100, and 1000 ppm polyelectrolyte concentration and the columns correspond to cationicity of polyelectrolyte used. It was shown above that the mean

diffusion coefficients for various cationicity polyelectrolytes were the same, but that polyelectrolyte concentration showed the means were not the same. Ratios of diffusion coefficients for polyelectrolytes with cellulase / polyelectrolyte without cellulase were used to compare whether differences in the diffusion coefficient are significant between polyelectrolytes with and without cellulase addition. ANOVA Two-Factor Without Replication (alpha=0.05 for a 95% confidence) was run to compare samples.

Table D.12. Raw PCC with and without cellulase data used for ANOVA analysis.

Polyelectrolyte (ppm)	10% Cationicity	40% Cationicity	80% Cationicity
10	1.47	1.72	1.54
100	1.38	1.31	1.32
1000	1.07	1.09	1.19

Table D.13. ANOVA PCC with and without cellulase summary.

Anova: Two-Factor Without Replication	Alpha	0.05		
SUMMARY	*Count*	*Sum*	*Average*	*Variance*
1.378424658	2	2.626684	1.313342	3.53E-05
1.073170732	2	2.281294	1.140647	0.004713
1.724806202	2	2.401245	1.200623	0.023552
1.54379562	2	2.506733	1.253367	0.008237

Table D.14. ANOVA results for PCC with and without cellulase.

Source of Variation	*SS*	*Df*	*MS*	*F*	*P-value*	*F crit*
Rows	0.029823	1	0.029823	15.16937	0.159998	161.4476
Columns	0.002782	1	0.002782	1.414999	0.445028	161.4476
Error	0.001966	1	0.001966			
Total	0.034571	3				

Here the P-values for the rows (i.e., polyelectrolyte concentration) is not less than alpha (0.05), so we can accept the hypothesis that all of the diffusion coefficients ratios with and without cellulase are the same. The P-value for columns (i.e., different cationicity polyelectrolytes) is not less than alpha, so we can accept the hypothesis that all of the diffusion coefficient ratios with different polyelectrolyte cationicities are the same.

D.2 Statistical Comparison of Binding Data

Next, a statistical comparison was performed for data for where cellulase was bound to cellulosic fiber. Unpaired t-test analysis was used for comparing data from Figure 5.34. A t test calculator was used from GraphPad Software. The data entry format required entering the sample mean, standard deviation, and number of observations. Table D.15 summarizes the unpaired (two sample) t-test comparing the mean of two groups.

Table D.15. Summary of t-test analysis for cellulase bound to polyelectrolyte treated cellulosic fiber.

Cellujlase (v/v)%	Two-tailed P-value	T	Statistically Significant (SS) or Not Statistically Significant (NSS)
0.25%			
Control - XP10023L	0.0001	19.4012	SS
Control - XP10025L	0.0001	19.2199	SS
Control - XP10033L	0.0001	17.8679	SS
XP10023L - XP10025L	0.9036	0.1289	NSS
XP10023L - XP10033L	0.0024	6.8212	SS
XP10025L - XP10033L	0.0026	6.6670	SS
0.50%			
Control - XP10023L	0.0001	21.2164	SS
Control - XP10025L	0.0001	20.5272	SS
Control - XP10033L	0.0001	20.7441	SS
XP10023L - XP10025L	0.3169	1.1428	NSS
XP10023L - XP10033L	0.0051	5.5638	SS
XP10025L - XP10033L	0.0118	4.3933	SS

Table D.16. Summary of statistical significance of binding data.

Unpaired t test for Data from Figure 5.34				
	Control	10%	40%	80%
Control	-	SS	SS	SS
10%		-	NSS	SS
40%			-	SS
80%				-

It was found that there was a positive statistical significance between all samples except samples where cellulase was bound to 10% and 40% cationicity treated samples. Both samples show significant binding, but compared to each other there was no statistical difference.

Next, a statistical comparison was performed for data for where cellulase was bound to cellulosic fiber treated with cationic polyelectrolyte. Unpaired t-test analysis was used for comparing data from Figure 5.37. A t-test calculator was used from GraphPad Software. The data entry format required entering the sample mean, standard deviation, and number of observations. The following table summarizes the unpaired (two sample) t-test comparing the mean of two groups.

Table D.17. Summary of t-test for binding data from Figure 5.37.

Test	Two-tailed P-value	t	Statistically Significant (SS) or Not Statistically Significant (NSS)
Control - XP10023L	0.0420	2.9485	SS
Control - XP10025L	0.0136	4.2113	SS
Control - XP10033L	0.1721	1.6607	NSS
XP10023L - XP10025L	0.2699	1.2793	NSS
XP10023L - XP10033L	0.2767	1.2585	NSS
XP10025L - XP10033L	0.0620	2.5693	NSS
Control – XP10025L	0.0136	4.2113	SS
Control – XP10025	0.0755	2.3858	NSS
Control – XP10025H	0.1928	1.5641	NSS
XP10025L - XP10025	0.1639	1.7025	NSS
XP10025L - XP10025H	0.0620	2.5693	NSS
XP10025 - XP10025H	0.8799	0.161	NSS

The results suggest that there is a statistical significance between the control and both 10% and 40% cationicity samples. There was not a statistical difference between the control and the 80% cationicity sample. As for molecular weight, there was statistical significance between the control and the XP10025L sample but the higher molecular weight samples (each 40% cationicity) did not show a statistical difference compared with the control or between themselves.

D.3 Statistical Comparison of Kinetics Data

ANOVA was used for comparing the difference in enzymatic hydrolysis (relative glucose production from handsheets) between temperatures (30, 40, 50^{o}C) and six different fiber furnishes. ANOVA Two-Factor Without Replication (alpha=0.05 for a 95% confidence) was run to compare samples.

Table D.18. ANOVA summary of handsheet data from Figure 5.44.

Anova: Two-Factor Without Replication	Alpha	0.05		
SUMMARY	*Count*	*Sum*	*Average*	*Variance*
60	5	192	38.4	300.3
100	5	240	48	683.5
19	2	58	29	72
20	2	58	29	8
24	2	68	34	8
32	2	88	44	0
35	2	160	80	392

Table D.19. ANOVA results summary of handsheet data from Figure 5.44.

ANOVA						
Source of Variation	*SS*	*df*	*MS*	*F*	*P-value*	*F crit*
Rows	230.4	1	230.4	3.692308	0.127046	7.708647
Columns	3685.6	4	921.4	14.76603	0.011559	6.388233
Error	249.6	4	62.4			
Total	4165.6	9				

Here the P-values for the rows (i.e., effect of temperature on relative glucose production) are not less than alpha (0.05), so we can accept the hypothesis that all of the relative glucose production at different temperatures are the same. The P-value for columns (i.e., effect of furnish on relative glucose production) is less than alpha, so we can reject the hypothesis that all of the relative glucose production are the same for the various fiber handsheet samples.

ANOVA was used for comparing the difference in enzymatic hydrolysis (relative glucose production from dispersed fiber) between temperatures (30, 40, 50^{o}C) and six different

fiber furnishes. ANOVA Two-Factor Without Replication (alpha=0.05 for a 95% confidence) was run to compare samples.

Table D.20. ANOVA summary of dispersed fiber data from Figure 5.44.

Anova: Two-Factor Without Replication	Alpha	0.05		
SUMMARY	*Count*	*Sum*	*Average*	*Variance*
168	5	417	83.4	2943.8
218	5	491	98.2	5923.7
42	2	95	47.5	12.5
29	2	86	43	50
72	2	159	79.5	12.5
70	2	161	80.5	12.5
106	2	407	203.5	1740.5

Table D.21. ANOVA results summary of dispersed fiber data from Figure 5.44.

Source of Variation	*SS*	*Df*	*MS*	*F*	*P-value*	*F crit*
Rows	547.6	1	547.6	1.710715	0.260994	7.708647
Columns	34189.6	4	8547.4	26.70228	0.003815	6.388233
Error	1280.4	4	320.1			
Total	36017.6	9				

Here the P-values for the rows (i.e., effect of temperature on relative glucose production) is not less than alpha (0.05), so we can accept the hypothesis that all of the relative glucose production at different temperatures are the same. The P-value for columns (i.e., effect of furnish on relative glucose production) is less than alpha, so we can reject the hypothesis that all of the relative glucose production are the same for the various dispersed fiber samples.

For softwood furnishes the SWD (28 mesh) and SWD furnishes do not show any significant temperature dependence when hydrolyzed as a handsheet or dispersed fibers as summarized in the following table.

Table D.22. ANOVA results summary of SWD fiber data from Figure 5.43.

Handsheets			
T (*C)	SWD (28 mesh)	SWD	Fines
30	32	24	35
40	44	32	66
50	44	36	94
Dispersed Fiber			
T (*C)	SWD (28 mesh)	SWD	Fines
30	70	72	106
40	78	82	174
50	83	77	233

However, the softwood fines for both handsheet and dispersed fiber hydrolysis do show significant temperature dependence, which was masked by the other data in the prior ANOVA analysis. However, t-tests comparison between the SWD (28 mesh) and fines shows that for the dispersed fiber samples each of the unpaired t-tests results were extremely statistically significant for each of the three temperatures. P-values were all equal to or less than 0.0007 and t values were all 9.2952 to 16.1126.

D.3 Statistical Comparison of Screening Kinetics

Finally, a statistical comparison was performed on data for a hydrolysis screening of cellulosic fiber and cornstarch both treated with cationic polyelectrolyte. Unpaired t-test analysis was used for comparing data from Figure 5.45. A t-test calculator was used from GraphPad Software. The data entry format required entering the sample mean,

standard deviation, and number of observations. The following table summarizes the unpaired (two sample) t-test comparing the mean of two groups.

For the fiber screening, 17 of 22 sample means were greater then the control (no polyelectrolyte added). Of the 22 samples, 9 were found to be positively statistically significant. The BS and BC series polyelectrolytes were found to be the most significant.

For the cornstarch screening, 19 of 22 sample means were greater then the control (no polyelectrolyte added). Of the 22 samples, 14 were found to be positively statistically significant. Overall, the emulsions series were found to be best for the cornstarch hydrolysis while the BS series also showed some significance with medium and higher cationicities.

REFERENCES

Adney, B., & Baker , J. (1996). *Measurement of Cellulase Activities: Laboratory Analytical Procedure (LAP): NREL/TP-510-42628*. Golden, CO: National Renewable Energy Laboratory.

Allen, L., Polverari, M., Levesque, B., Rancis, W. (1996). Effects of system closure on retention and drainage aid performance in TMP newsprint manufacture. *TAPPI Journal, 82*(4), 188-195.

Akerholm, M., Hinterstoisser, B., Salmena, L. (2004). Characterization of the crystalline structure of cellulose using static and dynamic FT-IR spectroscopy. *Carbohydrate Research, 339*, 569–578.

Arica, M.Y., Yavuz, H., Patir, S., Denizli, A. (2000). Immobilization of glucoamylase onto spacer-arm attached magnetic poly(methylmethacrylate) microspheres: characterization and application to a continuous flow reactor. *Journal of Molecular Catalysis B: Enzymatic, 11*, 127-138.

American Society for Testing and Materials. (1985). *Zeta Potential of Colloids in Water and Waste Water, ASTM Standard D 4187-82.* West Conshohocken, PA.

Baldy, M.W. (1997). *The University Wine Course* (Chapter 3). South San Francisco, CA: The Wine Appreciation Guild.

Banerjee, S., Reye, J. (2008), Systems and methods for altering rates of enzymatic processes, World Intellectual Property Organization, filing date:12/18/2008, publication date: 6/25/2009, www.wipo.int/pctdb/en/wo.jsp?WO=2009079634

Banka, R.R. & Mishra, S. (2002). Adsorption properties of the fibril forming protein from *Trichoderma reesei*, *Enzyme and Microbial Technology*, 31, 784-793.

Barr, B.K., Hsieh, Y.L., Ganem, B., Wilson, D.B. (1996). Identification of two functionally different classes of exocellulases. *Biochemistry, 35(2)*, 586-592.

Berghem, L.E.R., Pettersson, L.G., Axiofedriksson, U. (1975). The mechanism of enzymatic degradation. Characterization and enzymatic properties of a B-1,4-glucan cellobiohydrolase from Trichoderma viride. *European Journal of Biochemistry*, *53*, 55-62.

Biermann, C.J. (1993). *Essentials of pulping and papermaking*. San Diego, CA: Academic Press.

Binnig, G., Rohrer, H., Gerber, C., Weibel, E. (1982). Surface studies by scanning tunneling microscopy. *Physical Review Letters, 49,* 57-61.

Binnig, G. Quate, C. F., Gerber C. (1986). Atomic force microscope. *Physical Review Letters, 56,* 930-933.

BioAmerica Inc. (2010). Material Safety Data Sheet - Acryalamide Molecular Biology Grade, www.bioamerica-inc.com/pdf/bioamerica_msds_acrylamide.pdf, MSDS, accessed April 21, 2010

Blakeney, A.B., Matheson, N.K. (1984). Some properties of the stem and pollen starches of rice. *Starch, 36,* 265-269.

Boeris, V., Farruggia, B., Rommanini, D., Pico, G. (2009), How flexible polymers interact with proteins and its relationship with the protein separation method by protein-polymer complex formation. *Protein Journal, 28,* 233-239.

Bohmer, M.R., Evers, O.A., Scheutjens, J.M.H.M. (1990). Weak polyelectrolytes between two surfaces: adsorption and stabilization. *Macromolecules, 23*(8), 2288-2301.

Bohren, C.F., Huffman, D.R. (1998*). Absorption and scattering of light by small particles*. New York, NY: Wiley-VCH.

Bonnarme, P., & Jeffries, T.W. (1990). Mn(II) regulation of lignin peroxidases and manganese-dependent peroxidases from lignin-degrading white rot fungi. *Applied and Environmental Microbiology, 56*(1), 210-217.

Bradford, M.M. (1976). A rapid and sensitive method for the quantitation of microgram quantities of protein utilizing the principle of protein-dye binding. *Analytical Biochemistry, 72,* 248–254.

Brancato, A., Walsh F.L., Sabo, R., Banerjee, S. (2007). Effect of recycling on the properties of paper surfaces. *Industrial & Engineering Chemistry Research, 46*(26), 9103-9106.

Branden, C., & Tooze, J. (1999) *Introduction to protein structure* (Second Edition). Stockholm, Sweden: Garland Science.

Blanch, H.W., & Clark, D.S. (1997) *Biochemical Engineering*. New York, NY: Marcel Dekker.

Brethauer, S., & Wyman, C.E. (2010). Review: Continuous hydrolysis and fermentation for cellulosic ethanol production. *Bioresource Technology, 101*(13), 4862-4874.

Britt, K.W., & Unbehend, J.E. (1976). New methods for monitoring retention. *Tappi Journal, 59*(2), 67.

Brodkey, R.S., & Hershey, H.C. (1988). *Transport phenomena - a unified approach*. New York, NY: McGraw-Hill.

Brotherson, B.A. (2007). *Site blocking effects on adsorbed polyacrylamide conformation* (Doctoral Dissertation). Atlanta, GA: Georgia Institute of Technology.

Brotherson, B., Deng, Y. (2008). Site blocking effect on the conformation of adsorbed cationic polyacrylamide on a solid surface. *Journal of Colloid and Interface Science, 326,* 324-328.

Calvimontes, A., & Stamm, M. (2009). Effect of cellulase enzyme on cellulose nano-topography. *Tensile Surfactants Detergents, 46*(6), 368-372.

Chang, L.L., Raudenbush. D.L., & Dentel, S.K. (2001). Aerobic and anaerobic biodegradability of a flocculant polymer, *Water Science and Technology*, 44(2-3), 461-468

Chen, W. (2009). What is Zeta Potential?. American Filtration & Separations Society (AFS): Educating and Networking Industry Professionals. Richfield, MN

Christensen, G.L., & Dick, R.I. (1985). Specific resistance measurements – methods and procedures. *Journal of Environmental Engineering-ASCE, 111*(3), 258-271.

Chu, B. (1974). *Laser light scattering: basic principles and practice*. New York, NY: Academic Press.

De La Torre Ugarte, D. G., Walsh, M. E., Shapouri, H. and Slinsky, S. P. (2000*). The economic impacts of bioenergy crop production on U.S. agriculture.* USDA report form the Oak Ridge National Laboratory.

Delgado, A.V., Gonzalez-Caballero F., Hunter, R.J., Koopal, L.K., Lyklema, J. (2005). Measurments and interpretation of electrokinetic phenomena. *Pure Applied Chemistry, 77*(10), 1753-1805.

Diniz, J.M.B.F., Gil, M.H., Castro, J.A.A.M. (2004). Hornification - its origin and interpretation in wood pulps. *Wood Science and Technology, 37*(6), 489-494.

Duff, S.J.B., Cooper, D.G., Fuller, O.M. (1985). Cellulase and β -glucosidase production by mixed Culture of *Trichoderma reesi* RUT C30 and *Aspergillus phoenicis*. *Biotechnology Letters, 7*(3), 185-190.

Duff, S.J.B., Cooper, D.G., Fuller, O.M. (1987). Effect of media composition and growth conditions on production of cellulase and β-glucosidase by a mixed fungal fermentation. *Enzyme and Microbial Technology, 9,* 47-52.

Dunham, A.J., Tubergen, K.R., Govoni, S.T., Alfano, J.C. (2000). The effect of dissolved and colloidal substances on flocculation of mechanical pulps. *Journal of Pulp and Paper Science, 26*(3), 95-101.

Dunham, A.J., Sherman, L.M., Alfano, J.C. (2002). Effect of dissolved and colloidal substances on drainage properties of mechanical pulp suspensions. *Journal of Pulp and Paper Science, 28*(9), 298-304.

Eisenberg H, Mohan GR (1959). Aqueous solutions of polyvinylsulfonic acid: phase separation and specific. interactions with ions, viscosity, conductance and potentiometry. *Journal of Physical Chemistry, 63*(5), 671-680.

Eisenberg, H., & Casassa, E.F. (1960). Aqueous solutions of salts of poly(vinylsulfonic acid). *Journal of Polymer Science, 47*, 29-44.

Eklund, D. & Lindstrom, T. (1991). *Paper chemistry: an introduction.* Grankulla, Finland: DT Paper Science Publications.

Enarsson, L.E., Wagberg, L., Carlen, J., Ottosson, N. (2009). Tailoring the chemistry of polyelectrolytes to control their adsorption on cellulosic surfaces. *Colloids and Surfaces A: Physicochemical Engineering Aspects, 340*, 135-142.

Enayati, N. & Parulekar, S.J. (1995). Enzymatic saccharification of sybean hull-based materials. *Biotechnology Progress, 11*, 708-711.

Fan, Z., South, C., Lyford, K., Munsie, J., van Walsum, P., Lynd, L.R. (2004). Conversion of paper sludge to ethanol in a semicontinuous solids-fed reactor. *Bioprocess Biosystems Engineering, 26*, 93-101.

Fleer, G.J., Cohen-Stuart, M.A., Scheutjens, J.M.H.M., Cosgrove, T., Vincent, B. (Eds.), (1993). *Polymers at Interfaces* (pp. 343-375). London, UK: Springer.

Flory, P.J. (1941). Thermodynamics of high polymer solutions. *Journal of Chemical Physics, 9*(8), 660-661.

Flory, P.J. (1942). Thermodynamics of high polymer solutions. *Journal of Chemical Physics, 10*, 51-61.

Fundin, J., Brown, W., Vethamuthu, M.S. (1996). Poly((N,N,N-trimethylammonio)ethyl acrylate chloride salt) (PCMA)-SDS complex formation in dilute aqueous solution. Light scattering and time-resolved fluorescence quenching measurements. *Macromolecules, 29*(4), 1195-1203.

Fundin, J., Brown, W., Ilipoulos, I., Claesson, P.M. (1999). The interaction between sodium dodecylsulfate and the cationic-nonionic random copolymer (3-(2-methylpropionamide)propyl) trimethylammonium chloride-acrylamide of two different charge densities studied using dynamic light scattering and rheometry. *Colloid Polymer Science, 277*, 25-33.

Garcia-Conesa, M.-T., Kroon, P.A., Ralph, J., Mellon, F.A., Colquhoun, I.J., Saulnier, L., Thibault, J.-F., Williamson, G. (1999). A cinnamoyl esterase from Aspergillus niger can break plant cell wall cross-links without release of free deferulic acids. *European Journal of Biochemistry, 266*, 644-652.

Gardner-Chavis, R.A., Reye, J. (2003). Unified explanation of catalyzed and non-catalyzed chemical reactions, *Journal of Molecular Catalysis A-Chemical*, 206(1-2), 269-289.

Ghose, T.K. (1987). Measurement of cellulase activities. *Pure & Applied Chemistry, 59*, 257-268.

Goldstein, M.A., Takagi, M., Hashida, S., Shoseyov, O., Doi, R.H., Segil, I.H. (1993). Characterization of the cellulose-binding domain of the clostridium-cellulovorans cellulose-binding domain-A. *Journal of Bacteriology, 175*(18), 5762-5768.

Gomez, L.D., Steele-King, C.G., McQueen-Mason, S.J. (2008). Sustainable liquid biofuels from biomass: the writing's on the walls. *New Phytologist, 178*, 473-485.

Gong, C.S., Ladisch, M.R., Tsao, G.T. (1977). Cellobiase from *Trichoderma viride*: Purification, properties, kinetics, and mechanism. *Biotechnology and Bioengineering, 19*, 959-981.

Gray, K.A., Zhao, L., Emptage, M., (2006). Bioethanol. *Current Opinion in Chemical Biology, 10*, 141-146.

Griebel, T., Kulicke, W.M. (1992). Molecular characterization of water-soluble, cationic polyelectrolytes. *Makromolekulare Chemie-Macromolecular Chemistry and Physics, 193*(3), 811-821.

Grula, M.M., Huang, M. & Sewell, G. (1994). Interactions of certain polyacrylamides with soil bacteria. *Soil Science*, 158, 291–300.

Gurnagul, N., Howard, R C., Zou, X., Uesaka, T., Page, D.H. (1993). The mechanical permanence of paper: a literature review. *Journal of Pulp and Paper Science, 19*(4), J160-J166.

Hahn-Hägerdal, B., Galbe, M., Gorwa-Grauslund, M.F., Lidén, G., Zacchi, G. (2006). Bio-ethanol – the fuel of tomorrow from the residues of today. *Trends in Biotechnology, 24*(12), 549-556.

Harris, D., Stork, J., Debolt, S. (2009). Genetic modification in cellulose-synthase reduces crystallinity and improves biochemical conversion to fermentable sugar. Global Change Biology Bioenergy, 1(1), 51-61.

Hartley, W.H., & Banerjee, S. (2008). Imaging c-PAM-induced flocculation of paper fibers. *Journal of Colloid and Interface Science, 320*, 159-162

Hilden, L., Valjamae, P., Johansson, G. (2005). Surface character of pulp fibres studied using endoglucanases. *Journal of Biotechnology 118*(4), 386-397.

Ho, K.M., Mao, X.P., Gu, L.Q., Li, P. (2008). Facile route to enzyme immobilization: Core-shell nanoenzyme particles consisting of well-defines poly(methyl methacrylate) cores and cellulase shells. *Langmuir, 24* (19), 11036–11042.

Holtzapple, M.T., Caram, H.S., Humphrey, A.E., The HCH-1 model of enzymatic cellulose hydrolysis. *Biotechnology & Bioengineering*, *26*, 775-780.

Hu, G., Heitmann Jr., J.A., Rojas, O.J. (2009). In situ monitoring of cellulase activity by microgravimetry with a quartz crystal microbalance. *Journal of Physical Chemistry B, 113*, 14761-14768.

Hubbe, M.A. & Rojas, O.J. (2008). Colloidal stability and aggregation of lignocellulosic materials in aqueous suspension: A Review. *BioResources, 3*(4), 1419-1491.

Hubbe, M.A., Nanko, H., McNeal, M.R (2009). Retention aid polymer ineractions with cellulosic surfaces and suspensions: A Review. *Bioresource, 4*(2), 850-906.

Huggins, M.L. (1941). Solutions of long chain compounds. *Journal of Chemical Physics, 9*(5), 440.

Ikegami, A. & Imai, N. (1962). Precipitation of polyelectrolytes by salts. *Journal of Polymer Science, 56*, 133.

Ingesson, H., Zacchi, G., Yang, B., Esteghlalian, A.R., Saddler, J.N., (2001). The effect of shaking regime on the rate and extent of enzymatic hydrolysis of cellulose. *Journal of Biotechnology, 88,* 177-182.

Jenkel, E., Rumback, B., (1951). Adsorption of high polymers from solution. *Z. Elektrochem, 55*, 612-618.

Jeoh, T., Ishizawa, C.I., Davis, M.F., Himmel, M.E., Adney, W.S., Johnson, D.K., (2007). Cellulase digestibility of pretreated biomass is limited by cellulose accessibility. *Biotechnology and Bioengineering, 98*(1), 112-122.

Jung, Y.C., & Bhushan, B.. Contact angle, adhesion and friction properties of micro and nanopatterned polymers for superhydrophobicity. *Nanotechnology, 17*(19), 4970-4980.

Kadam, K.L. & J.D. McMillan, (2003). Availability of corn stover as a sustainable feedstock for bioethanol production. *Bioresource Technology, 88,* 17-25.

Kadirvelu, K., & Namasivayam, C. (2000). Agricultural by-product as metal adsorbent: Sorption of lead(II) from aqueous solutions onto coir-pith carbon. *Environmental technology, 21*(10), 1091-1097.

Kam, S., Gregory, J. (1999). Charge determination of synthetic cationic polyelectroyles by colloid titration. *Colloids and Surfaces A: Physicochemical and Engineering Aspects, 159,* 165-179.

Kamiti, M., Dabros, T., van de Ven, T.G.M. (1995). Kinetics of surface coagulation. *Journal of Colloid and Interface Science, 172*(2), 459-466.

Kamiti, M., van de Ven, T.G.M. (1995). Impinging jet studies of the kinetics of deposition and dissolution of calcium carbonate particles. *Colloids and Surface A: Physiochemical and Engineering Aspects, 100,* 117-129.

Keating, J.D., Panganiban, C., Mansfield, S.D. (2006). Tolerance and adaptation of ethanologenic yeast to lignocellulosic inhibitory yeast. *Biotechnology & Bioengineering, 93*(6), 1196-1206.

Kersten, P.J., & Cullen, D. (2004*). Enzymology and molecular biology of lignin degradation* (pp. 249-273). In *Biochemistry and Molecular Biology*. Springer-Verlag: Berlin-Heidelberg.

Kim, D.W., & Hong, Y.G. (2000). Ionic strength effect on adsorption of cellobiohydrolases I and II on microcrystalline cellulose. *Biotechnology letters,* 22(16) 1337-1342.

Kipper, K., & Väljamäe, P., Johansson, G. (2005). Processive action of cellobiohydrolase Cel7A from *Trichoderma reesei* is revealed as ‘burst’ kinetics on fluorescent polymeric model substrate. *Biochemical Journal, 385,* 527–535.

Kirk, T.K. & Jeffries, T.W. (1996*). Roles for microbial enzymes in pulp and paper processing.* ACS Symposium Series 655.

Kitahara, A., Katano, S., Fujii, T. (1971). Dependence of zeta-potential upon particle-size and capillary radius at streaming potential study in non-aqueous media. *Bulletin of the Chemical Society of Japan, 44*(12), 3242-3245.

Kontturi, E.J. (2005). Surface Chemistry of Cellulose: from natural fibres to model surface (Doctoral Dissertation). geboren te Espoo, Finland: Technische Universiteit Eindhoven.

Krahulec, S., Petschacher, B., Wallner, M., Longus, K., Klimacek, M., Nidetzky, B. (2010). Fermentation of mixed glucose-xylose substrates by engineered strains of Saccharomyces cerevisiae: role of the coenzyme specificity of xylose reductase, and effect of glucose on xylose utilization. *Microbial Cell Factories, 9*(16).

Kunst, A., Draeger, B., Ziegenhorn, J. (1988). *Methods of enzymatic analysis* (Vol.VI, 163-172). Cambridge, UK: VCH Publishers (UK) Ltd.

Lark, N., Xia, Y., Qin, C-G., Gong, C.S., Tsao, G.T. (1997). Production of ethanol from recycled paper sludge using cellulase and yeast, *Kluveromyces marxianus. Biomass & Bioenergy, 12*, 135-143.

Larsson, A., Walldal, C., Wall, S. (1999). Flocculation of cationic polymers and nanosized particles. *Colliods and Surfaces A: Physicochemical and Engineering Aspects, 159*, 65-76.

Lee, I., Evans, B.R., Woodward, J. (2000). The mechanism of cellulase action on cotton fibers: evidence from atomic force microscopy. *Ultramicroscopy, 82*, 213-221.

Lee, J.M., Heitmann, J.A., Pawlak, J.J. (2007). Local morphological and dimensional changes of enzyme-degraded cellulose materials measured by atomic force microscopy. *Cellulose, 14*, 643-653.

Lee, M., Cho, Y.D., Choe, E.K., Chung, C. (2007). On-line monitoring of cellulase treatment by differential refractometer. *Fibers and Polymers, 8*(4), 356-362.

Lee, Y.H. (1988). *Enzymatic hydrolysis of insoluble cellulose - a kinetic study*, in *department of chemical engineering* (pp. 340). Manhattan, KS: Kansas State University

Li, X., Kim, T.H., Nghiem, N.P. (2010). Bioethanol production from corn stover using aqueous ammonia pretreatment and two-phase simultaneous saccharification and fermentation (TPSSF). *Bioresource Technology, 101*(15), 5910-5916.

Lide, D.R. (1995). *Handbook of chemistry and physics* (76th ed.). New York, NY: CRC Press.

Linder, M, & Teeri, T.A. (1996). The cellulose-binding domain of the major cellobiohydrolase of *Trichoderma reesei* exhibits true reversibility and a high exchange rate on crystalline cellulose. *Proceedings of the National Academy of Science, USA, 93*, 12251-12255.

Lindstrom, T., & Carlsson, G. (1978). Proceedings from the EUCEPA Symposium: *The effect of chemical environment on fiber swelling* (pp. 32-52). Warsawa, Poland: Lodz.

Lindstrom, T. (1992). Chemical factors affecting the behavior of fibers during papermaking. *Nordic Pulp and Paper Research Journal, 7*(4), 181-192.

Lowry, O.H., Rosebrough, N.J., Farr A.L., Randall R.J. (1951). Protein measurement with the Folin Phenol Reagent. *Journal of Biological Chemistry. 193,* 267-75.

Lu J, Reye J.T., & Banerjee S. (2010). Temperature Dependence of Cellulase Hydrolysis of Paper Fiber. *Biomass & Bioenergy, 34,* 1973-1877

Magonov, S. N. (1993). Surface characterization of materials at ambient conditions by scanning tunneling microscopy and atomic force microscopy. *Applied Spectroscopy Review, 28,* 1-121.

Magonov, S.N., Whangbo, M.-H. (1996). *Surface Analysis with STM and AFM*. New York, NY: VCH.

Maguire, R.J. (1977). Kinetics of hydroysis of cellobiose and p-nitrophenyl-β-D-gucoside by cellobiase of trichoderma viride. *Canadian Journal of Biochemistry, 55*, 19-26.

Mandels, M., & Reese, E.T. (1964). *Fungal cellulases and the microbial decomposition of cellulosic fabric,* in *Developments in industrial microbiology, Volume 5*. Washington, DC: Society for Industrial Microbiology.

McCleary, B.V., & Codd, R. (1991). Measurement of (1-]3),(1-]4)-beta-d-glucan in barley and oats - a streamlined enzymatic procedure. *Journal of the Science of Food and Agriculture, 55*(2), 303-312.

McNeal, M.R., Nanko, H., Hubbe, M.A. (2005). Proceeding from the 13th Fundamental Research Symposium: *Imaging of macromolecular events occurring during manufacture of paper* (pp. 1225-1267). Cambridge, UK: Springer.

Medve, J., Stahlberg, J., Tjerneld, F. (1994). Adsorption and synergism of cellobiohydrolase I and II of *Trichoderma reesei* during hydrolysis of microcrystalline cellulose. *Biotechnology and Bioengineering*, 44, 1064-1073.

Miller, G.L. (1959). Use of dinitrosalicylic acid reagent for determination of reducing sugar. *Analytical Chemistry, 31,* 426-428.

Min, G., Bevan, M., Prieve, D., Patterson, G. (2002). Light scattering characterization of polystyrene latex with and without adsorbed polymer. *Colloids and Surfaces A: Physicochemical and Engineering Aspects, 202*, 9–21.

Mingjie, J., Lau, M.W., Balan, V., Dale, B.E. (2010). Two-step SSCF to convert AFEX-treated switchgrass to ethanol using commercial enzymes and *Saccharomyces cerevisiae* 424A(LNH-ST). *Bioresource Technology, 101*(21), 8171-8178.

Mosier, N., Wyman, C., Dale, B., Elander, R., Lee, Y.Y., Holtzapple, M., Ladisch, M. (2005). Features of promising technologies for pretreatment of lignocellulosic biomass. *Bioresource Technology, 96*(6) 673-686.

Munk, P., & Aminabhavi, T.M. (2002). *Introduction to Macromolecular Science* (2nd Edition). New York, NY: John Wiley & Sons.

Nam, K.H., Sung, M.W., Hwang, K.Y. (2010). Structural insights into the substrate recognition properties of β-glucosidase. *Biochemical and Biophysical Research Communications, 391*(1), 1131-1135.

Nanko, H., Pan, S. (2006). Proceedings from the Pan Pacific Conference - Advances in Pulp & Paper Sciences and Technologies: *Understanding wet-end polymer performance through visualization of macromolecular events by transmission electron microscopy* (pp. 1-18). Seoul, Korea: Korean Institute of Pulp and Paper.

Nanko, H., Pan, S., McNeal, M. (2003). Polymer adsorption on cellulose substrate visualized by transmission electron microscopy (TEM). *Abstracts Of Papers Of The American Chemical Society, 225*, 630.

Nasser, M.S., & James, A.E. (2006). Coacervate Complex Formation Between Cationic Polyacrylamide and Anionic Sulfonated Kraft Lignin. *Separation and Purification Technology, 52*(2), 241-252.

Nassman, J., Lindholm, J., Ekund, D. (1998). Proceedings from the 5th International Paper and Coating Symposium: *Visualization of polymer adsorption on pulp fiber* (23, pp.1-8). Montreal, Canada: Pulp and Paper Technical Association of Canada.

NCBI (2010). National Center for Biotechnology Information. Accessed July 29, 2010. www.ncbi.nlm.nih.gov/

Niemi, H., Paulapuro, H., Mahiberg, R. (2002). Review: Application of scanning probe microscopy to wood, fibre, and paper research. *Paperi JA Puu-Paper and Timber, 84*(6), 389-406.

Neimo, L. (1999). *Papermaking chemistry*. Norcross, GA: TAPPI.

Nurmi, M., Wallin, S., Eklund, D. (2003). Interactions between cationic polyacrylamide and TMP. *Wochenblatt FurPapierfabrikation, 131*(11-12), 678-682.

Odberg, L., Swerin, A., Tanaka, H. (1993). Kinetic aspects of the adsorption of polymers on cellulosic fibres. *Nordic Pulp and Paper Research, 8*(1), 6-9.

Ödberg, L., Sandberg, S., Welin-Klintström S., Arwin, H. (1995). Thickness of adsorbed layers of high molecular weight polyelectrolytes studied by ellipsometry. *Langmuir, 11*(7), 2621-2625.

Ogawa, K., Sato, S., Kokufuta, E. (2005). Formation of intra- and interparticle polyelectrolyte complexes between cationic nanogel and strong polyanion. *Langmuir, 21*(11), 4830-4836.

Oh, S.Y., Yoo, D.I., Shin, Y., Kim, H.C., Kim, H.Y., Chung, Y.S., Park, W.H., Youk, J.H. (2005). Crystalline structure analysis of cellulose treated with sodium hydroxide and carbon dioxide by means of x-ray diffraction and FTIR spectroscopy. Carbohydrate Research, 340(15), 2376-2391.

Ong, E., Gilkes, N.T., Miller, R.C. Jr, Warren, R.A.J., Kilburn, D.G. (1993). The cellulose-binding domain (CBDcex) of an exoglucanase from *Cellulomonas fimi:* production in Escherichia coli and characterization of the polypeptide. *Biotechnology & Bioengineering, 42*, 401-409.

Ooshima, H., Sakata, M., Harano, Y. (1983). Adsorption of cellulase from *Trichoderma viride* on cellulose. *Biotechnology & Bioengineering*, *25*, 3103-3114.

Ozeroglu, C., Guney, O., Sarac, A.S., Mustafaev, M.I. (1996). The polymerization of acrylamide initiated with Ce(IV) and KMnO4 redox systems in the presence of glycine. *Journal of Applied Polymer Science, 60*(5), 759-765.

Palonen, H.(2004). Role of lignin in the enzymatic hydrolysis of lignocellulose. In *VTT Biotechnology* (pp. 1-80). Espoo, Finland: Helsinki University of Technology

Palonen, H., Tenkanen, M., Linder, M. (1999). Dynamic interaction of *Trichoderma reesei* cellobiohydrolases Cel6A and Cel7A and cellulose at equilibrium and during hydrolysis. *Applied and Environmental Microbiology, 65*(12), 5229-5233.

Park, S.M., Jun, H.B., Jung, M.S., Koo, H.M. (2006). Effects of velocity gradient and mixing time on particle growth in a rapid mixing tank. *Water Science and Technology*, 53(7), 95-102.

Pelton, R.H., Allen, L.H., Nugent, H.M. (1980). Factors affecting the effectiveness of some retention aids in newsprint pulp. *Svensk Papperstidning, 83*(9), 251-258.

Perez, J., Munoz-Dorado, J., de la Rubia, T., Martinez, J. (2002). Biodegradation and biological treatments of cellulose, hemicellulose and lignin: an overview. *International Microbiology, 5*, 53-63.

Petlicki, J., van de Ven, T.G.M. (1994). Adsorption of polyethylenimine onto cellulose fibers. *Colliods and Surfaces A: Physicochemical and Engineering Aspects, 83*, 9-23.

Rao, R., Kuys, K. (1995). Proceedings from the 8th International Symposium on Wood and Pulping Chemistry: *Surface chemistry of fibers in recycling of newsprint and Magazines* (pp. 261-266). Helsinki, Finland: Kauppakirjapaino Oy.

Reye, J.T., Maxwell, K., Rao, S., Lu, J., Banerjee, S. (2009). Cationic polyacryamides enhance rates of starch and cellulose saccharification. *Biotechnology Letters, 31*(10), 1613-1616.

Reye, J.T., Lu, J., Maxwell, K., Mora, S., Banerjee, S. (2010), Enhancement of cellulase catalysis of wood pulp fiber by cationic polyelectrolytes, submitted to *Biomass & Bioenergy*, September 2010.

Reye, J.T., Maxwell, K., Banerjee, S. (2010). Cationic Polyacrylamides Promote Binding to cellulase and amylase, submitted to *Journal of Biotechnology*, November 2010.

Richards, E.G., Dover, S.D. (1980). *An introduction to the physical properties of large molecules in solution*. Cambridge, UK and New York, NY: Cambridge University Press.

Ring, G.J.F., Bacon, A.J. (1997). Multiple component analysis of fiber length distributions. *TAPPI Journal, 78*(7), 224-231.

Robertson, G., Olson, J., Allen, P., Chan, B., Seth, R. (1999). Measurement of fiber length, coarseness, and shape with the fiber quality analyzer. *TAPPI Journal, 82*(10), 93-98.

Romani, A., Yanez, R., Garrote, G., Alonso, J.L., Parajo, J.C. (2007). Sugar production from cellulosic biosludges generated in a water treatment plant of a Kraft pulp mill. *Biochemical Engineering Journal, 37*(3), 319-327.

Ryu, D.D.Y., Mandels, M. (1980). Cellulase: biosynthesis and applications. *Enzyme and Microbial Technology, 2*, 91-102.

Saarinen, T., Österberg, M. and Laine, J. (2009). Properties of cationic polyelectrolyte layers adsorbed on silica and cellulose surfaces studied by QCMD – Effect of polyelectrolyte charge density and molecular weight. *Journal of Dispersion Science and Technology, 30*(6), 969-979.

Salmi, J., Osterberg, M., Stenius, P., Laine, J. (2007). Surface forces between cellulose surfaces in cationic polyelectrolyte solutions: The effect of polymer molecular weight and charge density. *Nordic Pulp and Paper Journal, 22*(2), 248-257.

Sauer, B., Solomon, F., Baker, T. (20007) 7.51 Graduate Biochemistry, MITOPENCOURSEWARE, Massachusetts Institute of Technology, Lecture Notes, *Review of Chemical Equilibrium*, accessed 9/27/2010, http://ocw.mit.edu/courses/ biology/ 7-51-graduate-biochemistry-fall-2001/lecture-notes/fa01lec07.pdf.

Scallan, A.M., & Grignon, J. (1979). The effect of cations on pulp and paper properties. *Svensk Papperstidning, 75*(17), 699-703.

Schmuck, M., Pilz, I., Hayn, M., Esterbauer, H. (1986). Investigation of cellobiohydrolase from *trichoderma-reesei* by small-angle x-ray-scattering. *Biotechnology Letters, 8*(6), 397-402.

Schumann, H. & Kunst, S. (1991). Elimination von 14C-markierten polyelecktrolyten in biologischen Abwasserreinigungsprozessen. *Gas-Wasserfach, Wasser/Abwasser* 132, 376–383.

Scott, W.E. (1996) *Principals of wet end chemistry*. Roswell, GA: TAPPI Press.

Sluiter, A., Hames, B., Ruiz, R., Scarlata, C., Sluiter ,J., Templeton, D., Crocker, D. (2008) *Determination of structural carbohydrates and lignin in biomass. Laboratory Analytical Procedure, National Renewable Energy Laboratory Technical Report NREL/TP-510-4261*. Golden, CO: National Renewable Energy Laboratory.

Smith, P.K., Krohn, R.I., Hermanson, G.T., Mallia, A.K. (1985). Measurement of protein using bicinchoninic acid. *Analytical Biochemistry, 150,* 76-85.

Smook, G.A. (1982). *Handbook for Pulp & Paper Technologists* (pp. 3-7). Montreal, Canada: Canadian Pulp and Paper Association.

SNF (UK) Limited (2010). *Powders Beads SNF FLOERGER*. Accessed May 21, 2010, www.snf.co.uk/downloads/Powders.pdf.

Soderstrom, J., Pilcher, L., Galbe, M., Zacchi, G. (2003). Two-step steam pretreatment of softwood by dilute H_2SO_4 impregnation for ethanol production. *Biomass & Bioenergy, 24*, 475-486.

Solberg, D. (2003). On the mechanism of cationic-polyacrylamide-induced flocculation and re-dispersion of a pulp fiber dispersion. *Nordic Pulp and Paper Research, 18*(1), 51-55.

Solberg, D.,& Wagberg ,L. (2003). Adsorption and flocculation behavior of cationic polyacrylamide and colloidal silica. *Colloids and Surfaces A: Physicochemical and Engineering Aspects, 219*, 161-172.

Song, D.L., Zhao, Y.L., Dong, C.X., Deng, Y.L. (2009). Surface modification of cellulose fibers by starch grafting with crosslinkers. *Journal of Applied Polymer Science, 113*(5), 3019-3026.

Song, Y., Mathias, P.M., Tremblay, D., Chen, C.C. (2003). Liquid viscosity model for polymer solutions and mixtures. *Industrial & Engineering Chemistry Research, 42*, 2415-2422.

Southwick, J.G., Jamieson, A.M., Blackwell, J. (1982). Conformation of xanthan dissolved in aqueous urea and sodium chloride solutions. *Carbohydrate Research,99,* 117-127.

Spindler, D.D., Wyman, C.E., Grohmann, K., Mohagheghi, A. (1989). Simultaneous saccharification and fermentation of pretreated wheat straw to ethanol with selected yeast strains and b-glucosidase supplementation. *Applied Biochemistry and Biotechnology, 20/21*, 529-540.

Stenius, P., & Pakarine, H. (1991). *Forest products chemistry*. In *Papaermaking science and technology* (Volume 3). Helsinki, Finland and Atlanta, Georgia: TAPPI.

Sternberg, D., Vijayakumar, P., Reese E.T. (1977). B-glucosidase: microbial production and effect on enzymatic hydrolysis of cellulose. *Canadian Journal of Biochemistry, 23,* 139-147.

Stockton, B.C, Mitchell, D.J., Grohmann, K., Himmel, M.E. (1991). Optimum B-glucosidases supplementation of cellulase for efficient conversion of cellulose to glucose. *Biotechnology Letters, 13*(1), 57-52.

Stov, S.V., Izumrudov, V.A., Muronetz, V.I. (2010). Structural changes of a protein bound to a polyelectrolyte depend on the hydrophobicity and polymerization degree of the polyelectrolyte. *Biochemistry-Moscow, 75*(4), 437-442.

Sun, Y., Cheng, J. (2002). Hydrolysis of lignocellulosic materials for ethanol production: a review. *Bioresource Technology, 83*, 1-11.

Sun, Y. (2002). Enzymatic hydrolysis of rye straw and bermudagrass for ethanol production (Doctoral Dissertation). Raleigh, NC: North Carolina State University.

Swerin, A., Odberg, L. (1997). Proceedings from the 11th Fundamental Research Symposium: *Some aspects of retention* aids (pp. 265-350). In*: The fundamentals of papermaking materials.* Cambridge, UK: Pira International.

Tangnu, S.K., Blanch, H., Wilke, C.R. (1981). enhanced production of cellulase, hemicellulase and B-xylosidase by Trichoderma reesi (RUT-C30). *Biotechnology & Bioengineering, 23*, 1837-1849.

TAPPI (2006). *TAPPI 205 sp-06, Forming handsheets for physical tests of pulp*. Atlanta, GA: TAPPI Press.

TAPPI (2006). *TAPPI 233 cm-06, Fiber length of pulp by classification*. Atlanta, GA: TAPPI Press.

TAPPI (2007). *TAPPI 271 om-07, Fiber length of pulp and paper by automated optical analyzer using polarized light*. Atlanta, GA: TAPPI Press.

Trinder, P. (1969). Determination of glucose in blood using glucose oxidase with an alternative oxygen acceptor. *Annals Clinical Biochemistry, 6,* 24.

Van de Steeg, H.G.M., Cohen Stuart, M.A., de Keizer, A., Bijsterbosch, B.H. (1992). Polyelectrolyte adsorption - a subtle balance of forces. *Langmuir, 8*(10), 2538.

Vesilind, P.A. (1988). Capillary suction time as a fundamental measure of sludge dewaterability. *Journal Water Pollution Control Federation, 60*(2), 215-220.

Vesilind, P.A., Ormeci, B. (2000). A modiefied capillary suction time apparatus for measuring the filterability of super-flocculated sludges. *Water Science and Technology, 42*(9), 135-139.

Volk, D., Vollmer, D., Schmidt, M., Oppermann, H.K. (2004). Conformation and phase diagrams of flexible polyelectrolytes. *Advanced Polymer Science, 166,* 29-65.

Vries, R.P.D. & Visser, J. (2001). Aspergillus enzymes involved in degradation of plant cell wall polysaccharides. *Microbiology and Molecular Biology Reviews, 65*(4), 497-522.

Wagberg, L., Aselli, I. (1995). The action of cationic polymers in the fixation of dissolved and colloidal substances. 2. *Colloids and Surfaces A, 104*(2-3), 169-184.

Wagberg, L., & Odberg, L. (1989). Polymer adsorption on cellulosic fibres. *Nordic Pulp and Paper Research Journal, 4*(2), 135.

Wagberg, L. (2001). *Polyelectrolyte adsorption on cellulose fibres – a review (pp.1-30).* Mid-Sweden University, Fibre Science and Communication Network, Report number: R-00-7.

Walldal, C., & Akerman, B. (1999). Effect of ionic strength on the dynamic mobility of polyelectrolytes. *Langmuir, 15*(16), 5237-5243.

Wang, T.K., & Audebert, R. (1988). Adsorption of cationic copolymers of acrylamide at the silica—water interface: Hydrodynamic layer thickness measurements. *Journal of Colloidal Interface Science, 121,* 32-41.

Wann, S.R., & Rakestraw J.L. (1998) Proceedings from Improving Forest Productivity for Timber, A Key to Sustainability: *Maximizing Hardwood Plantation Productivity in the Southern United States – Lessons Learned From Loblolly Pine*. Duluth, Minnesota: Springer.

Weil, J.R., Dien, B., Bothast, R., Hendrickson, R., Mosier, N.S., Ladisch, M.R. (2002). Removal of fermentation inhibitors formed during pretreatment of biomass by polymeric adsorbents. *Industrial & Engineering Chemistry Research, 41*(24), 6132-6138.

Wiechelman, K., Braun, R., Fitzpatrick, J. (1988). Investigation of the bicinchoninic acid protein assay: Identification of the groups responsible for color formation. *Analytical Biochemistry, 175,* 231-7.

Wien, Q.X., Chen, Z.Q., Zhao, Y., Zhang, H.C., Feng, Y.J. (2010). Biodegradation of polyacrylamide by bacteria isolated from activated sludge and oil-contaminated soil, *Journal of Hazardous Materials*, 175(1-3), 955-959.

Wittemann, A., Ballauff, M. (2006). Interactions of proteins with linear polyelectrolytes and spherical polyelectrolyte brushes in aqueous solution. *Physical Chemistry Chemical Physics, 8*, 5269-5275.

Wood, T.M. (1968). Cellulytic enzyme system of trichoderma kiningii. Separation of components attacking native cotton. *Biochemical Journal, 109*(2), 217-227.

Woodward, J. (1982). Fungal and other B-D-glucosidases – Their properties and applications. *Enzyme and Microbial Technology, 4*, 73-79.

Wu, J., Ju, K.L. (1998). Enhancing enzymatic saccharification of waste newsprint by surfactant addition. *Biotechnology Progress, 14*, 649-652.

Wyman, C.E. (Editor) (1996). *Handbook on bioethanol: production and utilization* (Applied Energy Technology Series). Philadelphia, PA: Taylor and Francis.

Wyman, C.E., Dale, B.E., Elander, R.T., Holtzapple, M., Ladisch, M.R., Lee, Y.Y. (2005). Coordinated development of leading biomass pretreatment technologies. *Bioresource Technology, 96*(18) 1959-1966.